Aus dem Bereich Physiologie
Theoretische Medizin und Biowissenschaften
der Medizinischen Fakultät
der Universität des Saarlandes, Homburg/Saar

Characterization of the sigma-1 receptor in the mouse central nervous system

Dissertation

zur Erlangung des Grades eines Doktors der Naturwissenschaften

**der Medizinischen Fakultät
der Universität des Saarlandes**

2023

vorgelegt von: Qing Liu
geb. am: 02. March 1991 in Tianjin, China

Date of oral examination: 19.12.2023

Dean of the faculty: **Univ.-Prof. Dr. med. Michael D. Menger**

Examinants: **Prof. Dr. Frank Kirchhoff** - University of Saarland

Prof. Dr. Robert Ernst - University of Saarland

_____

_____

_____

This work was supported by grants from the Deutsche Forschungsgemeinschaft, Sino-German joint project KI 503/14-1, the Fritz Thyssen Foundation (10.21.1.021MN) and the medical faculty of the University of Saarland (HOMFORexzellent2016). I was supported by a PhD student stipend from the Chinese Scholarship Council.

CONTENTS

List of Abbreviations

AD	Alzheimer's disease
AEP	anterior entopeduncular area
ALS	amyotrophic lateral sclerosis
Ab	antibody
AR	antigen retrieval
ATF6	transcription factor 6
BAF	barrier-to-autointegration factor
BCAS1	breast carcinoma amplified sequence 1
BDNF	brain-derived neurotrophic factor
BiP	binding immunoglobulin protein
cc	corpus callosum
CC1	adenomatous polyposis coli (APC) clone CC1
cKO	conditional knockout
CNPase	2',3'-cyclic nucleotide 3'-phosphodiesterase
CNTF	ciliary neurotrophic factor
CNS	central nervous system
CPu	caudate putamen
ctx	cortex
CXCL1	chemokine (C-X-C motif) ligand 1
DM	dextromethorphan
DSB	double strand break
EGF	epidermal growth factor
ENPP6	ectonucleotide pyrophosphatase/phosphodiesterase 6
ER	endoplasmic reticulum
F-actin	filamentous polymers
FST	forced swimming test
G-actin	globular monomers
GalC	galactocerebroside
GPR17	G-protein receptor 17
GRP78	glucose-regulated protein 78
GSTπ	glutathione-S-transferase pi

GS	glutamine synthetase
GM	grey matter
HDAC	histone deacetylase
hip	hippocampus
IFN-γ	interferon-gamma
IGF	insulin-like growth factor
IHC	immunohistochemistry
IL-6	interleukin-6
IL-1β	interleukin-1 beta
IP3Rs	inositol 1,4,5-trisphosphate receptors
IRE1	inositol-requiring protein 1
KO	knockout
LGE	lateral and caudal ganglionic eminences
LPS	Lipopolysaccharide
LTP	long-term potentiation
MACS	magnetic-activated cell sorting
MAM	mitochondria-associated ER membrane
MAG	Myelin Associated Glycoprotein
MAOB	Monoamine oxidase B
mOL	mature myelinating oligodendrocyte
MBP	Myelin Basic Protein
MFs	Microfilaments
MFI	Mean Fluorescence Intensity
MTs	Microtubules
MGE	medial ganglionic eminence
MOG	Myelin-Oligodendrocyte Glycoprotein
MTOC	microtubule organizing center
Myrf	myelin regulatory factor
NMDA	N-methyl-D-aspartate
NRGs	Neuregulins
NRG1	neuregulin 1 type III
NSC	neural stem cells

OL	oligodendrocyte
OPC	oligodendrocyte progenitor cell
PERK	protein kinase RNA-like ER kinase
PNS	peripheral nervous system
Pα	platelet-derived growth factor receptor alpha subunit
preOL	premyelinating oligodendrocyte
PSA-NCAM	The polysialic acid (PSA) modification of neural cell adhesion molecule
RyRs	ryanodine receptors
S1R	sigma-1 receptor
SDS	sodium dodecyl sulfate
sgRNA	single guide RNA
Shh	Sonic hedgehog
Sp3	Specific protein 3
TBI	Traumatic brain injury
TCF7I2	Transcription factor 7-like 2
TGF-β	Transforming growth factor-beta
TNF-α	Tumor necrosis factor-alpha
TH	tyrosine hydroxylase
UPR	Unfolded Protein Response
VGCC	L-type voltage-gated calcium channels
W	week
WM	white matter
6-OHDA	6-hydroxydopamine

List of Figures

List of Tables

List of Supplementary Figures

1 Abstract

The sigma-1 receptor (S1R) is a chaperon protein, and S1R exogenous ligands have shown therapeutic potential for several neurological disorders. Extensive *in vitro* studies have demonstrated the localization of S1Rs in the membrane of endoplasmic reticulum (ER) but *in vivo* cell type specific expression pattern of S1Rs remains unclear, mainly due to the lack of a reliable detection method.

In this study, we established a highly specific immunohistochemical protocol for the detection of S1Rs which was validated using S1R knock-out (KO) mice. Next, we characterized S1R expression in the mouse brain, demonstrating that S1Rs are widely expressed in principal neurons, interneurons, and all glial cell types. Particularly, the expression of S1Rs in oligodendrocyte progenitor cells (OPCs) was detected for the first time. Employing neuronal and glial cell specific Cre-expressing mice, we generated Cre-dependent S1R conditional KO mice. Taken together, we provide a powerful tool for cell-specific detection, deletion, and functional characterization of S1Rs *in vivo*.

We detected an increase of S1R expression during OPC differentiation into oligodendrocytes (OLs), suggesting a potential role of S1Rs in regulating OL development. Since we found a transit delay of myelination in the cortex of S1R KO mice at postnatal day 14 (P14), we traced the fate of OPCs after Cre activity induction at P7-8 using the NG2-CreERT2 knock-in and Rosa26-tdTomato reporter mice. Although no difference was found in the density or proportion of Pα (OPC marker), APC CC1 or Myrf (both OL markers) immunoreactive cells at P14, P21, and P30, we observed an increase in GSTπ$^+$ (mature OL marker, mOLs) in the *corpus callosum* of KO mice. Similarly, the OPC-specific deletion of S1R did not influence the proliferation and differentiation of OPCs into OLs during development. Again, we observed the increased density and proportion of GSTπ$^+$ mOLs in the brain (cortex and *corpus callosum*) and spinal cord of cKO mice at P21 and P30. In addition, we detected increased expression of myelin-related proteins (MBP and MOG) in the brain. We also found increased GSTπ$^+$ and GSTπ$^+$tdT$^+$ mOLs in cKO brains four weeks after the Cre activity induction in adult OPCs at P30. Altogether, our results suggest that S1R deletion in OL lineage cells may lead to precocious maturation of OLs during development.

In conclusion, our findings indicate that S1Rs are involved in regulating OL lineage cell maturation but do not affect the OPC proliferation and differentiation during OL development. Unravelling the mechanisms underlying S1Rs regulating OL maturation is required in the further study to develop novel therapies for demyelination-related diseases.

2 Graphical Abstract

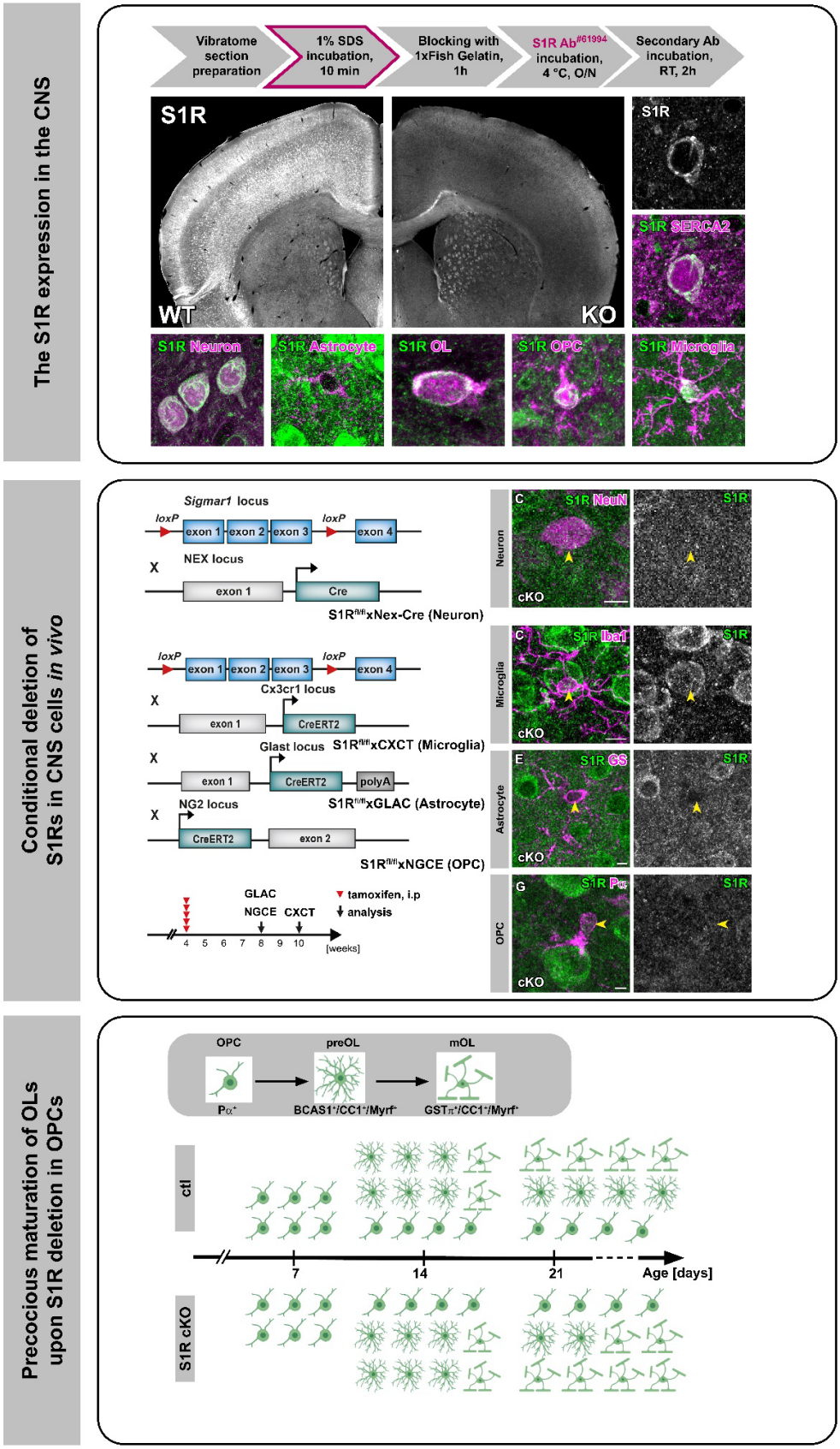

3 Zusammenfassung

Der Sigma-1-Rezeptor (S1R) ist ein Chaperon-Protein, und S1R exogene Liganden haben sich als therapeutisches Potenzial für mehrere neurologische Erkrankungen gezeigt. Intensive in vitro-Studien haben die Lokalisierung von S1Rs in der Membran des endoplasmatischen Retikulums (ER) gezeigt, aber das in vivo zelltypspezifische Expressionsmuster von S1Rs bleibt unklar, hauptsächlich aufgrund des Mangels an einer zuverlässigen Nachweismethode.

In dieser Studie haben wir ein hochspezifisches immunohistochemisches Protokoll zur Detektion von S1Rs etabliert, das mit S1R-Knock-out (KO)-Mäusen validiert wurde. Anschließend charakterisierten wir die S1R-Expression im Gehirn der Maus und zeigten, dass S1Rs in den Hauptneuronen, Interneuronen und allen Gliazelltypen weit verbreitet sind. Insbesondere wurde die Expression von S1Rs in Oligodendrozyten-Progenitorzellen (OPCs) zum ersten Mal nachgewiesen. Unter Verwendung von Mäusen mit neuronalen und glialen zellspezifischen Cre-Expression generierten wir Cre-abhängige S1R-Bedingte KO-Mäuse. Zusammenfassend liefern wir ein leistungsstarkes Werkzeug für die zellspezifische Detektion, Deletion und funktionelle Charakterisierung von S1Rs *in vivo*.

Wir stellten eine Zunahme der S1R-Expression während der Differenzierung von OPCs zu Oligodendrozyten (OLs) fest, was auf eine potenzielle Rolle von S1Rs bei der Regulation der OL-Entwicklung hinweist. Angesichts unserer Feststellung einer Verzögerung der Myelinisierung in der Großhirnrinde von S1R-KO-Mäusen am 14. postnatalen Tag (P14) haben wir mithilfe von NG2-CreERT2-Knock-in- und Rosa26-tdTomato-Reporter-Mäusen das Schicksal von OPCs nach der Induktion der Cre-Aktivität am P7-8 verfolgt. Obwohl kein Unterschied in der Dichte oder dem Anteil von Pα (OPC-Marker), APC CC1 oder Myrf (beide OL-Marker) immunreaktiven Zellen bei P14, P21 und P30 festgestellt wurde, beobachteten wir eine Zunahme von GSTπ$^+$ (reifer OL-Marker, mOLs) im Corpus callosum von KO-Mäusen. Ebenso beeinflusste die OPC-spezifische Deletion von S1R weder die Proliferation noch die Differenzierung von OPCs zu OLs während der Entwicklung. Erneut beobachteten wir bei den cKO-Mäusen bei P21 und P30 eine erhöhte Dichte und einen höheren Anteil von GSTπ$^+$ mOLs im Gehirn (Großhirnrinde und Corpus callosum) und Rückenmark. Darüber hinaus stellten wir eine erhöhte Expression von Myelin-verwandten Proteinen (MBP und MOG) im Gehirn fest. Wir fanden auch erhöhte GSTπ$^+$ und GSTπ$^+$tdT$^+$ mOLs in den cKO-Gehirnen vier Wochen nach der Cre-Aktivitätsinduktion bei erwachsenen OPCs am P30. Insgesamt deuten unsere Ergebnisse darauf hin, dass die Deletion von S1R in OL-Linienzellen zu einer vorzeitigen Reifung von OLs während der Entwicklung führen kann.

Zusammenfassend deuten unsere Ergebnisse darauf hin, dass S1Rs an der Regulation der Reifung von OL-Linienzellen beteiligt sind, aber die Proliferation und Differenzierung von OPCs während der OL-Entwicklung nicht beeinflussen. Die Aufklärung der Mechanismen, die der Regulation der OL-Reifung durch S1Rs zugrunde liegen, ist für weitere Studien zur Entwicklung neuartiger Therapien für demyelinisierungsbedingte Erkrankungen erforderlich.

4 Introduction

4.1 Structural and pharmacological functional properties of the sigma-1 receptor

The sigma-1 receptor (S1R) was originally identified as a G-protein-couped opioid receptor in 1976 (Martin et al., 1976). However, this classification was corrected in 1982 and S1Rs were recognized as non-opioid, non-phencyclidine receptors (Su, 1982). There are two subtypes of sigma receptors namely sigma-1 receptors and sigma-2 receptors. Receptor binding studies have shown that S1Rs have a high affinity for their ligands, whereas sigma-2 receptors have lower ligand affinity (Hellewell and Bowen, 1990). S1Rs have been cloned and found to be conserved in their amino acid sequences across different mammalian species (Hanner et al., 1996).

S1Rs are single transmembrane proteins containing of 223 amino acids (~25kD). The crystal structure of the human S1R provides a high-resolution view of its structure (Schmidt et al., 2016; Meng et al., 2022) (Figure 1A). The S1Rs exhibit a homotrimeric structure: each protomer includes a single transmembrane helix at the amino-terminus, followed by a cupin-fold β-barrel body containing a ligand-binding site, and a V-shaped two-helix bundle (α4/α5) adjacent to the membrane at the carboxy-terminus, covering the cupin-fold domain (Schmidt et al., 2016; Schmidt et al., 2018). The carboxy-terminal domain of S1Rs faces the cytosolic surface of endoplasmic reticulum (ER), with a hydrophobic ligand-binding pocket buried in the center (Schmidt et al., 2016). Previous studies have demonstrated that S1R agonists and antagonists exert their effects through oligomer dissociation and stabilization, respectively (Mishra et al., 2015). Moreover, the entry mechanism of ligands into the binding site of S1Rs has gained increasing interest, providing new insights into the understanding of this protein (Schmidt et al., 2018; Rossino et al., 2020; Meng et al., 2022).

Based on their structural characteristics, S1Rs have become a pharmacological target of interest in clinical trials and hold potential therapeutic significance in the treatment of various diseases, including neurological disorders and cancer. S1Rs exhibit different binding affinities for different exogeneous ligands and possess diverse pharmacological applications (Cobos et al., 2008), including cocaine and methamphetamine for the treatment of drug abuse (Matsumoto et al., 2002; Nguyen et al., 2005), antidepressants such as fluvoxamine (Narita et al., 1996), and the drugs meperidine and donepezil for the treatment of Alzheimer's disease (Maurice, 2016; Kargbo, 2021). Additionally, several selective and high-affinity drugs have been used in research that specifically target S1Rs, including the S1R agonists PRE-084 (Maurice et al., 1994; Motawe et al., 2020) and SA4503 (Maurice and Privat, 1997; Ono et al., 2014), as well as the S1R antagonists BD1047 (Matsumoto et al., 1995; Skuza and Rogóz, 2006) and NE-100 (Okuyama et al., 1993).

In addition to exogenous ligands, Su and his colleagues proposed a natural interaction between neurosteroids and S1Rs, suggesting that neurosteroids could serve as possible endogenous ligands for S1Rs (Su et al., 1988). It has been demonstrated that progesterone has the same effect as S1R antagonists, while pregnenolone sulfate and DHEA act as S1R agonists (Maurice et al., 2001; Hayashi and Su, 2004b; Hong et al., 2004). However, this concept remains controversial as the affinity of these steroids for S1Rs is lower compared to that of normal endogenous ligands (Hayashi and Su, 2004b). Nevertheless, benefiting

from *in vivo* studies of biological functions, the discovery of potent endogenous ligands may provide new therapeutic candidates for the future.

4.2 The distribution of S1Rs in the CNS

S1Rs are widely distributed in the central nervous system (CNS) and in different peripheral organs such as lungs, liver, urinary bladder, kidney, and muscles (Gundlach et al., 1986; Mei and Pasternak, 2001; Zhang et al., 2014a; Su et al., 2016).

Previous studies using immunohistochemistry and mRNA expression profiling experiments showed wide expression of S1Rs in neurons and glial cells (astrocytes, oligodendrocytes, microglia and ependymocytes) (Hayashi and Su, 2004a; Francardo et al., 2014; Su et al., 2016). However, controversy remains with respect to the exact cellular localization of S1Rs in the CNS. For example, using a custom-made antibody, Alonso et al. detected S1Rs only in neurons located in the granular layer of the olfactory bulb, various hypothalamic nuclei, the septum of brain, motor nuclei of the hindbrain and the dorsal horn of the spinal cord (Alonso et al., 2000). Palacios et al. observed S1R expression in OLs as well, using independently tailored antibodies (Palacios et al., 2003). Using a commercial antibody, Ruscher et al. observed that S1R immunoreactivity co-localized with the cytoskeleton indicated by glial fibrillary acidic protein (GFAP) as well as with the galactocerebroside-enriched membrane microdomains of reactive astrocytes in the peri-infarct area of rat brains after cerebral stroke (Ruscher et al., 2011). However, the exact expression pattern of S1Rs in oligodendrocyte progenitor cells (OPCs) and microglia has not been elucidated previously.

Notably, it is unclear whether the specificity of the antibodies used in the mentioned studies was tested by S1R knock-out (KO) mice/cell lines as a rigorous control. To date, only one custom-made antibody against S1R (termed Ab^{Ruoho}) generated by Arnold Ruoho's group has been validated by S1R KO mice, showing high specificity for immunohistochemistry in the brain and spinal cord (but worse performance for immunoblotting) (Mavlyutov et al., 2010; Mavlyutov et al., 2016; Nakamura et al., 2019). However, in these studies, the fine structures of Ab^{Ruoho} stained cells in brain slices were not displayed with high magnification, neither co-immunostaining for different cell type markers performed. Therefore, it is hard to verify the detailed expression patterns of S1Rs in neurons and glial cells *in vivo*.

4.3 Involvement of S1R activation in various cellular functions

S1Rs have been shown to be involved in various aspects of cellular functions upon ligand targeting (Reviewed by Su et al., 2016) (Figure1B). Unlike traditional receptors activation mechanisms, S1Rs function as molecular chaperone proteins: agonists of S1Rs act through dissociation of S1Rs and chaperone proteins, while antagonists stabilize target proteins (Gromek et al., 2014).

S1Rs are mainly localized at the mitochondria-associated ER membrane (MAM), where are involved in the regulation of calcium (Ca^{2+}) homeostasis, lipid synthesis, and ER stress response. Under normal physiological conditions, S1Rs bind to another chaperone glucose-regulated protein 78 (GRP78, also known as BiP, binding immunoglobulin protein), which is thought to stabilize inositol 1,4,5-trisphosphate receptors (IP3Rs). Upon agonist binding or stress stimulation, S1Rs dissociated from Bip, ensuring the Ca^{2+} influx from the ER to

mitochondria, suggesting a role of S1Rs for the maintenance of calcium homeostasis (Hayashi and Su, 2007; Hayashi, 2015).

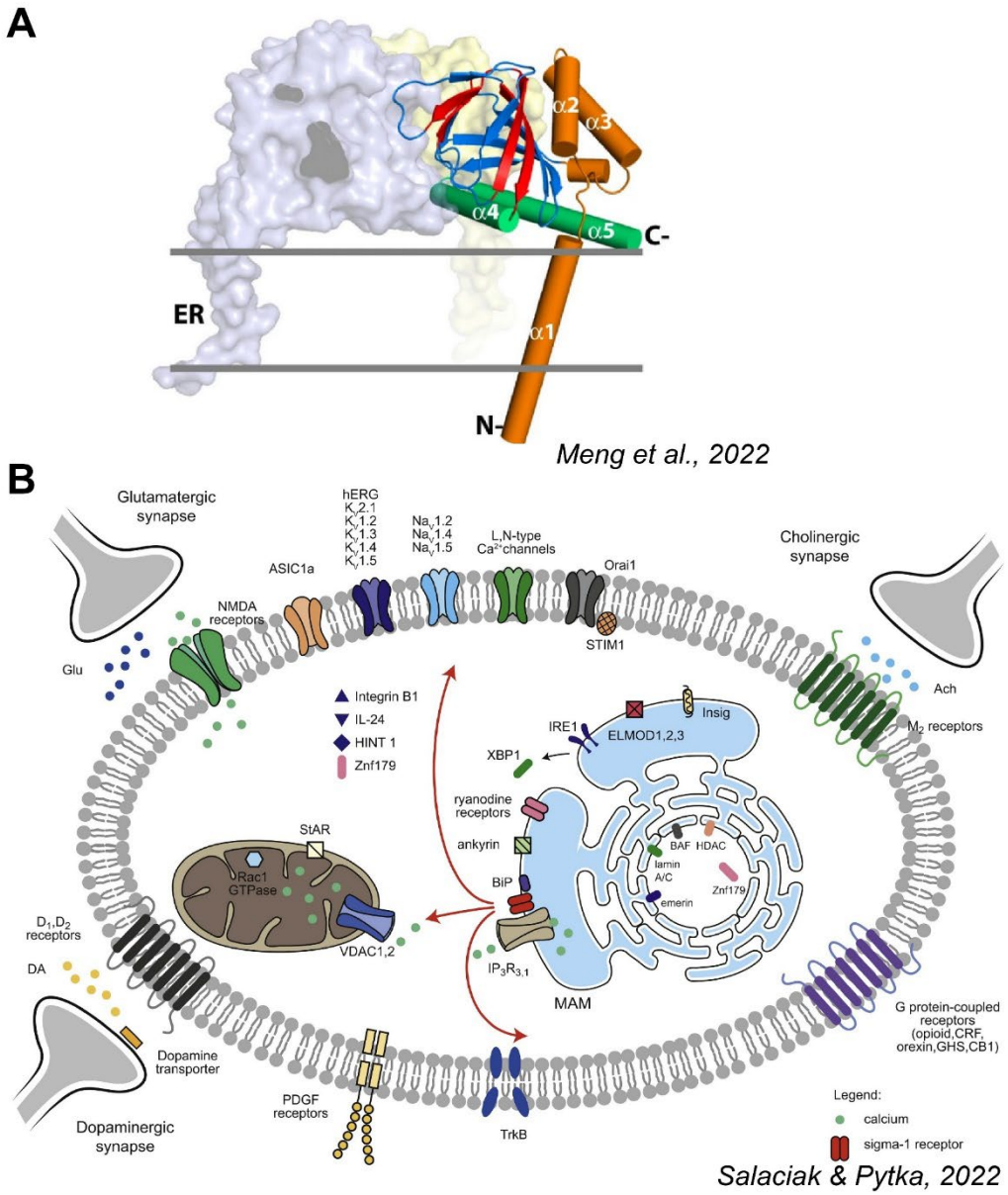

Figure 1. Schematic representation of the 3D-structure of S1Rs and the cellular functions of S1Rs. A. The diagram illustrates the homotrimeric structure of S1Rs, indicating the three subunits that form the receptor. Adapted from Meng et al., 2022 (Meng et al., 2022). **B.** The diagram represents the cellular functions of S1Rs upon their activation. It highlights various processes and pathways associated with S1R activation, such as modulation of calcium signalling, regulation of mitochondrial function, neuroprotection, and modulation of neurotransmitter release. Adapted from Salaciak and Pytka, 2022 (Sałaciak and Pytka, 2022).

Furthermore, S1Rs are involved in the regulation of cellular survival under ER stress (Mori et al., 2013). The ER is responsible for protein folding and assembly. Accumulation of misfolded or unfolded proteins can lead to a disruption of homeostatic environment in the ER, which is known as ER stress. The unfolded protein response (UPR) is an adaptive cellular response to ER stress that reduces the protein load to maintain correct cellular functioning (Hetz, 2012). Under physiological conditions, as with Bip, S1Rs chaperone with

ER stress sensors such as inositol-requiring protein 1 (IRE1), transcription factor 6 (ATF6) and protein kinase RNA-like ER kinase (PERK). Upon ER stress, S1Rs dissociate from IRE1 and regulate cell survival (Mori et al., 2013). In a model of lipopolysaccharide (LPS)-induced septic shock, Rosen et al. showed that activation of S1Rs by their agonist fluvoxamine exerted an anti-inflammatory function and decreased cytokine expression via modulation of IRE1 (Rosen et al., 2019).

Moreover, increasing evidence suggests that S1Rs are involved in the regulation of autophagy, a process associated with the clearance of damaged cellular components. Dysfunctional autophagy is observed in neurodegenerative diseases (Christ et al., 2019; Zhang et al., 2020; Prasanth et al., 2021). Yang et al. showed that S1R deficiency resulted in impaired clearance of autophagosomes and accumulation of autophagosome markers (LC3-II and p62), which was mainly associated with dysfunctional of autophagosome-lysosome fusion (Yang et al., 2019). Extensive studies have demonstrated that S1Rs chaperone with the nucleus protein POM121 to recruit KPNB1/importinβ1, facilitating the transportation of TFEB from the cytosol into the nucleus. This process is crucial for initiating autophagy in NSC34 cells. These findings were confirmed using the S1R agonist pridopidine, suggesting that S1Rs could represent novel targets for pharmacological treatment of diseases involving impairments in autophagy (Wang et al., 2023).

S1Rs have been implicated in the regulation of various ion channels in neurons, including calcium channels (N-type and L-type voltage-gated calcium channels), potassium channels (Kv1.2, Kv1.3, Kv1.4 and Kv1.5 channels), and sodium channels (Nav1.2/1.4 and Nav1.5) (Balasuriya et al., 2012; Gao et al., 2012; Kourrich et al., 2013; Abraham et al., 2019). For example, it has been shown that the S1R agonist (+)-SKF 10047 directly inhibits Nav1.2/1.4 (Gao et al., 2012). Fontanilla et al. demonstrated that S1Rs interact with N, N-dimethyltryptamine (DMT) and inhibit activation of Nav1.5 channel in cardiac myocytes (Fontanilla et al., 2009). Furthermore, S1Rs are involved in the regulation of neurotransmitter systems. Low dose agonists of S1Rs potentiate N-methyl-D-aspartate (NMDA)-induced neuronal firing in the CA3 of the hippocampus (Monnet et al., 1990). Upon ligand activation, S1Rs enhance the response to the NMDA-dependent long-term potentiation (LTP), indicating the potential role of S1Rs in the regulation of learning and memory in the hippocampus (Sabeti et al., 2007; Maurice and Su, 2009).

Furthermore, S1Rs can translocate from the ER to the nuclear envelope upon activation by S1R agonists. Here, S1Rs interact with Emerin and recruit chromatin remodeling molecules, including lamin A/C, barrier-to-autointegration factor (BAF), and histone deacetylase (HDAC) in NG108 cells. The S1R/Emerin/BAF/HDACs complex is then formed and is associated to the regulation of monoamine oxidase B (MAOB) gene transcription through the linkage of specific protein 3 (Sp3) (Tsai et al., 2015).

Indeed, most of these studies have been conducted *in vitro* or using pharmacological models. The involvement of S1Rs in mediating various cellular functions primarily relies on their ligand-binding properties. However, the biological functions of S1Rs in different cell types *in vivo* remains to be elucidated.

4.4 Implications of S1R functions from S1R knockout mice

Several decades of research have been shown that S1Rs play an important role in CNS diseases such as Alzheimer's disease (AD), amyotrophic lateral sclerosis (ALS), multiple sclerosis, and neuropsychiatric disorders. Several pharmacological studies have

demonstrated the neuroprotective functions of S1Rs upon activation (Mishina et al., 2008; Tsai et al., 2012). In a Parkinson's disease model induced by 6-hydroxydopamine (6-OHDA), administration of the S1R agonist PRE-084 resulted in increased expression of tyrosine hydroxylase (TH)-positive neurons in the lesion region and improved functional recovery (Francardo et al., 2014). Likewise, in an ALS model using SOD1G93A mice, treatment with S1R agonists PRE-084 and SA4503 led to a reduction in motor neuron loss and damage (Mancuso et al., 2012; Ono et al., 2014). Moreover, Gaja-Capdevila et al. demonstrated that not only S1R agonists but also a S1R antagonist BD1063 reduced spinal motoneuron degeneration and exerted neuroprotective effects (Gaja-Capdevila et al., 2021). In AD, several studies have shown that S1R ligands (e.g., ANAVEX2-73, donepezil, PRE-084) have neuroprotective roles and can prevent memory impairment and AD pathology (Maurice, 2016; Borbély et al., 2022).

Neuroinflammation is another common neuropathological manifestation of neurological disorders, mainly involving the activation of microglia and astrocytes. Increasing evidence suggests that activation of S1Rs exerts an anti-inflammatory function and promotes neuronal survival in CNS diseases such as traumatic brain injury (TBI), chronic neurodegenerative diseases, and systemic inflammation-induced encephalopathy (e.g., sepsis-associated encephalopathy). In an embolic stroke model, administration of the S1R agonist PRE-084 reduced the expression levels of pro-inflammatory cytokines, demonstrating a neuroprotective effect (Allahtavakoli and Jarrott, 2011). In cultured astrocytes, activation of S1Rs by the agonist SA4503 attenuate oxidative and inflammatory responses induced by LPS (Wang and Zhao, 2019). Similarly, in cultured microglia, S1R activation by SKF83959 prevented the activation of M1 microglia and inhibited the expression of pro-inflammatory cytokines in an LPS-induced neuroinflammation model (Wu et al., 2015).

Despite the clear effects of S1Rs observed in pharmacological studies, studies addressing the physiological functions of S1Rs using S1R KO mice have shown modest alterations, particularly in cognitive, psychiatric, and motor dysfunctions (Couly et al., 2022). Different research groups have reported variable performance of S1R KO mice in different behavioral tests, and the results can vary with age and gender. For instance, Chevallier et al. found deficits in working memory and spatial memory in female S1R KO mice using the Y-maze and Morris water maze tests (Chevallier et al., 2011). However, Xu et al. reported comparable performance in the water maze between wild-type (WT) and KO mice. Moreover, no difference in spontaneous locomotion, as assessed by the open field test, was observed between WT and KO mice (Xu et al., 2017). Aging KO mice (> 12 weeks old) exhibited more pronounced deficits in the Rotarod test, suggesting that the absence of S1Rs leads to abnormal motor coordination. S1R KO mice, and particularly male mice, also displayed depressive-like behaviors in the forced swimming test and tail suspension test (Sabino et al., 2009). In addition, several studies on ALS using S1R KO mice have demonstrated more severe pathological performance and reduced activity in motoneurons compared to WT mice (Mavlyutov et al., 2013).

Although most of these studies have focused on neuronal cells, growing evidence suggests that S1Rs also play important roles in the regulation of glial functions, particularly in astrocyte and microglia. In the TBI model, S1R KO mice exhibited reduced expression of GFAP in Bergmann glia cells and reduced motor impairment over the long-term (up to 12 months) (Stelfa et al., 2021). In an ischemic stroke model, microglia/macrophage from S1R

KO mice displayed impaired phagocytosis, affecting efferocytosis and consequence to worsened brain damage and neurological deficits (Zhang et al., 2023).

Neurons and glial cells interact to orchestrate diverse CNS functions, and the changes observed in S1R KO mice are multifactorial. Therefore, it is essential to focus on cell-type-specific S1Rs to modulate neural network activity under physiological and pathological conditions, which can be achieved by inducing S1R deletion or overexpression in specific cells *in vivo*.

Although oligodendrocytes (OLs) are one of the major glial cell populations in the CNS, the role of S1Rs in OL lineage cells has been less studied. Hayashi and Su demonstrated that the differentiation of CG-4 cells was inhibited after transfection with S1R siRNA (Hayashi and Su, 2004b). In the current study, we aim to investigate the biological functions of S1Rs in OL lineage cells by specifically ablating S1Rs in OPCs *in vivo*.

4.5 Oligodendrocytes in the CNS during development

In the CNS, myelination of neuronal axons is essential for the proper conduction of action potential and providing axonal trophic support. OLs in the CNS, as well as Schwann cells in the peripheral nervous system (PNS), are myelin-forming cells and are continuously generated through a process called oligodendrogenesis during development as well as in adulthood. The development of OLs is tightly regulated and involves three classical steps: the specification of OPCs, differentiation of OPCs into premyelinating OLs (preOL), and maturation of OLs into mature myelinating OLs (mOL). Specific markers for each stage of OL development are widely used to study the generation and myelination of OLs (Elbaz and Popko, 2019) (Figure 2).

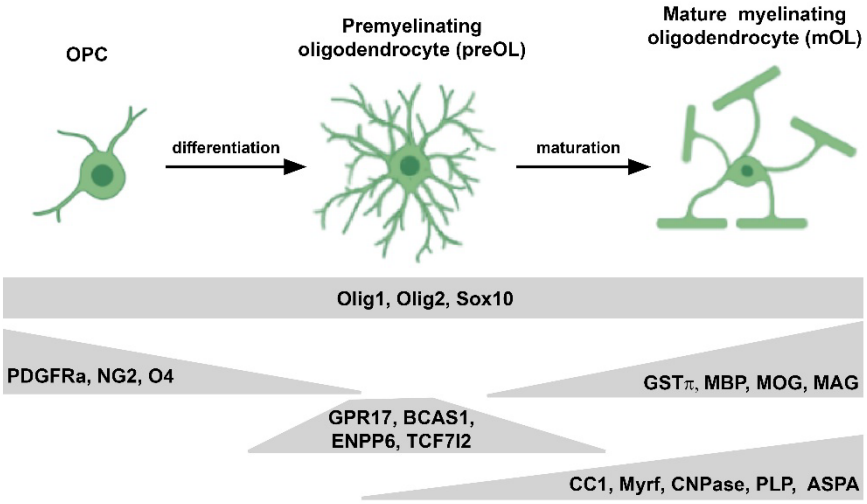

Figure 2. Schematic depiction of oligodendrocyte developmental stages. The diagram illustrates the different stages of oligodendrocyte (OL) development. There are three classical stages described: OPCs, premyelinating OL (preOL, immature), and mature myelinating OL (mOL). The bottom panel of the figure displays the markers associated with each stage of OL development.

4.5.1 Oligodendrocyte precursor cells: a reservoir of OLs

OPCs act as a pool for OLs generation and have been extensively studied in the CNS. In the forebrain, OPCs originate from neural stem cells (NSCs) in the neuroepithelial zone, and their generation occurs in three consecutive waves from ventral to dorsal regions (van Tilborg et al., 2018). The first wave of OPCs arise approximately at embryonic day 12.5

(E12.5), from the medial ganglionic eminence (MGE) and anterior entopeduncular area (AEP) of the ventral forebrain, and predominantly express a region-specific marker Nkx2.1. The second wave of OPCs emerges from the lateral and caudal ganglionic eminences (LGE) starting at E15.5 and is characterized by the transcription marker Gsh2. The third wave of OPCs arises from the dorsal cortical area after E17.5 until birth, and is associated with the expression of Emx1 (Kessaris et al., 2006; Richardson et al., 2006). It has been observed that OPCs generated in the first wave are almost completely replaced after birth. Therefore, OPCs that exit after postnatal time are derived from the medial and dorsal waves, identified by the expression of the cell surface protein platelet-derived growth factor receptor alpha subunit (PDGFRα) and proteoglycan (NG2). Once OPCs are generated, they proliferate and migrate to the peripheral regions. In the early postnatal period (~P2-P3), OPCs start to differentiate into OLs in the forebrain, but this happens earlier in the spinal cord (around E18).

In the adult brain, parenchymal OPCs serve as a persistent source of OL generation by maintaining specific densities, and retaining proliferative and differentiative capabilities (El Waly et al., 2014). These OPCs express the same markers as their developmental stages, including PDGFRα and NG2. They are commonly referred to as NG2 glia due to their characteristic expression of the NG2 proteoglycan (Nishiyama et al., 2009). NG2 glia represents the largest population of resident progenitor cells in the postnatal and adult brain. Extensive evidence supports their ability to generate OLs in the brain and spinal cord during development and in adult mice (Huang et al., 2014; Dimou and Gallo, 2015). To track the fate of OPCs, transgenic mice with NG2 promoter driving Cre-expression are widely used (Guo et al., 2021).

4.5.2 Premyelinating OLs: a checkpoint for OL maturation

Along the differentiation of OPCs into OLs, there is an intermediate stage known as premyelinating OLs (preOLs) or newly formed immature OLs. These cells are considered terminally differentiated but have not yet initiated myelination (Hughes and Stockton, 2021). RNA-sequencing studies further characterized these newly formed OLs (immature OLs) in the murine cortex (Zhang et al., 2014a; Marques et al., 2016). Correspondence of this stage, the morphology of OPCs transitions from a polygonal soma with bipolar processes to a multipolar morphology with radial processes. Several markers, such as G-protein receptor 17 (GPR17), breast carcinoma amplified sequence 1 (BCAS1), Ectonucleotide Pyrophosphatase/Phosphodiesterase 6 (ENPP6), and the transcription factor 7-like 2 (TCF7l2), are used to identify preOLs and newly formed OLs (Chen et al., 2009; Xiao et al., 2016; Fard et al., 2017; Guo and Wang, 2023).

The premyelinating stage of OL development is considered a critical checkpoint in the maturation process. It has been observed that a significant proportion (20-50%) of preOLs undergo apoptosis following differentiation during development (Barres and Raff, 1993; Hughes et al., 2018). This suggests that apoptosis plays a role in regulating oligodendrogenesis and may influence the overall process of OL maturation.

4.5.3 Mature myelinating oligodendrocytes (mOLs)

After the premyelinating stage, OLs further differentiate into mOLs, which are characterized by their ramified or T-shape-like branches. These cells highly express myelin-related proteins, including myelin basic protein (MBP), myelin-oligodendrocyte glycoprotein (MOG), myelin associated glycoprotein (MAG) as well as galactocerebroside (GalC). In addition, the myelin regulatory gene Myrf is also upregulated in mOLs, and its expression

is restricted to postmitotic lineage cells. It has been suggested that Myrf plays a key role in initiating myelination (Koenning et al., 2012; Bujalka et al., 2013; Hornig et al., 2013). The glutathione-S-transferase pi form (GSTπ) is a cytosolic enzyme expressed in both OLs and myelin (Tansey and Cammer, 1991). Both Myrf and GSTπ are used as markers for OLs.

During the myelination, the processes of OLs convert into the flat sheath that form the multilamellar myelin structure, which wrap around axons and isolates them. Myelination is a complex and well-coordinated process involving proper axon recognition, myelin synthesis and transport, as well as the wrapping and compaction of myelin sheaths.

4.6 The mechanisms regulating OL generation and myelination

OL maturation is a well-orchestrated and complex processes that ensures the proper OL differentiation at the expected time. Moreover, to reach the required area of myelination, the maintenance of OL number should also be taken. Several intrinsic and extracellular factors have been shown to be involved in this process such as transcription factors, ion channels, and the interaction of axons with other neighboring cells. Here are some of the key mechanisms involved in OL generation and myelination.

4.6.1 Transcription factors

Transcription factors are critical in regulating OL maturation. The Olig family, including Olig1 and Olig2, as well as the SoxE group genes, such as Sox8, Sox9, and Sox10, have been extensively studied for their involvement in OL development and myelination. Olig1 and Olig2 are bHLH transcription factors that are induced by Sonic hedgehog (Shh) signalling during development (Lu et al., 2000; Lu et al., 2002; Ligon et al., 2006). Olig1 has been shown to play roles in the development and maturation of OLs. Studies using different Olig1 null mice have shown a delay in OL differentiation in the brain, but the effect on myelination is still under debate (Lu et al., 2002; Xin et al., 2005). On the other hand, Olig2 is crucial for early OL development and is required for OL and motor neuron specification in the spinal cord (Takebayashi et al., 2002). In addition, the interplay between Olig1 and Olig2 is region- or stage-dependent, and their compensatory expression contributes to OL development. For instance, in the spinal cord of Olig1 null mice, myelination deficits were observed only in the early stage, with subsequent recovery due to the upregulation of Olig2 (Dai et al., 2015). Deletion of Olig2 in OPCs inhibited differentiation, while deletion in immature OLs enhanced maturation and accelerated myelination (Mei et al., 2013). SoxE group genes are involved in the development of OLs, Schwann cells and astrocytes: Sox9 is involved in OL specification; Sox8 and Sox10 have function on the terminal differentiation of OLs and induction of myelin formation (Kordes et al., 2005; Kiefer, 2007; Turnescu et al., 2018).

Another important transcription factor involved in OL myelination is Myrf. It acts as a transcriptional regulator and is required for OL myelination during development. Deletion of Myrf in mOLs led to severe myelin loss (Koenning et al., 2012; Bujalka et al., 2013). Studies have further shown that Myrf is actived by Sox10 and cooperatively drives the myelination process in OLs (Hornig et al., 2013; Aprato et al., 2020).

4.6.2 Calcium signalling in OL development

In OL development, calcium (Ca^{2+}) signalling contributes to OL differentiation and myelination (Yoo et al., 1999; Soliven, 2001). OPCs/NG2 glial cells express L-type voltage-gated calcium channels (VGCC), specifically Cav1.2 and Cav1.3 subtypes. The expression of these channels decreases as OPCs differentiate into OLs (Kirischuk et al., 1995). *In vitro* and *in vivo* investigations have elucidated the essential contributions of Cav1.2 and Cav1.3

in OL development and myelination (Cheli et al., 2016; Zhao et al., 2021). Using a BAC transgenic NG2-CreER mice, Cheli et al. showed in mice with Cav1.2 deletion in NG2 glia cells a reduction in the number of mOLs and an impairment in myelination (Cheli et al., 2016). However, a recent study from our group showed that a double ablation of Cav1.2 and Cav1.3 in NG2 glial cells (using NG2-CreERT2 knock-in mice) did not affect OL differentiation and myelination, but rather affected the proliferation of NG2 glia cells (Zhao et al., 2021). The different results obtained from various studies could be attributed to differences in the genetic models and recombination efficiency (Guo et al., 2021).

The ER represents an intracellular pool of Ca^{2+} in which release is driven by IP3Rs and ryanodine receptors (RyRs) (Haak et al., 2001; Li et al., 2018). Both these receptors play a role in mediating Ca^{2+} release from the ER in OPCs (Haak et al., 2001). Li et al. showed that the expression of RyR3 was decreased following OPC differentiation. Inhibition or downregulation of RyR3 inhibited OL differentiation, suggesting the involvement of RyR3-mediated Ca^{2+} signalling in the regulation of OL development (Li et al., 2018).

4.6.3 Regulation of the oligodendrocyte cytoskeleton

During OL development, OL lineage cells undergo a morphological change that are associated with the remodelling of cytoskeleton. After the terminal differentiation of OLs, their processes extend to contact with axons and then wrap the targeted axons. The main components of the cytoskeleton are microtubules (MTs) and microfilaments (MFs), which provide structural support and facilitate cellular processes (Lunn et al., 1997; Rumsby et al., 2003; Bauer et al., 2009).

MTs are composed of α- and β-tubulin heterodimers and form dense bundles in OL processes (Lunn et al., 1997). They are anchored to the microtubule organizing center (MTOC) near the nucleus and extend to the periphery of the OL. It has been proven that the link between MTs and MTOC is beneficial in OL differentiation (Song et al., 2001). Furthermore, Terada et al. observed a specific isoform of β-tubulin (βIV tubulin) which is not anchored to MTOC. Given the high expression of βIV tubulin in the PreOLs and mOLs, βIV tubulin may play a role in OL myelination (Terada et al., 2005). Moreover, MT proteins undergo a number of post-translational modifications associated with high stability of mOLs (Song et al., 2001).

MFs are associated with the ATP-binding protein actin, which exists in two states: globular monomers (G-actin) and filamentous polymers (F-actin). MFs are present at the tip and edge of rapidly forming processes in the OLs, indicating their role in the progress outgrowth (Bacon et al., 2007). The Rho family of GTPases, including RhoA, Rac1, and Cdc42, has been shown to regulate morphological changes in OLs by regulating actin polymerization. Wolf et al. showed that activation of RhoA inhibited the elongation of OL process (Wolf et al., 2001). However, the expression of activated Rac1 and Cdc42 led to highly branched and hyperextended processes in cultured OLs. The integrin-Fyn-Rho family GTPases pathway has been proposed to be involved in controlling OL morphological changes and myelination (Liang et al., 2004).

4.6.4 Neuronal regulation in OL development

Neurons actively regulate the extensive aspects of OL development, including the control of OL number, the timing of OL differentiation, and the selection of axons for myelination (Barres and Raff, 1993; Boiko and Winckler, 2006). Several molecules derived from neurons have been identified as regulators of OL development and myelination. OLs

receive signals and recognize target axons, form an axon-OL interaction domain, and then wrap them to form the myelinated segments.

During development, OLs are always overproduced and only OLs that enwrap the axons can survive. Therefore, the balance between proliferation and apoptosis is important. Several molecules derived from neurons are involved in the regulation of OL survival. For example, neuregulins (NRGs) are a family of polypeptide growth factors containing epidermal growth factor (EGF)-like domains that are related to the activation of the membrane associated ErbB2, ErbB3 and ErbB4 receptor tyrosine kinases. An *in vitro* study showed that NRGs promote OPC survival in developing optic nerve (Fernandez et al., 2000). Park et al showed that in ErbB2 KO mice, OLs failed to terminally differentiate and wrap axons, without altering OL cell death in the spinal cord (Park et al., 2001). In cultured Schwann cells, activation of ErbB2/ErbB3 receptor complex has been implicated in promoting OL survival through the PI3K/Akt/Bad pathway (Li et al., 2001).

It is known that axons with a diameter larger than 0.2 μm are myelinated, and axons with large caliber tend to be myelinated preferentially, which then increases the length of the myelin sheath (Friede, 1972; Hildebrand and Waxman, 1984; Bechler et al., 2015). For example, sympathetic postganglionic axons, which are usually unmyelinated, were myelinated when their caliber was increased induced by an increase in the diameter of peripheral target they innervate, suggesting that axon diameter is important for the regulation of myelination (Voyvodic, 1989). Many studies have demonstrated that neuregulin 1 type III (NRG1) which is expressed on large diameter axons plays a role in initiating myelination and determining myelin thickness in the PNS (in Schwann cell) (Michailov et al., 2004; Taveggia et al., 2005; Taveggia et al., 2008). However, in the CNS, there are regional differences in the promotion of myelination by NRG1, which is more pronounced in the forebrain (Taveggia et al., 2008). Furthermore, in Pten conditional KO mice, artificially increasing the caliber of parallel fiber (Pf) axons, which are normally unmyelinated, can trigger myelination through activation of PI3K–AKT1–mTOR pathway in cerebellar granule cells, further suggesting that axon caliber influences the initiation of myelination (Goebbels et al., 2017).

However, even with sufficient diameter, some axons are unmyelinated, suggesting that there are other mechanisms regulating axonal selection. Several *in vitro* and *in vivo* studies showed that axonal activity promotes OPC proliferation, OL generation, and myelination (Demerens et al., 1996; Stevens et al., 2002; Gibson et al., 2014). Blocking neuronal activity in the optic nerve has been shown to decrease OPC proliferation, indicating the dependence of OL development on axonal activity (Barres and Raff, 1993). In a zebrafish study, the deficit in neuronal activity resulted in the formation of OL membrane sheaths that did not extend, indicating that neuronal activity guides myelination. Also, shorter sheaths retract more frequently, which indicates that the axon selection for myelination is biased by neuronal activity (Hines et al., 2015).

Several studies have shown that axonal derived cell-adhesion molecules (including permissive and repulsive cues) are involved in the regulation of myelination. Permissive regulators include Ncad (Schnädelbach et al., 2001), L1CAM (Laursen et al., 2009), Necl1 (Park et al., 2008), Nrg1-III, and EphA/B (Linneberg et al., 2015). Repulsive regulators include LINGO-1 (Lee et al., 2007; Jepson et al., 2012), Jam2 (Redmond et al., 2016), Jagged1 (Wang et al., 1998; Zhang et al., 2009), PSA-NCAM (The polysialic acid (PSA)

modification of neural cell adhesion molecule) (Jakovcevski et al., 2007), ephrin-A/B (Pasquale, 2008) and Gal-4 (Díez-Revuelta et al., 2017; Almeida, 2018).

The specific mechanisms by which OLs select axons for myelination and initiate myelination are still largely unknown. For example, the interaction between synaptic of unmyelinated axons and OPCs may regulate the timing and coordination of myelination (e.g., the release of glutamate and GABA/glutamate).

4.6.5 The roles of astrocytes and microglia in regulating OL development

Some extracellular factors released from astrocytes and microglia also contribute to OL differentiation and myelination.

Astrocytes release growth factors that contribute to OL maturation and myelination. Studies using BDNF KO mice have shown that myelination requires brain-derived neurotrophic factor (BDNF) released by astrocytes (Cellerino et al., 1997; Djalali et al., 2005). The platelet-derived growth factor (PDGF) produced by astrocytes promotes OPC survival and proliferation (Gard et al., 1995; McKinnon et al., 2005). Produced by astrocytes and neurons, the ciliary neurotrophic factor (CNTF) promotes OPC differentiation by regulating OL survival (Stankoff et al., 2002; Nash et al., 2011). Furthermore, astrocytes have also been suggested to provide lactate to OLs, which is necessary for lipid synthesis and myelin production (Rinholm et al., 2011).

In addition, some evidence suggests that growth factors derived from microglia play a role in the maturation of OLs. Insulin-like growth factor (IGF) signalling, including IGF-1 and IGF-2, derived from microglia, is involved in OL maturation and myelination. IGF-1 KO mice showed reduced expression of myelin proteins (MBP, PLP) and increased expression of IGF-2 during development, suggesting a role of IGF-1 in the regulation of myelination (Ye et al., 2002). IGF-2 has been shown to promote OL survival in CG4 cell line (Nicholas et al., 2002). Moreover, activated microglia release cytokines and chemokines, such as transforming growth factor-beta (TGF-β), interleukin-6 (IL-6), interferon-gamma (IFN-γ), tumor necrosis factor-alpha (TNF-α), interleukin-1 beta (IL-1β), and chemokine (C-X-C motif) ligand 1 (CXCL-1), which play a role in regulating OL maturation and myelination (Tsai et al., 2002; Chew et al., 2005; Shigemoto-Mogami et al., 2014).

Collectively, these mechanisms work together to ensure the proper generation, differentiation, and myelination of OLs in the CNS. Dysregulation of these processes can lead to developmental abnormalities or impaired myelination, contributing to various neurological disorders.

4.7 Involvement of S1Rs in the regulation of OL development

At the cellular level, S1Rs have been found to co-localize with cholesterol and form cholesterol-rich microdomain in the ER membrane, which are involved in protein recruiting for secretion and signalling (Hayashi and Su, 2010; Zhemkov et al., 2021).

Pharmacological experiments have provided further insights into the effects of S1R activation on OL maturation. Treatment with S1R agonists or overexpression of S1Rs enhanced differentiation of CG-4 cells, while inhibition of S1Rs using siRNA inhibited differentiation (Hayashi and Su, 2004a). Lisak et al. showed that activation of S1Rs by using their agonists (ANAVEX2-73 or dextromethorphan) promotes the proliferation of OPCs without altering OL maturation *in vitro* (Lisak et al., 2020). Additionally, in a stroke model of

diabetic patients, activation of S1Rs using the agonist PRE-084 has been shown to promote oligodendrogenesis (Song et al., 2023).

While these findings suggest the potential role of S1Rs in OL development and maturation, further research is required to understand the precise mechanisms and effects of S1Rs in OLs *in vivo*, as well as their impact on different stages of OL development. Further studies using animal models and genetic approaches will help elucidate the biological functions of S1Rs in OLs and their potential therapeutic implications for OL-related disorders.

5 Aims of the Study

S1Rs have been discovered over forty years ago. However, due to the lack of reliable detection tools, their expression pattern as well as their biological functions in specific CNS cell types, particularly in OL lineage cells, still remain elusive. The current study aims to provide a deeper understanding of these aspects as follows:

Aim 1: Characterization of S1R expression pattern in CNS cells *in vivo*.
Previous studies indicate that S1Rs are widely expressed in the CNS. However, the immunohistochemical results of individual studies showed strong variability. Firstly, I will validate the specificity of different commercial antibodies in S1R KO mice by immunoblot. Moreover, I will establish an antigen retrieval method for immunohistochemistry of S1R. To detect cellular expression pattern of S1Rs in brain cells, I will perform S1R immunostaining with neuron and glial cell-specific markers on both brain and spinal cord tissue.

Aim 2: To achieve cell-type specific S1Rs deletion *in vivo.*
To achieve cell-type specific deletion of the *sigmar1* gene, we generated a floxed S1R mouse ($S1R^{fl/fl}$) in which the exon 1-3 of the *sigmar1* gene are flanked by loxP sites. To delete S1Rs in targeted cell types using this mouse line, we will crossbreed $S1R^{fl/fl}$ mice with different Cre mouse lines (Nex-Cre mice for pyramidal neurons, CX3CR1-CreERT2 mice for microglia, Glast-CreERT2 mice for astrocytes, and NG2-glia-CreERT2 mice for OPCs). I will detect the deletion of S1Rs in different cell types by immunohistochemistry.

Aim 3: To investigate the role of S1Rs in regulating OL development *in vivo*.
Some pharmacological studies suggested that S1Rs may play a role in regulating OL maturation. In this study, we will crossbreed $S1R^{fl/fl}$ mice with NG2-CreERT2 mice to generate S1R conditional knockout mice in NG2 glia cells (cKO). To map the fate of OL development, we will take advantage of th Cre dependent reporter-expressing mice Rosa26-tdTomato. Inducing Cre recombination by tamoxifen injection at postnatal day 7 (P7) and P8, we will detect the potential OL lineage cell changes in cKO mice during development by immunohistochemistry using specific-stage markers of OL combined with tdT expression. We will detect myelin protein expression by immunohistochemistry and immunoblot.

6 Materials and Methods

6.1 Materials

6.1.1 Consumables

The following consumables were used in this study: Eppendorf reaction tubes (0.5 ml, 1.5 ml, 2ml, and 5ml), Eppendorf (Hamburg); Falcontubes, Greiner Bio-One (Frickenhausen); Pipette tips, Sarstedt (Nümbrecht); glass pipettes, VWR International (Darmstadt); 48 well culture plates, Sarstedt (Nümbrecht); object slides, Karl Hecht Glaswarenfabrik (Sondheim); cover slips, Menzel-Gläser (Braunschweig); 96-well-PCR-reaction-tubes, 4titude (Berlin); RT-PCR-96-well-plates, Axon (Kaiserslautern).

6.1.2 Kits

The kits used in this study are listed in the table.

Kit Name	Application	Company	Cat no.
NucleoSpin RNA Plus XS	RNA extraction	Macherey-Nagel	40990.50
Omniscript kit		QIA-GEN	205113
Western blotting detection kit	Western Blot	Advansta	K-12042-D20
Pierce BCA Protein Assay Kit		Thermo Scientific	23225
Adult Brain Dissociation Kit	Magnetic-associated cell sorting of glial cells	Miltenyi Biotec	130-107-677
Anti-ACSA-2 MicroBead Kit		Miltenyi Biotec	130-097-678
Anti-CD11b MicroBead Kit		Miltenyi Biotec	130-093-634
Anti-NG2 MicroBead Kit		Miltenyi Biotec	130-097-170
Anti-O4 MicroBead Kit		Miltenyi Biotec	130-096-670
Anti-CD140 MicroBead Kit		Miltenyi Biotec	130-101-502

Table 1. List of kits.

6.1.3 Devices

Device	Producer
Centrifuges-Theromo	Eppendorf
Centrifuges (RT)	neoLab
Shaker DRS-12	neoLab
Precellys 24 (Homogenizer)	Peqlab Biotechnologie GmbH
Preparations- and perfusion instruments	F.S.T., Pharmacia
peQ ThermoCyclers	Peqlab Biotechnologie GMBH
Gel chambers and supplies for agarose gels	Workshop of the CIPMM
Vibratome VT1000S	Leica Biosystems

CFX96 Real-Time PCR Detection System	BioRad
Infinite PRO 200 microplate reader	Tecan
Electrophoresis power supply (PCR)	Consort
Western Running Electrophoresis power supply	BioZym
ChemiDoc Imaging System	BioRad
AxioScan.Z1	Zeiss
Confocal microscope LSM 800	Zeiss

Table 2. List of devices.

6.1.4 Buffers

Some buffers that are routinely used (e.g., PBS, PFA and TAE buffer) in the experiment are not listed in detail here.

Homogenization sucrose buffer

Sucrose	320 mM
Tris (pH 7.4)	10 mM
$NaHCO_3$	1 mM
$MgCl_2$	1 mM

1x protease inhibitor and phosphorylation inhibitor were added freshly before use.

10x transfer buffer for western blotting

Glycine	38.63 mM
Tris	47.87 mM
SDS	1.28 mM

1x transfer buffer was used with 20 (v/v) Methanol. Keep at 4 °C before use.

10x Tris-base buffer (PH 7.4, 1L)

Tris-base	24.2 g
Nacl	80 g

Blotting buffer in PBS for immunohistochemistry (regular protocol)

Horse Serum	5% (v/v)
Triton x-100	0.5% (v/v)

Blotting buffer in PBS for immunohistochemistry (AR^{SDS} and $AR^{SDS\text{-}EtOH}$ protocol)

Fish Gelatin	1x (v/v)
Triton x-100	0.5% (v/v)

Karlsson-Schultz Fixative Solution in phosphate buffer (PH 7.4, 200ml)

Formaldehyde	4% (v/v)
Glutaraldehyde	0.2% (v/v)
NaCl	0.5% (v/v)
NaH_2PO_4 H_2O	0.013 mM
Na_2HPO_4 $2H_2O$	0.087 mM

The fixing solution was filtered with a Nalgene unit before use.

Toluidine Blue Staining Solution

Toluidine blue	1% (v/v)
Sodium tetraborate	2% (v/v)

Dissolve the sodium tetraborate powder in ddH_2O, then add toluidine blue powder. Filter the solution before use.

6.1.5 Primers

6.1.5.1 Primers for genotyping PCR

Gene	Sequence (5'-3')	Product size (bp)
Sigma1r flox forward	AAGCAGAAGAGCAGCTAGTGCTG	KI 440
Sigma1r flox reverse	TGAGACAGGGTTTCTCTGTATAGCC	WT 335
Oprs1 KO forward	CAACATGGATACCCTTGAGAGATG	
Oprs1 KO reverse	GCTGGCATGGAACTTGCATAG	KO 736
Oprs1 WT forward	CACTAGCCGACACTTTCTTCAGC	WT 524
Oprs1 WT reverse	GAATGAGGCATCAGAGTGAGGTAG	
Nex-Cre forward	GAGTCCTGGAATCAGTCTTTTTC	KI 520
Nex-Cre reverse	CCGCATAACCAGTGAAACAG	WT 770
Nex-Cre reverse	AGAATGTGGAGTAGGGTGAC	
Cx3cr1-CreERT2 forward	TCAGTGTTTTCTCCCGCTTGC	KI 825
Cx3cr1-CreERT2 reverse	GTAGTGGTTGTCGGGCAGCAG	WT 407
Cx3cr1-CreERT2 reverse	CAGTGATGCTCTTGGGCTTCC	
Glast-CreERT2 forward	GAGGCACTTGGCTAGGCTCTGAGGA	KI 400
Glast-CreERT2-WT reverse	GAGGAGATCCTGACCGATCAGTTGG	WT 700
Glast-CreERT2 (KI)	GGTGTACGGTCAGTAAATTGGACAT	
NG2-CreERT2 forward	GGCAAACCCAGAGCCCTGCC	KI 829
NG2-CreERT2 WT reverse	GCTGGAGCTGACAGCGGGTG	WT 557
NG2-CreERT2 KI reverse	GCCCGGACCGACGATGAAGC	
Rosa26-tdTomato KI forward	GGCATTAAAGCAGCGTATCC	KI 196
Rosa26-tdTomato KI reverse	CTGTTCCTGTACGGCATGG	

Table 3. List of primer sequencing.

6.1.5.2 Primers used for real-time qPCR

Gene	Forward primer (5'-3')	Reverse primer (5'-3')
sigmar1	CTGGGCACTCAAAACTTCGTC	CTCCACGATCAGCCGAGAGA
gfap	GCCACCAGTAACATGCAAGA	CAGCGTCTGTGAGGTCTG
Itgam	CAATAGCCAGCCTCAGTGC	GAGCCCAGGGGAGAAGTG
Pdgfra	ACCTCCCACCAGGTCTTTCT	CTTCACTCTCCCCAACGCAT
Actb	CTTCCTCCCTGGAGAAGAGC	ATGCCACAGGATTCCATACC

Table 4. List of primers for qPCR.

6.1.6 Antibodies

6.1.6.1 Primary antibodies used for immunoblotting and immunohistochemistry

Antigen	Host Species	Antibody type	Source	Catalog no.	Dilution

SIGMAR1 (D4J2E)	Rabbit	monoclonal	Cell Signaling	#61994	WB: 1:1000
					IHC: 1:500
SIGMAR1(D7L1M)	Rabbit	monoclonal	Cell Signaling	#74807	WB: 1:1000
					IHC: 1:500
Anti-Sigma Receptor (B-5)	Mouse	monoclonal	Santa Cruz	sc-137075	WB: 1:500
					IHC: 1:500
Sigma-1 Receptor	Rabbit	polyclonal	Invitrogen	#42-3300	WB: 1:500
					IHC: 1:500
Sigma1-receptor C-terminal	Rabbit	polyclonal	Abcam	Ab53852	WB: 1:500
					IHC: 1:500
SIGMAR1	Rabbit	polyclonal	Proteintech	15168-1-AP	WB: 1:500
					IHC: 1:500
CD11b	Rabbit	monoclonal	Abcam	Ab133357	WB: 1:1000
					IHC: 1:500
GFAP	Rabbit	Polyclonal	Dako	Z 0334	WB: 1:1000
GAPDH	Mouse	monoclonal	Sigma	G8795	WB: 1:5000
					IHC: 1:500
HA-tag	Mouse	monoclonal	Covance	MMS-101P	IP: 1:100
α-Tubulin	Mouse	monoclonal	Sigma-Aldrich	T6074	WB: 1:8000
					IHC: 1:500
GS	Mouse	monoclonal	BD	610518	IHC: 1:500
GFAP	Goat	polyclonal	Abcam	Ab53554	IHC: 1:500
Iba1	Goat	polyclonal	Abcam	ab5076	IHC: 1:500
S100 beta SH-B1	Mouse	monoclonal	Abcam	ab66028	IHC: 1:500
NeuN Clone A60	Mouse	monoclonal	Millipore	MAB377	IHC: 1:500
Calbindin-D28K	Mouse	monoclonal	Sigma	C9848	IHC: 1:500
PDGFRα (Pα)	Goat	polyclonal	R&D Systems	AF1042	IHC: 1:500
APC (Ab-7) clone CC-1	Mouse	monoclonal	Calbiochem	OP80	IHC: 1:200
a-Actinin (Sarcomeric) clone EA-53	Mouse	monoclonal	Sigma	A7811	IHC: 1:500
SERCa2 ATPase	Mouse	monoclonal	Sigma	S1439	IHC: 1:500
MBP Myelin Basic Protein (MBP)	Mouse	monoclonal	Biolegend	SMI99	IHC: 1:500
					WB: 1:4000
MOG (8-18C5)	Mouse	monoclonal	homemade		WB: 1:2000
Myrf	Rabbit	polycolonal	homemade		IHC: 1:500
GSTπ	Mouse	monoclonal	BD Pharmingen	610718	IHC: 1:500
GPR17	Rabbit	polyclonal	Cayman	10136	IHC: 1:400
					WB: 1:500

NaBC1(BCAS1)	Mouse	monoclonal	Santa Cruz	sc-136342	IHC: 1:1000

Table 5. List of primary antibodies.

6.1.6.2 Secondary antibodies

Antibody	Source	Catalog no.	Dilution
goat anti-rabbit IgG HRP	Dianova	111-035-045	WB: 1: 5000
goat anti-mouse IgG HRP	Sigma	A9044	WB: 1: 10000
Alexa Fluor 488 donkey anti-mouse	Invitrogen	A21202	IHC: 1: 1000
Alexa Fluor 488 donkey anti-goat	Invitrogen	A11055	IHC: 1: 1000
Alexa Fluor 546 donkey anti-mouse	Invitrogen	A10036	IHC: 1: 1000
Alexa Fluor 647 donkey anti-rabbit	Invitrogen	A31573	IHC: 1: 1000
DAPI (stain for nuclei)	Biochimica	A10010010	IHC: 1: 1000

Table 6. List of secondary antibodies.

6.1.7 Reagents and chemical components

Name	Company	Cat no.
RIPA buffer	ThermoFischer	89900
Fish Gelatin Blocking Agent (10x)	BioTium	22010
Triton X-100	AppliChem	A1388
SDS powder	Roth	CN30.1
ß-Mecapthoethanol	Sigma-Alrich	M6250
Phosphorylation Inhibitor Cocktail Tablets	Roch	04906 845 001
cOmplete™ Proteasehemmer-Cocktail	Roche	11697498001
Tween-20	AppliChem	A7564.0500
RNasin	Promega	N2511
Protein G-Dynabeads	Thermo Fisher Scientific	10003D
Tris-base	Sigma-Alrich	T1503
Glycine	AnalaR NORMAPUR	10119CU
Sucrose	Roth	4621.1
NaCl	Grüsing	12155
di-sodium hydrogen phosphate dihydrate (Na2HPO4 7H2O)	Roth	X987.2
Sodium dihydrogen phosphate dihydrate (NaH2PO4 2H2O)	Grüsing	13472-35-0
NaHCO3	Grüsing	144-55-8
Methanol	Fisher Chemical	701229
Nonidet P40 Substitude (NP-40)	SIGMA	74385
2x SDS sample buffer (for SDS-PAGE)	SERVA	42526

10x SDS running buffer (for SDS-PAGE)	SERVA	42556
Western blot stripping buffers	ThermoFischer	21059
5x HotStart Taq EvaGreen qPCR Mix	Axon	27490
Tamoxifen powder	Carbobution	CC99648
Glutaraldehyde	Sigma-Alrich	8143931000
Paraformaldehyde	Sigma-Alrich	441244
Miglyol	Caesar & Loretz	3274
Ketamin (100 mg / ml)	bela-pharm	E1670041
Xylazinhydrochlorid (20 mg / ml)	Elanco GmbH	87226794

Table 7. List of reagents and chemical components.

6.1.8 Animals

6.1.8.1 Ethics Statement

All animal experiments were ethically conducted at the animal facility of CIPMM, University of Saarland, adhering to strict compliance with European and German guidelines for the welfare of experimental animals. The animal experiments were approved by the Saarland state's 'Landesamt für Gesundheit und Verbraucherschutz' in Saarbrücken/Germany. The animal licenses used in this project are 34/2016, 36/2016, 03/2021 and 08/2021.

6.1.8.2 Animal strains

All mice used in this study were housed at the animal facility of the CIPMM in a temperature-(22°C ± 2°C) and humidity-controlled facility with a 12-h light/dark cycle. Each mouse was assigned an animal ID used ear punches, which were recorded in an animal administrative system (PyRAT, Python-based Relational Animal Tracking, Scionics Computer Innovation, Dresden).

Sigmar1 global knockout (S1R KO) mice were generated by GemPharmatech (Nanjing, China) by deleting the entire encoding region (~10359bp) of *Sigmar1*.

TgN (Thy1-HcRed) (Hirrlinger et al., 2005) mice in which excitatory neurons express HcRed fluorescent proteins under the Thy1 promoter, allowing for the identification of S1R expression in excitatory neurons.

RiboTag mice (Rlp22HA) (Sanz et al., 2009) express HA (human influenza hemagglutinin)-tagged ribosomes, which can be used for immunoprecipitation and collection of translated mRNA in specific glial cells. They were crossbred with different glia-specific Cre-driver mice, including GLAST-CreERT2 mice for astrocytes (Mori et al., 2006), CX3CR1-CreERT2 mice for microglia (Yona et al., 2013), and NG2-CreERT2 mice for OPCs (Huang et al., 2014) (n = 3 mice per mouse line).

The *sigmar1* flox ($S1R^{fl/fl}$) mouse line was generated using CRISPR/Cas9 technology through the "Dalmatian Mouse Action" of GemPharmatech (Nanjing, China). The *sigmar1* gene (Oprs1) was modified using single guide RNA (sgRNA) and a donor vector containing exons 1-3 of Sigmar1 flanked by two loxP sites. Cas9, sgRNA and the donor vector were microinjected into the fertilized eggs of C57BL/6J mice. sgRNA directed Cas9 endonuclease cleavage at about 6 kb upstream of exon1 and downstream of 3'UTR and create a double strand break (DSB).

For antibody testing, 4 to 8 week-old mice of both sexes were used. For S1R deletion testing, 8 to 10 week-old adult mice aged were used. For the OL developmental study,

postnatal pups at P14, P21, and P30 were used. The transgenic reporter mouse line Rosa26tdTomato was used for the fate mapping experiments.

The transgenic mouse lines used in this study are listed in Table 8.

Abbrevation	Mouse line
S1R KO	*Sigmar1* global knockout
$S1R^{fl/fl}$	*Sigmar1* flox
NEX	NEX-Cre
Thy1	TgN (Thy1-HcRed)
RiboTag	Rlp22HA
GLAC	GLAST-CreERT2
NGCE	NG2-CreERT2
CXCT	CX3CR1-CreERT2
Rosa26-tdTomato	TgH (Rosa26-CAG-flSTOPfl-tdTomato)

Table 8. List of transgenic mouse lines.

6.2 Methods

6.2.1 Genotyping PCR

Genotyping PCR was performed following the regular protocol established in our laboratory. The primer sequences used for genotyping PCR are listed in Table 3.

6.2.2 Tamoxifen injection

Tamoxifen powder (cat. no.: CC99648, Carbobution) was dissolved in Miglyol (cat. no.: 3274, Caesar & Loretz, Hilden) at a concentration of 10 mg/ml. Depending on the specific experimental requirements, mice were intraperitoneally injected with tamoxifen at a dose of 100 mg/kg bodyweight. The injection was administered either for five consecutive days at the age of 4 weeks or two days on P7 and P8 in pups.

6.2.3 Magnetic-associated cell sorting (MACS) of glial cells

MACS was performed according to the manufacturer's instruction (Miltenyi Biotec) with some modifications as previously described (Fang et al., 2022). Briefly, 4-week-old mice were perfused with cold Hank's balanced salt solution without Ca^{2+} and Mg^{2+} (HBSS, cat. no.: H6648, Gibco) and cortices were dissected in ice-cold HBSS. After debris removal (cat. no.: 130–107-677, Miltenyi Biotec), cells were resuspended in 1 ml of re-expression medium containing NeuroBrew-21 (1:50 in MACS neuro Medium) (cat. no.: 130–093-566 and 130–093-570, Miltenyi Biotec) and 200 mM L-glutamine (1:100, cat. no.: G7513, Sigma-Aldrich), and incubated at 37°C for 30 min.

For OPC sorting, cells were incubated with Fc-receptor blocker (provided with the CD140 microbeads kit) for 10 min at 4°C, followed by a 15 min incubation with a 10 µl mixture of microbeads containing antibodies against CD140 (cat. no.: 130–101-502, Miltenyi Biotec), NG2 (cat. no.: 130–097-170, Miltenyi Biotec) and O4 (cat. no.: 130–096-670, Miltenyi Biotec) in a 1:1:1 ratio at 4°C.

For sorting of astrocytes, microbeads containing antibodies directed against ACSA-2 (cat. no.: 130–097-678, Miltenyi Biotec) were used.

For microglia sorting, microbeads containing antibodies directed against CD11b (cat. no.: 130–093-634, Miltenyi Biotec) were used.

6.2.4 Ribosome immunoprecipitation (IP)

After the mice were perfused with ice-cold HBSS, cortical samples were carefully dissected from the brain and immediately stored at −80°C until further use. Tissues were subsequently homogenized in ice-cold lysis buffer (comprising 50 mM Tris, pH 7.4, 100 mM KCl, 12 mM MgCl2, 1% NP-40, 1 mM DTT, 1x protease inhibitor, 200 units/ml RNasin (Promega) and 0.1 mg/ml cycloheximide (Sigma-Aldrich) in RNase-free deionized H_2O) 10% w/v using a homogenizer (Precellys 24, PeQlab). Subsequently, the homogenates were centrifuged at 10,000 g at 4°C for 10 min to remove cell debris. The supernatants were then collected, and a 50 µl aliquot was removed for input analysis. To capture the protein of interest, Anti-HA antibody (diluted 1:100, cat. no.: # MMS-101P, Covance) was added to the supernatant, which was then slowly rotated at 4°C. Protein G-Dynabeads (Thermo Fisher Scientific) were pre-treated with lysis buffer through three washes for equilibration. Following a 4 h incubation with the HA-tag Ab, 100 µl of pre-equilibrated beads were added to each sample, and the mixture was further incubated overnight at 4°C. After 10-12 h, the samples were washed with high-salt buffer (composed of 50 mM Tris, 300 mM KCl, 12 mM MgCl2, 1% NP-40, 1 mM DTT, 1x protease inhibitor, 100 units/ml RNasin and 0.1 mg/ml cycloheximide in RNase-free deionized H_2O) three times for 5 min at 4°C. At the end of the washing, the beads were magnetized and 150 µl of RA1 lysis buffer from NucleoSpin RNA Plus XS Kit (cat. no.: 40990.50, Macherey-Nagel) was added to the beads. Subsequently, RNA extraction was performed following the manufacturer's instructions (Macherey-Nagel).

6.2.5 Quantitative real time PCR (qPCR)

RNA concentration was determined using NanoDrop from the immunoprecipitation (IP) and input RNA samples. 100 µg of RNA was used to synthesize first-strand complementary DNA (cDNA) using Omniscript kit (cat. no.: 205113, QIA-GEN). qPCR was performed using EvaGreen (cat. no.: 27490, Axon) in a CFX96 Real-Time System (BioRad). The standard two-step program was used: 94 °C for 10 min, followed by 40 cycles at 94 °C for 15 sec, and 60 °C for 1 min. The expression levels of *sigmar1*, *gfap*, *Itgam*, and *Pdgfra* were measured. Primer sequences are listed in Table 4. The relative expression of the targeted genes was determined using the ΔΔCt method with normalization to *Actb* expression.

6.2.6 Western Blot analysis

Protein extraction was performed using either sucrose buffer or RIPA lysis buffer (cat. no.: 89900, Thermo Scientific), both supplemented with 1x protease inhibitor cocktail (cat. no.: 05892970001, Roche). Protein concentration was determined using the Bicinchoninic Acid (BCA) assay kit (Thermo Fisher Scientific). After adding 1x protein loading buffer (cat. no.: 42526.01, SERVA) containing 5% ß-Mercaptoethanol (M6250, Sigma-Aldrich), protein samples were denatured at 95°C for 5 min. Equal amounts of lysates (10-30 µg) from each mouse were separated by either 10% or 4-20% gradient SDS-polyacrylamide gel electrophoresis (PAGE, cat. no.: 43289.01, SERVA) and transferred onto nitrocellulose (NC) membranes (cat. no.: QP0907015, neoLab). Homogeneous protein-transfer onto NC membranes was confirmed by Ponceau S staining. After blocking with 5% non-fat milk powder (cat. no.: A0830,0500, PanReac AppliChem,) in 1x PBS for 1 h at room temperature (RT), the NC membranes were incubated with primary antibodies at 4°C overnight (Table 5) in TBST solution (Tris-base buffer with 0.1% Tween-20). The following day, membranes were washed three times with TBST and incubated with corresponding horseradish peroxidase (HRP) conjugated secondary antibodies (Table 6) in TBST for 1 h at RT. For detecting different proteins on the same NC membrane, the previous antibodies were

stripped off using a stripping buffer for 20 min, followed by incubation with other primary antibodies.

For MACS-purified cells, 40 µl RIPA lysis buffer (cat. no.: 89900, Thermo Scientific) and an equal volume of 1x loading buffer with 5% ß-Mercaptoethanol were added per sample. After denaturation for 5 min at 95°C, 10 µl of each protein samples were separated by SDS-PAGE and subjected to western blot analysis as described above. All primary and secondary antibodies are listed in Table 5 and Table 6, respectively.

Immunoblots were developed using enhanced chemiluminescence (ECL) reagent (cat. no.: 541015, Biozym) and imaged using a ChemiDoc Imaging System (BioRad). The immunoblot intensity was quantified with ImageJ software (ImageJ 1.53q, NIH, USA).

6.2.7 Brain tissue preparation

After anesthesia with 1 mg/kg ketamine and 0.5 mg/kg xylazine (i.p.), mice were transcardially perfused with 20 ml of ice-cold PBS. For antibody testing, the dorsal region of the cortex was dissected from coronal brain slices (1 mm). Segments from the cervical spinal cord segment were collected. For functional studies involving S1Rs, the entire cortex and the corpus callosum from rostral to caudal coronal slices were collected. Additionally, the cervical spinal cord segment was dissected. All specimens were stored at -80°C until further analysis.

6.2.8 Vibratome sections preparation

After anesthesia with 1 mg/kg ketamine and 0.5 mg/kg xylazine (i.p.), mice were transcardially perfused with 5 ml PBS and followed with 15 ml 4% PFA. Dissected tissues were post-fixed in 4% PFA at 4℃ overnight. Then, coronal brain sections or transverse spinal sections were collected by cutting with a vibratome (VT1000S, Leica).

6.2.9 Immunohistochemistry

Regular free-floating immunostaining was performed as previously described (Huang et al., 2020). Additionally, two new protocols with antigen retrieval (AR) were established for S1R staining using antibody #61994 (Fig. 2A):

AR^{SDS} protocol for immunostaining of S1Rs in the brain: brain slices were pre-treated with 1% SDS (cat. no.: CN30.1, Roth) in 1x PBS for 10 min at RT to facilitate antigen retrieval (Brown et al., 1996). After three washes with 1x PBS, blocking buffer (1x Fish Gelatin Blocking Agent (cat. no.: 22010, BioTium), 0.5% Triton x-100 in PBS) was added to the slices and incubated for 40 min at RT to reduce background signal. All primary antibodies were diluted in the blocking buffer.

$AR^{EtOH\text{-}SDS}$ protocol for S1R immunostaining in the spinal cord: spinal slices were incubated with 100% ethanol (EtOH) at 4°C overnight with gentle shaking to remove lipids. After washing with 1x PBS, 1% SDS pre-treatment was performed as described in the AR^{SDS} protocol above.

For co-immunostaining of S1R with the ER marker SERCA2, blocking buffer containing 0.5% NP-40 (instead of Triton X-100) in PBS was used for SERCA2 staining prior to S1R staining. After incubation with the secondary antibody against the SERCA2 antibody, slices were fixed with 2% PFA for 30 min, followed by immunostaining of S1R using AR^{SDS} protocol.

For functional studies, different combinations of antibodies specific to different stages of OL development were used with the regular immunohistochemistry (IHC) protocol.

Brain and spinal cord sections were incubated at 4°C for two nights with primary antibodies at appropriate dilutions as shown in Table 5. After washing with 1x PBS, sections were incubated with the corresponding secondary antibodies (Table 6) for 2 hours at RT. DAPI was used for nuclear staining. Following three washes with 1x PBS, the slices were mounted with Immu-Mount (cat. no.: 9990402, Thermo).

6.2.10 Semithin sections preparation and Toluidine blue staining

After anesthesia with 1 mg/kg ketamine and 0.5 mg/kg xylazine (i.p.), mice were transcardially perfused with the fixative solution containing 0.2% Glutaraldehyde and 4% PFA in phosphate buffer for 30 mins. Following perfusion, the cervical spinal cords were collected and kept overnight at 4°C in the same fixative solution. All fixed tissues were subsequently stored in 1% formaldehyde in 0.1M phosphate buffer at 4°C until use. Coronal semithin sections with a thickness of 0.5 µm were prepared using a Leica ultramicrotome and a diamond knife and mounted onto glass slides. The mounted sections were then stained with 1% toluidine blue solution.

6.2.11 Image acquisition and quantification

Images were acquired using two microscopy systems: the epifluorescence microscope system AxioScan.Z1 (Zeiss, Oberkochen, Germany) equipped with a Plan-Apochromat 20x/0.8 M27 objective, and the Zeiss confocal microscope system LSM 880 with Plan-Apochromat 40x/1.3 Oil DIC UV-IR M27 objective and 63x/1.4 Oil DIC UV-IR M27 objective (Zeiss, Oberkochen, Germany).

For each immunostaining, two randomly selected coronal brain sections per mouse were collected at the hippocampus level. Epifluorescence AxionScan images were used for quantification of different immunostaining using ZEN 3.1 (blue edition) software. For the deletion of S1Rs in different glial cells, non-overlapping confocal image stacks were arbitrarily captured from either three areas of the somatosensory cortex or two different areas from corpus callosum.

To quantify S1R expression levels in individual neurons and glial cells, non-overlapping confocal image stacks were arbitrarily taken from deep cortical layers (L5 and 6) from two slices per mouse (n=3 mice) with consistent imaging settings (laser power: 2%, gain: 0.9). Cell counting and mean fluorescence intensity were performed using ZEN 3.0 SR (black edition) software (Carl Zeiss, 16.0.2.306), and blinding was not performed.

Four to five randomly selected transversal sections from the cervical spinal cord were collected per mouse. Epifluorescence AxionScan images of the spinal cord were captured and analysed using ZEN 3.1 (blue edition).

To study MBP immunoreactivity, two brain slices per mouse were used. Confocal stack images from one region of interest (ROI) in the cortex (~layer 2-4) and the middle region of the corpus callosum were captured with the same settings. The threshold function of ImageJ was used for data analysis. The stack images of the cortex were converted to maximum intensity projections, and the area occupied by MBP in the analysed region was measured. A single layer of stack image from the corpus callosum was used for data analysis.

To study the structure of myelin, three spinal cord semithin sections per mouse were used. Light microscope images from two ROIs in the ventral white matter were captured with a 63x objective. The myelin thickness and axon diameter were measured using ZEN 3.1 (blue edition).

6.2.12 Statistical analysis

Data were analysed using GraphPad Prism 9.3.1 software (GraphPad, San Diego, CA). All data points were included in the analysis and were given as mean ± SEM, with n indicating the number of mice. The normality of the data was assessed using the Shapiro–Wilk test. Two-tailed Student's t-test was used for comparisons between two groups, and one-way ANOVA was used for comparisons among more than two groups, followed by Tukey's post-hoc test. P values of ≤ 0.05 were considered statistically significant.

7 Results

7.1 Characterization of S1R expression in CNS cells

7.1.1 Specific detection of the S1R by immunoblot

To identify reliable S1R antibodies, we screened six commercially available antibodies on tissue homogenates of WT and S1R KO mice by immunoblot. The total protein from the cerebral cortex (ctx) and spinal cord tissues was prepared using RIPA buffer containing 1% Triton X-100. Protein samples ranging from 5-30 µg were used for western blot analysis. To detect potential nonspecific signals, each membrane was exposed for up to 15 min. Based on the blot results, we observed that one monoclonal rabbit antibody from Cell Signalling (#61994, $Ab^{\#61994}$) showed a strong signal at the expected size of S1Rs (25 kD) in WT mice but was absent in the KO mice (Figure3A, left). Even with the long exposure time (15 min), we only detected faint bands at higher molecular weights. Another monoclonal rabbit antibody from Cell Signalling (#74807) only showed some unspecific bands at higher molecular weights in both WT and KO mice. The monoclonal mouse antibody from Santa Cruz (sc-137075, $Ab^{sc\text{-}137075}$) showed relatively weak but specific bands at 25 kD, consistent with previous studies (Moreno et al., 2014; Yang, Shen, Li, Stanford, & Guo, 2020). However, we also observed many other nonspecific bands of different sizes in both WT and KO mice. The other polyclonal rabbit antibodies, i.e. 42-3300 from Invitrogen, ab53852 from Abcam and 15168-1-AP from Proteintech, showed bands at 25 kD and other sizes in both WT and KO mice ($Ab^{15168\text{-}1\text{-}AP}$ showed weaker bands at 25 kD in KO mice), indicating nonspecific detection of S1Rs by those antibodies for immunoblot (Figure 3A).

Previous transcriptome profiling studies using purified cells from postnatal mice have shown that *Sigmar1* is widely expressed in neurons and glial cells, with even higher expression levels in microglia and OPCs compared to other cells (Figure S1A) (Zhang et al., 2014a). To detect *Sigmar1* expression levels in glial cells of adult mice, we purified translated mRNA directly from astrocytes, microglia, and OPCs of cerebral ctx using a Cre- dependent RiboTag approach (Figure S1B-D). Quantitative real-time PCR (qPCR) results suggested that adult astrocytes, microglia and OPCs all expressed *Sigmar1* mRNA, albeit at variable levels when normalized to Actb expression per se (Figure S1E). Additionally, we investigated the expression of S1R protein in adult glial cells. By employing magnetic-activated cell sorting (MACS), we purified astrocytes, microglia and OPCs from the cortex of adult WT mice and performed immunoblot using the specific $Ab^{\#61994}$ (Figure 3B-C). As shown in Figure 3C, we detected S1Rs in protein samples from purified astrocytes, microglia, and OPCs. Notably, western blotting and qPCR analysis of target genes typically rely on normalization to expression levels of house-keeping genes (e.g., β-actin, α-tubulin), which can vary among different cell types (Zhang et al., 2014b; Zhang et al., 2014a; Ximerakis et al., 2019). This makes it challenging to quantitatively compare S1R expression in purified CNS cells using these methods. Instead, *in situ* immunolabelling will help to better determine the expression pattern of S1Rs.

7.1.2 Establishment of a reliable protocol for S1R immunohistochemistry

To visualize the detailed expression pattern of S1Rs *in situ*, it is crucial to have a highly specific antibody for immunohistochemistry (IHC). Here, in this project, we utilized free-

floating vibratome sections of formaldehyde-fixed tissue to preserve the antigen integrity. To test the S1R antibodies, we initially used the regular protocol that had been successfully

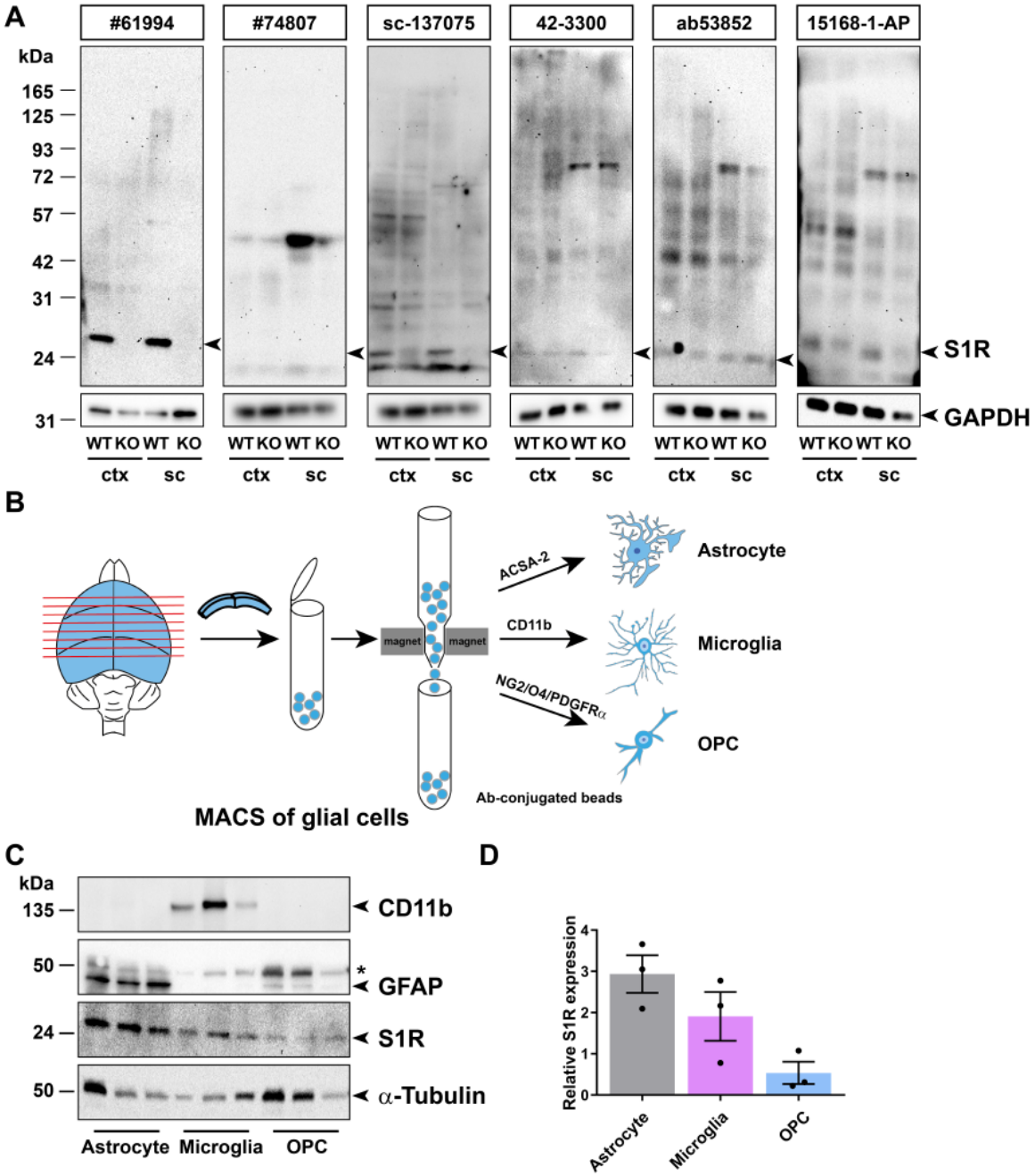

Figure 3. Detection of S1Rs in the CNS by immunoblot. A. Full-length scans of immunoblots detecting S1Rs in protein lysates from cortex (ctx) and spinal cord (sc) tissue of WT and S1R KO mice. S1R antibodies from Cell Signaling (#61994 and #74807), Santa Cruz (sc-137075), Invitrogen (42-3300), Abcam (ab53852), and Proteintech (15168-1-AP) were used. The molecular weight of S1Rs is indicated at 25 kDa. GAPDH was used as loading control. **B.** Schematic illustration of magnetic-associated cell sorting (MACS) method used to purify glial cells (astrocytes, microglia, and OPCs) from mouse ctx. The specific antibodies ACSA-2, CD11b, and NG2/O4/PDGFRα were used to isolate the respective cell types. **C.** Immunoblots showing the expression of S1Rs in sorted astrocytes, microglia and OPCs from ctx. CD11b and GFAP immunoblots demonstrate the purity of microglia and astrocyte from MACS. α-Tubulin was used as loading control. Asterisk (*) indicates the band of α-Tubulin which was not totally stripped off. **D.** The quantification of grey values from the blots showing the relative expression of S1R proteins in microglia, astrocyte, and OPC. All results were normalized to α-Tubulin. n = 3 mice.

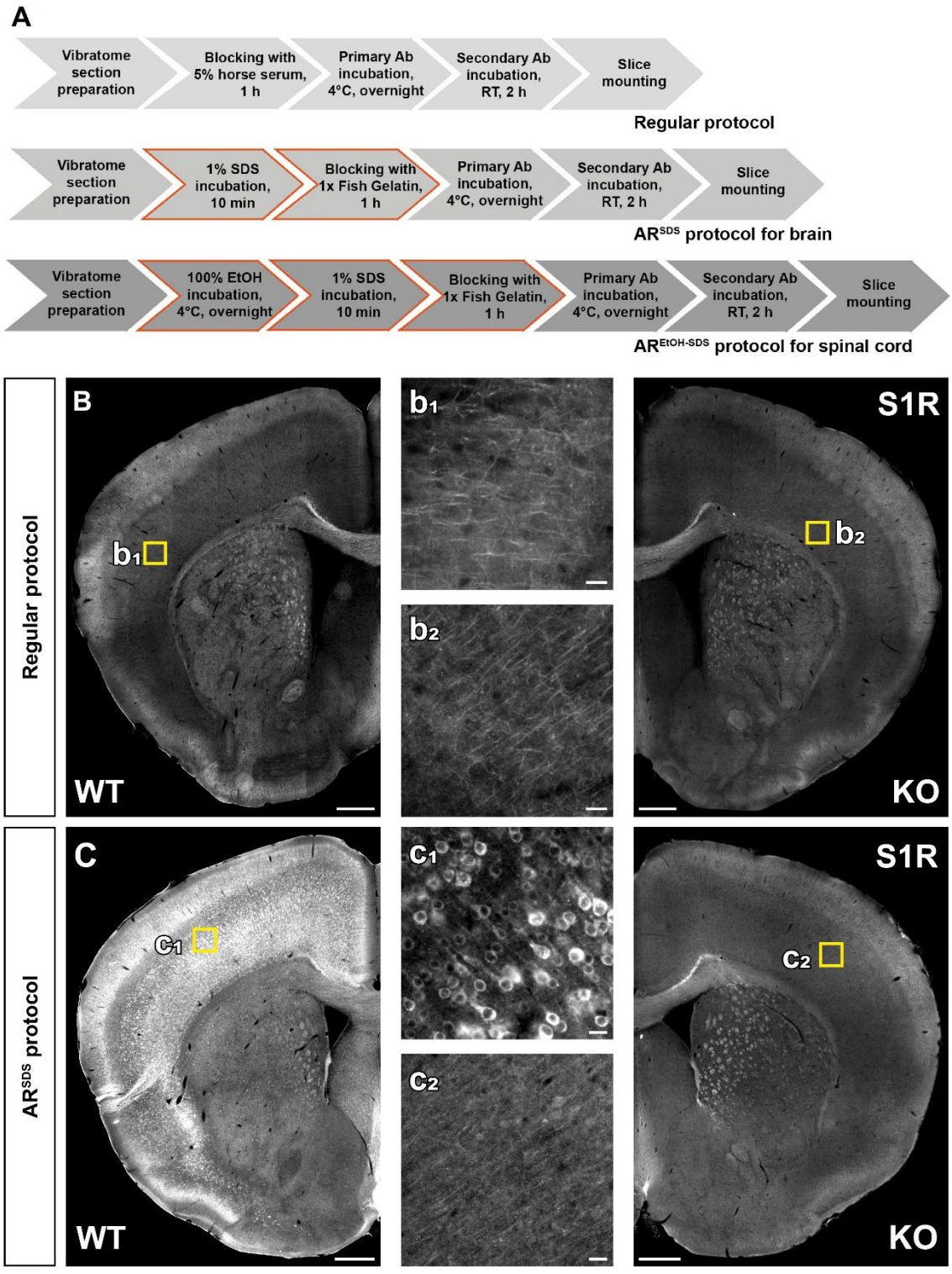

Figure 4. Establishing immunohistochemical protocols for specific detection of S1Rs. A. Immunohistochemical protocols tested on vibratome sections of brain and spinal cord. The regular protocol was modified by antigen retrieval (AR) using 1% SDS (AR^{SDS}) and used for brain sections. The modified ARSDS protocol with AR using 100% ethanol and 1% SDS sequentially was used for spinal sections ($AR^{EtOH-SDS}$). **B-C.** Representative fluorescent images of S1R immunostaining performed with the regular protocol (**B**) or AR^{SDS} protocol (**C**) using $Ab^{\#61994}$. Magnified images (b_1, b_2, c_1, c_2) corresponding to the yellow boxes depicted in the ctx of WT (b_1, c_1) and KO (b_2, c_2) mice. Scale bars = 200 µm in B-C, 5 µm in b_1, b_2, c_1, c_2.

used in our previous studies (Huang et al., 2019; Huang et al., 2020) (Figure 4A). We observed that Ab$^{\#61994}$, Ab$^{\#74807}$ (data not shown), and Ab$^{sc\text{-}137075}$ did not show any labelling in WT and KO mice (Figure 4B and Supplementary Figure 2A). With Ab^{ab53852} and Ab$^{15168\text{-}1\text{-}AP}$, weak immunostaining of neuron-like cell bodies was observed in both WT and KO mice (Supplementary Figure 2B and C). In addition, Ab^{ab53852} and Ab$^{15168\text{-}1\text{-}AP}$ strongly labelled many cells in a pattern similar to anti-GFAP staining, particularly in the corpus callosum (cc) and hippocampus (hip) of both WT and KO mice. Such GFAP-like staining was the only immuno-labelling of Ab$^{42\text{-}3300}$, in both WT and KO mice (Figure S2D). Consequently, these antibodies were deemed unsuitable for IHC and specific labelling of cells in the mouse brain.

Sodium dodecyl sulfate (SDS) has been suggested as an antigen retrieval (AR) reagent for antibodies detecting denatured proteins in IHC (Brown et al., 1996; Wilson and Bianchi, 1999). Considering that Ab$^{\#61994}$ specifically recognized SDS-denatured S1Rs for immunoblotting, we investigated the use of SDS as an AR reagent prior to the blocking step (AR^{SDS}) for IHC (Figure 4A).

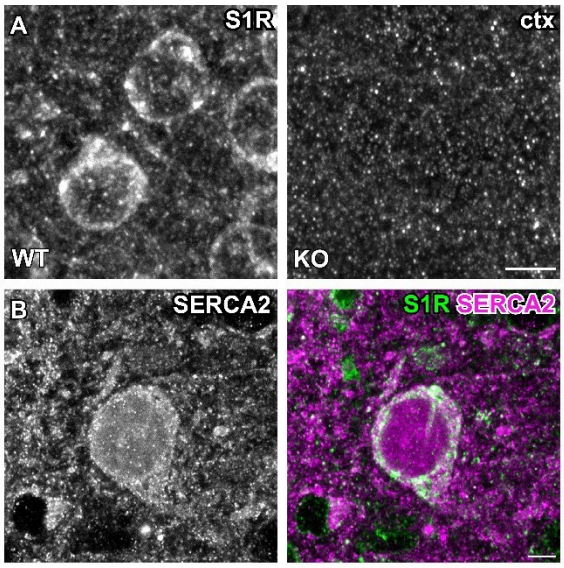

Figure 5. Subcellular distribution of S1R immuno-labelling *in situ*. A. The S1R immunostaining in WT mice shows punctate background signal in both WT and KO mice. **B.** S1R immunoreactivity was colocalized with an ER marker SERCA2 *in situ*. Scale bars = 5 µm in A-B.

By using the AR^{SDS} protocol (i.e., 1% SDS for AR + Ab$^{\#61994}$), we observed bright and clear immunoreactivity of S1R specifically detected in WT mice, which was absent in S1R KO mice (Figure 4C). This indicates that Ab$^{\#61994}$ has the potential to specifically detect S1Rs in IHC. Although tiny punctual background staining was observed in both WT and KO mice in images with higher magnifications (Figure 5A), Ab$^{\#61994}$ immunolabelling clearly displayed a ER-like perinuclear ring structure (Figure 5B), consistent with previous studies using EYFP-tagged S1Rs in cultured cells (Hayashi and Su, 2007). Furthermore, we demonstrated that S1R expressing cells were distributed throughout the brain, with strong immunolabelling of S1Rs observed in the cerebral ctx, hip, thalamus, and olfactory bulb area (Supplementary Figure 3A), along with nonspecific staining in the white matter tracts of brain stem and cerebellum (Supplementary Figure 3B). Additionally, we detected using this protocol immunolabeled S1Rs in other organs such as the liver (Supplementary Figure 4A-D) and heart (Supplementary Figure 4E-H). Therefore, the AR^{SDS} protocol reliably identifies S1R expression *in situ*.

We tested the effect of 1% SDS pre-treatment on other S1R antibodies as well. However, we did not observe improved immunostaining for Ab$^{sc\text{-}137075}$ compared to the protocol

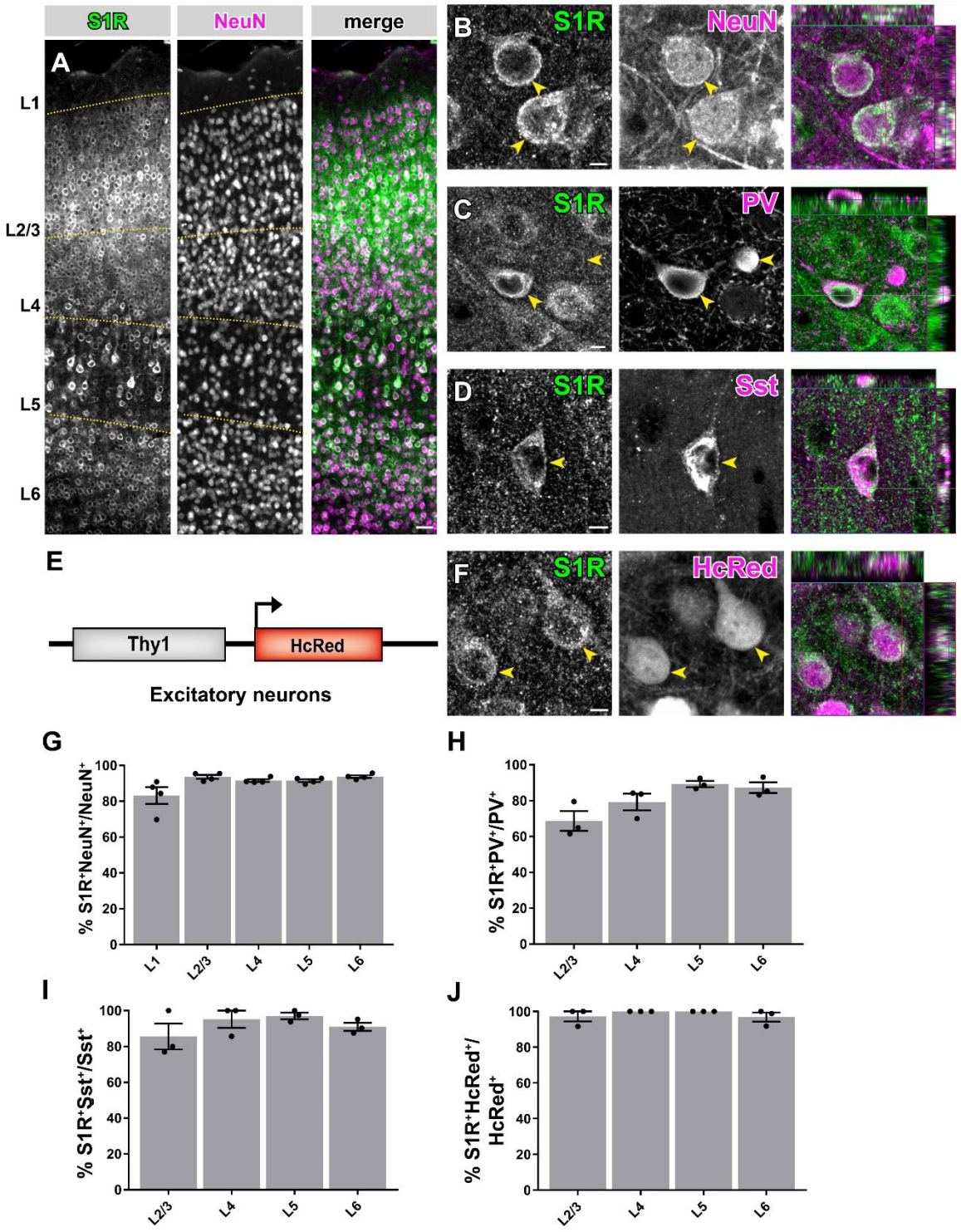

Figure 6. S1Rs are abundantly expressed in neurons. A. Immunohistochemical detection of S1Rs in NeuN$^+$ cells of different cortical layers (L1-L6). Almost all NeuN$^+$ cells co-localized with S1R immunostaining. **B.** Confocal images depicting the ring-like structure of S1R immunostaining in NeuN$^+$ cells. **C-D.** Detection of S1R in Parvalbumin$^+$ (PV, **C**) and Somatostatin$^+$ (Sst, **D**) interneurons. **E.** Scheme of the gene construct Thy1-HcRed used to visualize excitatory neurons. **F.** Confocal images showing the S1R immunolabelling in HcRed$^+$ excitatory neurons. The rightmost images of B-F show the orthogonal views. **G-J.** The proportions of S1R$^+$ cells in NeuN$^+$ (G), PV$^+$ (H), Sst$^+$ (I) and HcRed$^+$ (J) neurons in different cortical layers. n = 3 mice. Scale bars = 50 µm in A, 5 µm in B-F.

without SDS (Supplementary Figure 5A). The immuno-labelling by $Ab^{15168\text{-}1\text{-}AP}$ was improved in WT mice, but weak immunoreactivity was still observed in KO mice. For $Ab^{42\text{-}3300}$, $Ab^{ab53852}$, and $Ab^{15168\text{-}1\text{-}AP}$, the GFAP-like staining was still observed both in WT and KO mouse even after SDS treatment. Taken together, except for $Ab^{\#61994}$, the other commercial S1R antibodies failed to provide reliable immunolabelling of S1Rs for IHC.

7.1.3 Expression of S1Rs in CNS cells in the forebrain

By using the newly established AR^{SDS} protocol, we performed co-immunostaining for S1R ($Ab^{\#61994}$) and various cell markers to investigate the expression of S1Rs in the CNS.

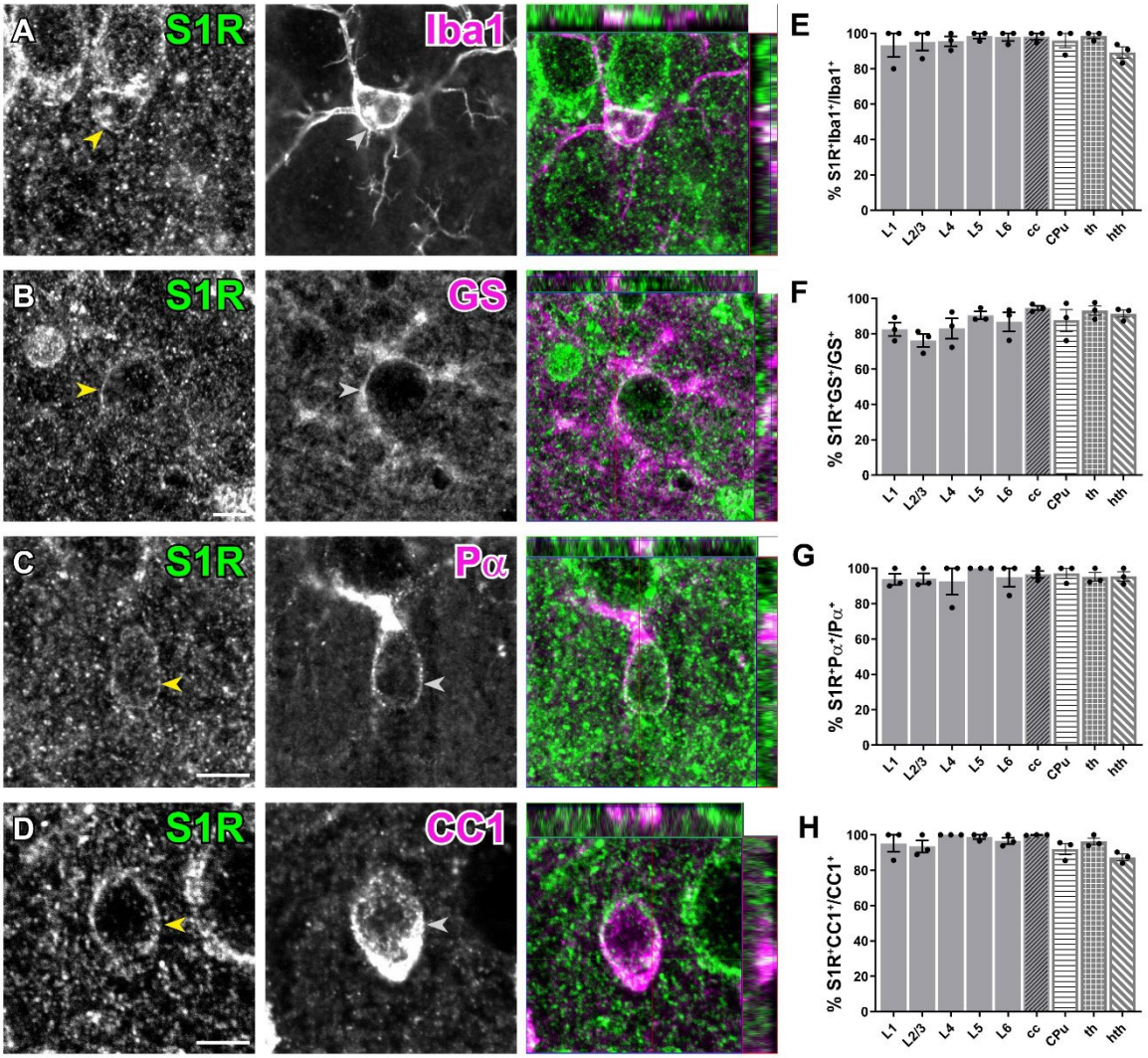

Figure 7. Detection of S1R expression in glial cells in the forebrain. A-D. S1R immunoreactivity in $Iba1^+$ microglia (**A**), GS^+ astrocytes (**B**), $PDGFR\alpha^+$ (Pα) OPCs (**C**), and $CC1^+$ OLs (**D**) in the ctx of adult mouse brain. The rightmost images in each panel show orthogonal views. **E-H.** Quantification of the proportion of S1R-expressing glial cells in different cortical layers (L1-L6), corpus callosum (cc), caudate putamen (CPu), thalamus (th) and hypothalamus (hth). n = 3 mice. Scale bars = 20 µm in A-D.

By combining NeuN (a pan-neuronal marker) and S1R immunostaining, we evaluated the expression of S1Rs in neurons. We found that most neurons were immune-positive for S1R throughout the forebrain (Figure 6A-B): S1R immunolabelling was found in ~85% of $NeuN^+$ cells in layer (L) 1 and in more than 90% of $NeuN^+$ cells in L2-6 (Figure 6G). Since NeuN

also labels interneurons in addition to principal neurons, we further detected the expression of S1Rs in two major interneuron types: parvalbumin (PV)$^+$ and somatostatin (Sst)$^+$ interneurons (Figure 6C-D). We found that the majority of PV$^+$ or Sst$^+$ interneurons expressed S1Rs, but with different proportions. The proportion of PV$^+$ interneurons immunolabelled for S1R was ~70% in L1, ~80% in L2/3, and ~90% in L5 and L6 (Figure 6H), while ~90% of Sst$^+$ interneurons showed immunoreactivity for S1Rs in L2-L6 (Figure 6I). Notably, virtually no PV$^+$ or Sst$^+$ cells were found in L1. To determine the S1R expression in excitatory neurons, we performed S1R immunostaining on brain sections from fluorescent transgenic mice where excitatory neurons were labelled by HcRed expression under the Thy1 promoter (Figure 6E). We found that more than 90% of HcRed-labelled cells were expressing S1Rs in L2-6 (Figure 6J).

To study the S1R expression in microglia, we performed co-immunostaining for Iba1 (a microglia marker) and S1R. The characteristic ring-like immunostaining of S1Rs was observed in Iba1$^+$ cells (Figure 7A). Quantification results suggested that virtually all Iba1$^+$ cells were expressing S1Rs, at least in the ctx, cc, caudate putamen (CPu), thalamus (th) and hypothalamus (hth) (Figure 7E).

For the detection of S1R expression in astrocytes, we used glutamine synthetase (GS) immunostaining to label astrocytes. The perinuclear ring structure of S1Rs in GS$^+$ cells appeared thinner than in neurons (Figure 7B). We found approximately 80-90% GS$^+$ cells were expressing S1Rs in cortical layers and cc, CPu, th and hth (Figure 7F). Notably, both in the cc and hip (Supplementary Figure 6A-B), we did not observe S1R staining in astrocytes resembling the typical GFAP-containing cytoskeleton, as indicated by anti-GFAP immunostainings.

To explore S1R expression in OL lineage cells, we performed PDGFRα (Pα, an OPC marker) and APC CC1 (an OL marker) immunostainings. With the AR^{SDS} protocol, we were able to detect S1R expression in almost all OPCs (Figure 7C and G) and OLs (Figure 7D and H), both in the grey matter (e.g., the ctx) and white matter (e.g., the cc), as well as in other studied ventral brain areas. To our knowledge, this is the first time that S1R expression has been observed in OPCs by immunolabeling.

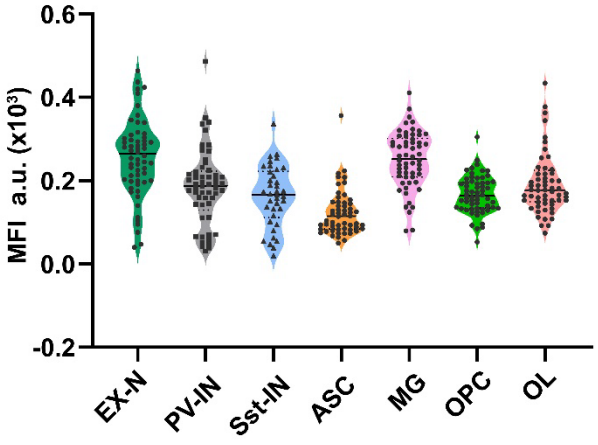

Figure 8. S1R expression levels in different brain cells *in situ*. S1R staining was performed with different brain cellular markers (excitatory neurons identified by Thy1-HcRed$^+$). The mean fluorescence intensity (MFI) of S1R immunostaining in single cells was measured. The violin plots depict the relative expression level of S1Rs in excitatory neuron (EX-N, n = 60 cells), parvalbumin$^+$ interneuron (PV-IN, n = 57 cells), somatostatin$^+$ interneuron (Sst-IN, n = 38 cells), astrocytes (ASC, n = 58 cells), microglia (MG, n = 58 cells), OPC (n = 60 cells) and OL (n = 60 cells) *in situ*. The dotted line represents the median value of all data. n = 3 mice.

The specific S1R immunolabelling enabled us to compare relative expression levels of S1Rs in different CNS cell types within defined regions *in situ*. By measuring the mean fluorescence intensity (MFI) of S1Rs in each cell, we observed relatively higher levels of S1Rs in excitatory neurons and microglia compared to other cell types (excitatory neurons

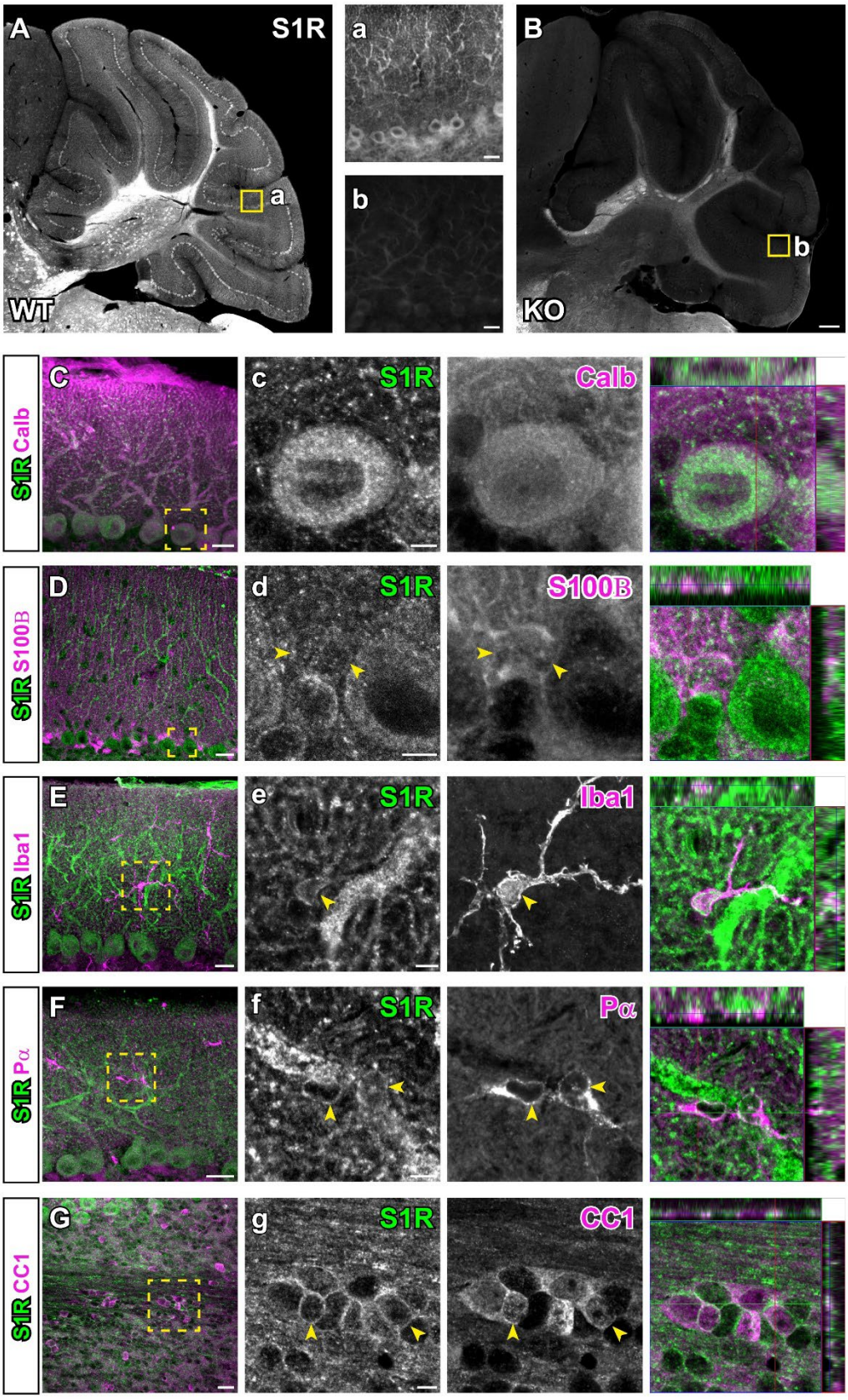

Figure 9. The expression pattern of S1Rs in the cerebellum. A-B. Sagittal sections of cerebellum were stained for S1Rs using the AR^{SDS} protocol. Specific immunostaining for S1Rs in WT cerebellum (**A**) is absent in KO mice (**B**). **a-b.** Magnified views showing the molecular layer as indicated in A and B. **C-G.** Cerebellar sections were double immune-stained for S1Rs, calbindin^{+} (calb) (**C**), S100B^{+}

(**D**), Iba1$^+$ (**E**), Pα$^+$(**F**) and CC1$^+$(**G**), respectively. **c-g.** Magnified images of the boxed area in C-G. Scale bars = 200 µm in A-B, 20 µm in a-b, C-G, and 5 µm in c-g.

> microglia > PV$^+$ interneurons > Sst$^+$ interneurons ≈ OLs > OPCs > astrocytes) (Figure 8).

In conclusion, using specific S1R immunolabeling, we demonstrated that the majority of neurons and all types of glial cells express S1Rs in the forebrain.

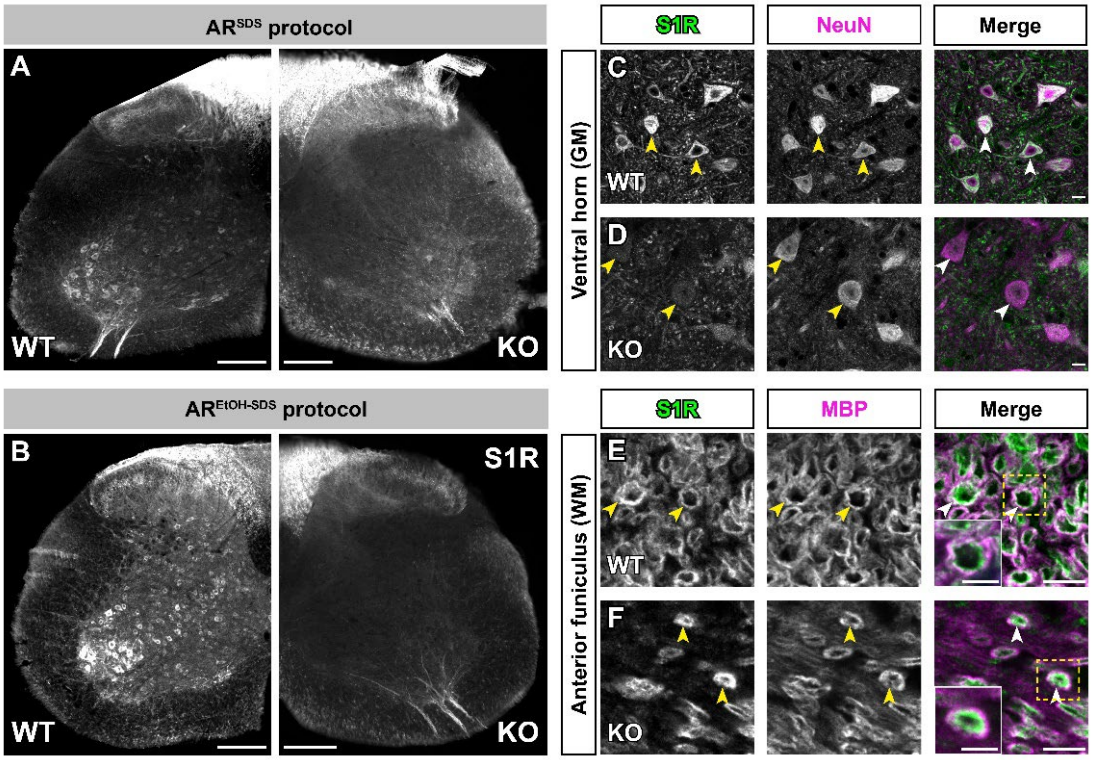

Figure 10. A modified AR^{SDS} protocol for immunolabeling S1Rs in the mouse spinal cord. A. Representative overview image of spinal cord sections stained with the specific S1R antibody (Ab$^{\#61994}$) using the AR^{SDS} protocol. Unspecific myelin-like staining is observed in both WT and S1R KO mice. **B.** The additional delipidation step using 100% EtOH prior to 1% SDS treatment (AR$^{SDS\text{-}EtOH}$ protocol) reduces the unspecific staining of S1R in KO mice, while improving the quality of S1R staining in WT mice. **C-D.** Confocal images showing the double-immunostaining of S1R and NeuN in the ventral horn (grey matter, GM) of the spinal cord in WT and KO mice. Some faint signal of S1R staining can be detected in NeuN$^+$ cells in the ventral horn of KO mice. **E-F.** Confocal images showing the immunoreactivity of S1R and MBP (a myelin marker) in the spinal white matter (WM) of WT and KO mice. Magnified images represent the boxed regions in E and F. Arrowheads indicate the localizations of S1R and MBP immunolabelling. Scale bars = 200 µm in A-B, 10 µm in C-F, and 5 µm in magnified images.

7.1.4 Expression of S1Rs in CNS cells in the cerebellum

In addition to the forebrain, we also examined the applicability of the AR^{SDS} protocol for S1R staining in the cerebellum. As depicted in Figure 9A and B, specific immunolabeling of S1R was observed in the cerebellum. In particular, we observed a high expression of S1Rs in the cell bodies and neurites of Purkinje neurons, as confirmed by Calbindin staining (Figure 9C). Further investigations using other cell type markers revealed that S1Rs were widely expressed in astrocytes including Bergmann glia (S100B$^+$), microglia (Iba1$^+$), OPCs (Pα$^+$), and OLs (CC1$^+$) in the cerebellum (Figure 9D-G). This finding indicates that S1Rs have a broad expression pattern in various cell types within the cerebellum.

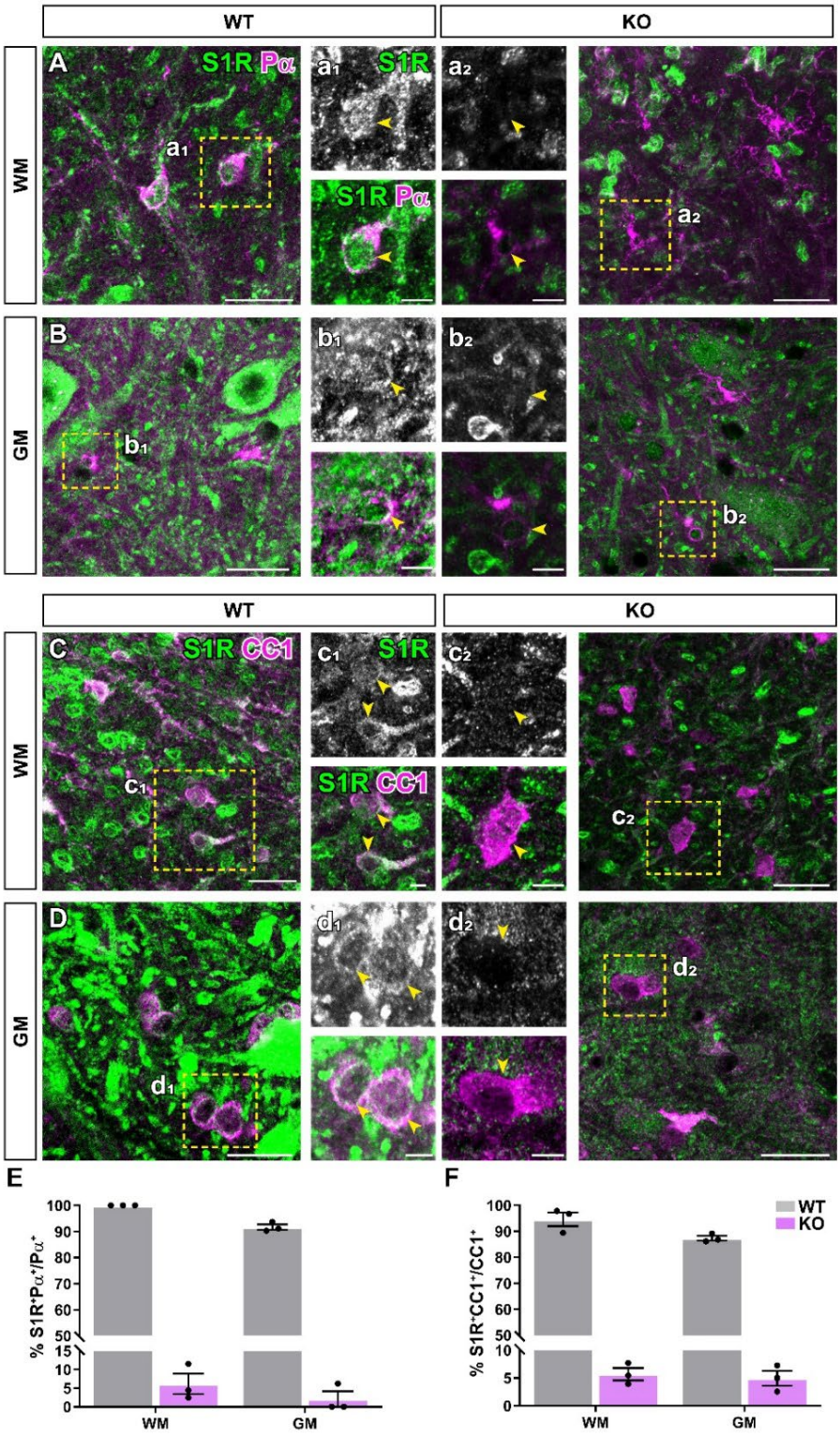

Figure 11. Specific detection of S1Rs in OL lineage cells in the mouse spinal cord. A-B. Confocal images showing S1R immunoreactivity in Pα$^+$ OPCs in both spinal WM (**A**) and GM (**B**) of WT and KO mice. **a_1-a_2 and b_1-b_2**. Magnified images correspond to areas in the yellow boxes in A and B. Arrowheads indicate the colocalization of S1R and Pα immunostaining. **C-D.** Confocal images showing S1R and CC1 immunoreactivity in spinal WM (**C**) and GM (**D**) of WT and KO mice. **c_1-c_2, d_1-d_2**. Magnified views in boxed areas from C and D. Arrowheads indicated colocalization of S1R and CC1 immunostaining. **E-F.** The quantification of the proportions of Pα$^+$ (E) or CC1$^+$ (F) cells showing S1R immunoreactivity in the spinal GM and WM of WT and KO mice. Scale bars = 20 μm in A-D, 5 μm in a_1-d_2. n = 3 mice per group.

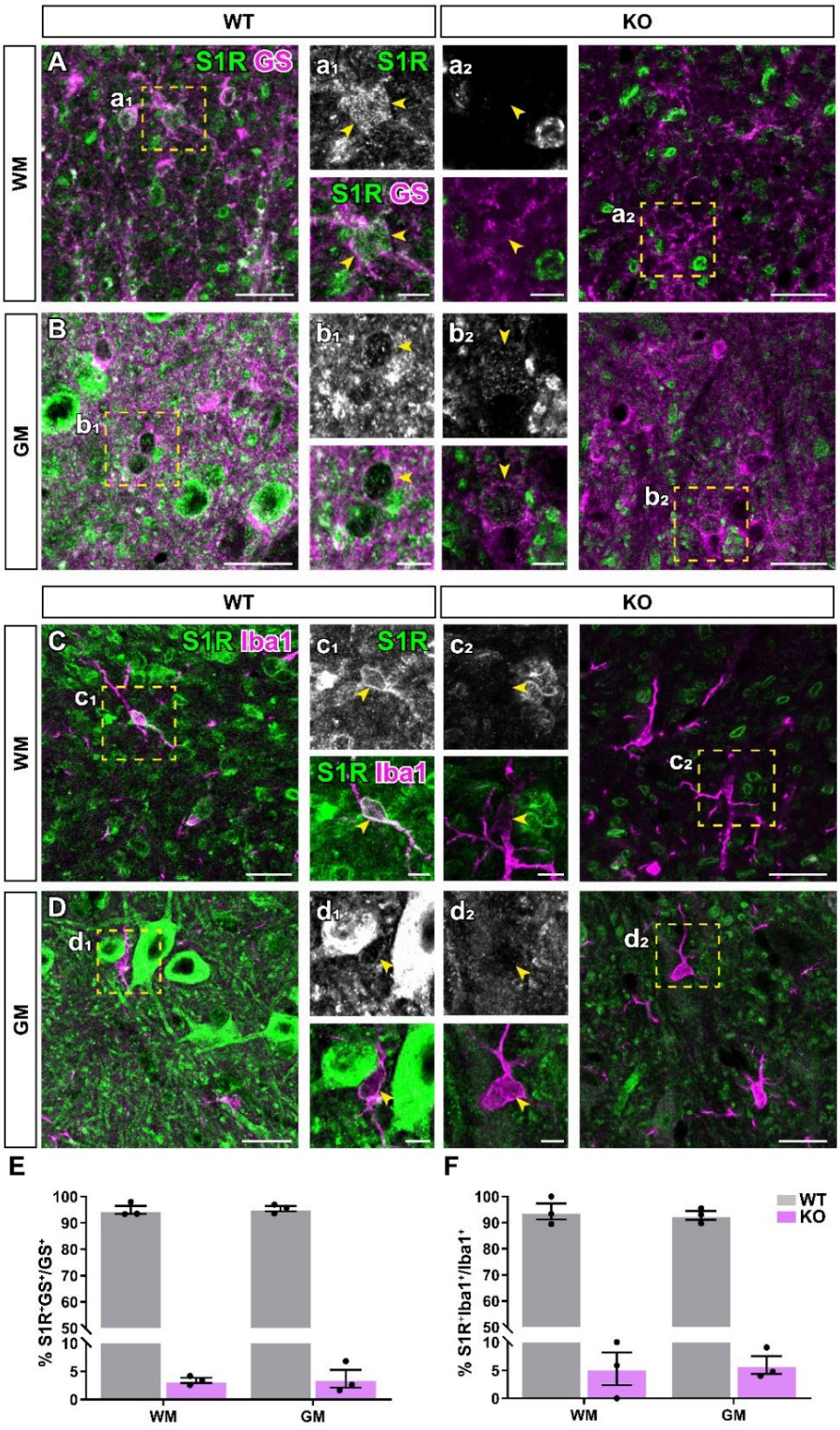

Figure 12. Specific immunolabeling of S1Rs in spinal astrocytes and microglia. A-B. Confocal images illustrating the S1R immunoreactivity in GS^+ astrocyte in both spinal WM (A) and GM (B) of WT and KO mice. **a_1-a_2, b_1-b_2**. Magnified images correspond to boxed areas in A and B. Arrowheads indicate the colocalization of S1R and GS immunostaining. **C-D**. Confocal images showing S1R immunoreactivity in $Iba1^+$ microglia in spinal WM (C) and GM (D) of WT and KO mice. **c_1-c_2, d_1-d_2**. Magnified views in boxed areas from C and D. Arrowheads indicate the colocalization of S1R and Iba1 immunostaining. **E-F.** Quantification of the proportions of GS^+ (E) and $Iba1^+$ (F) cells bearing S1R immunoreactivity in the spinal GM and WM of WT and KO mice. Scale bars = 20 µm in A-D, 5 µm in a_1-d_2. n = 3 mice per group.

7.1.5 Expression of S1Rs in CNS cells in the spinal cord

Previous studies using Ab^{Ruoho} showed that high expression of S1Rs in motor neurons of the spinal ventral horn. However, the S1R expression in other cell types has not been mentioned. In the current work, we also tested the performance of the AR^{SDS} protocol for S1R IHC in the spinal cord. We observed high expression of S1Rs in the ventral horn of WT mice, but associated with a strong background (Figure 10C-D). Moreover, unspecific staining using the AR^{SDS} protocol could be observed in KO mice, mainly in the white matter (WM) myelin structures (Figure 10A). Considering that delipidation of myelin is useful to decrease background for the detecting of myelin proteins (Ishii, Fyffe-Maricich, Furusho, Miller, & Bansal, 2012; Jahn, Tenzer, & Werner, 2009), we modified our protocol by pre-treating 100% ethanol overnight (more than 16 h). With this protocol ($AR^{EtOH\text{-}SDS}$, i.e., 100% ethanol + 1% SDS + $Ab^{\#61994}$; Figure 4A), we observed substantial reduction in background staining both in WT and KO mice (Figure 10B). However, for yet unknown reasons, myelin-like staining could still be observed in both groups of mice. We used MBP (a myelin marker) to further investigate the nonspecific staining components. The unspecific S1R immunolabelling did not totally overlap with MBP staining but appeared to be in the inner layers of the myelin sheath (Figure 10E and F). By co-immunostaining of S1R and NeuN, we found that all neurons express S1Rs in the spinal cord (Figure 10C). In addition, we performed co-immunostaining for S1Rs and glial markers with the $AR^{EtOH\text{-}SDS}$ protocol on spinal cord sections (Figure 11A-D and 12A-D). Given the still relatively high immunostaining background in the spinal cord compared to the brain, we quantified S1R immuno-positive cells in WT and KO spinal cords. We found that more than 90% of all types of glial cells in both the spinal grey matter (GM) and WM of WT mice were immunolabeled for S1Rs, whereas in KO mice, this proportion was no more than 5% (Figure 11E-F and 12E-F). The current results obtained using the $AR^{EtOH\text{-}SDS}$ protocol demonstrated that the majority of neurons and glial cells in the spinal cord express S1Rs.

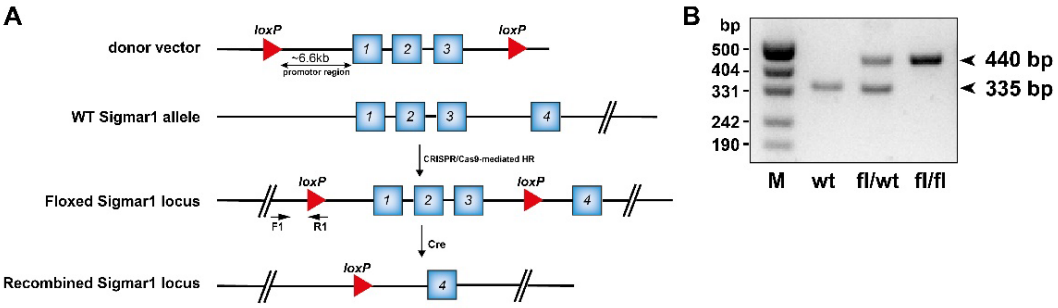

Figure 13. Generation of Cre-dependent Sigmar1 flox mice. A. Schematic representation of Cas9/CRISPR-mediated generation of the *Sigmar1* flox mice. Arrows indicate the positions of primers that were used for genotyping PCR. **B.** Results of genotyping PCR using primers F1 and R1 for wt, floxed *Sigmar1* heterozygous (fl/wt) and floxed *Sigmar1* homozygous (fl/fl) mice, respectively. The products sizes are indicated. M: DNA ladders.

7.2 Cell-type specific deletion of S1Rs *in vivo*

Using constitutive S1R KO mice, previous studies have shown that S1Rs are involved in various psychoneurological disorders including ALS, AD, and depression (Couly et al., 2022). However, the role of S1Rs in specific cell types is not well understood. To achieve this, the conditional knockout mice based on the Cre/loxp systerm was used in the current work.

7.2.1 Generation of S1R flox mice

To achieve cell-specific deletion of S1Rs, we generated a S1R flox mouse line ($S1R^{fl/fl}$). The CRISPR/Cas9 technology was used to modify the *Sigmar1* gene (*Oprs1*). Briefly, a single guide RNA (sgRNA) was transcribed *in vitro*, and a donor vector containing exons 1-3 of *Sigmar1* flanked by two loxP sites was constructed and co-injected into zygotes. Then, the sgRNA directed Cas9 endonuclease cleavage at about 6 kb upstream of exon1 and downstream of 3'UTR and create a double strand break (DSB) (Figure 13A). Such breaks will be repaired and result in the insertion of loxP sites by homologous recombination. Genotyping PCR for $S1R^{fl/fl}$ mice with the designed primers results in only one wild-type

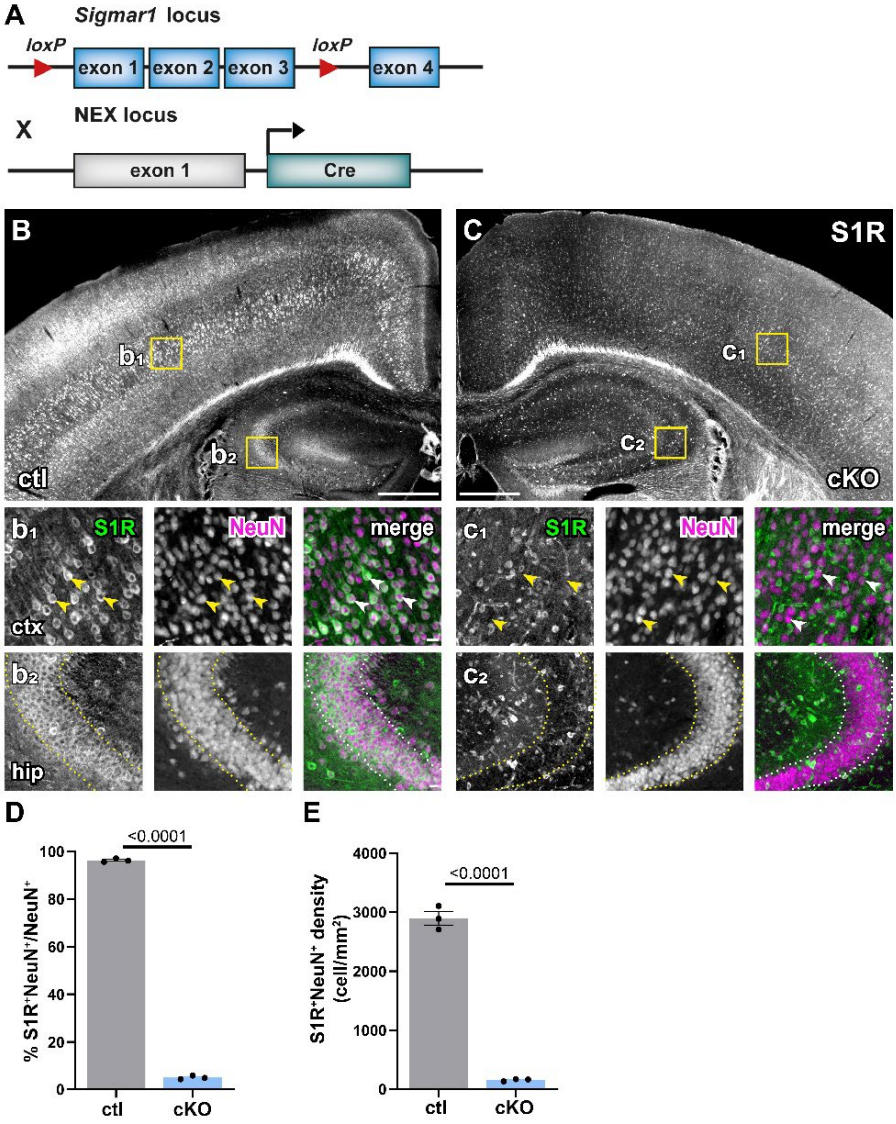

Figure 14. Successful knockout of S1Rs in principal neurons within the neocortex and hippocampus. A. Scheme with transgenic structures of NEX-Cre x $S1R^{fl/fl}$ mice used to delete S1Rs in principal neurons. **B-C.** Overviews of S1R immunostaining in the dorsal brain of control (ctl, B) and cKO (C) mice. **b_1-b_2, c_1-c_2.** Magnified views (yellow boxes in B and C). Arrowheads indicate reduced S1R expression in cortical $NeuN^+$ cells in cKO (c1) compared to ctl (b_1). Dotted lines indicate reduced expression of S1Rs in pyramidal neurons in the hippocampal CA2 region of cKO (c_2) compared to ctl (b_2) mice. **D-E.** Histograms highlighting decreased proportion and density of $S1R^+$ cells in $NeuN^+$ cells in cKO mice. n=3 mice per group. Scale bars = 500 µm in B-C, 50 µm in b_1-b_2, c_1-c_2.

band of 335 bp for WT, only one transgenic band of 440 bp for homozygous and two bands for heterozygous (Figure 13B)

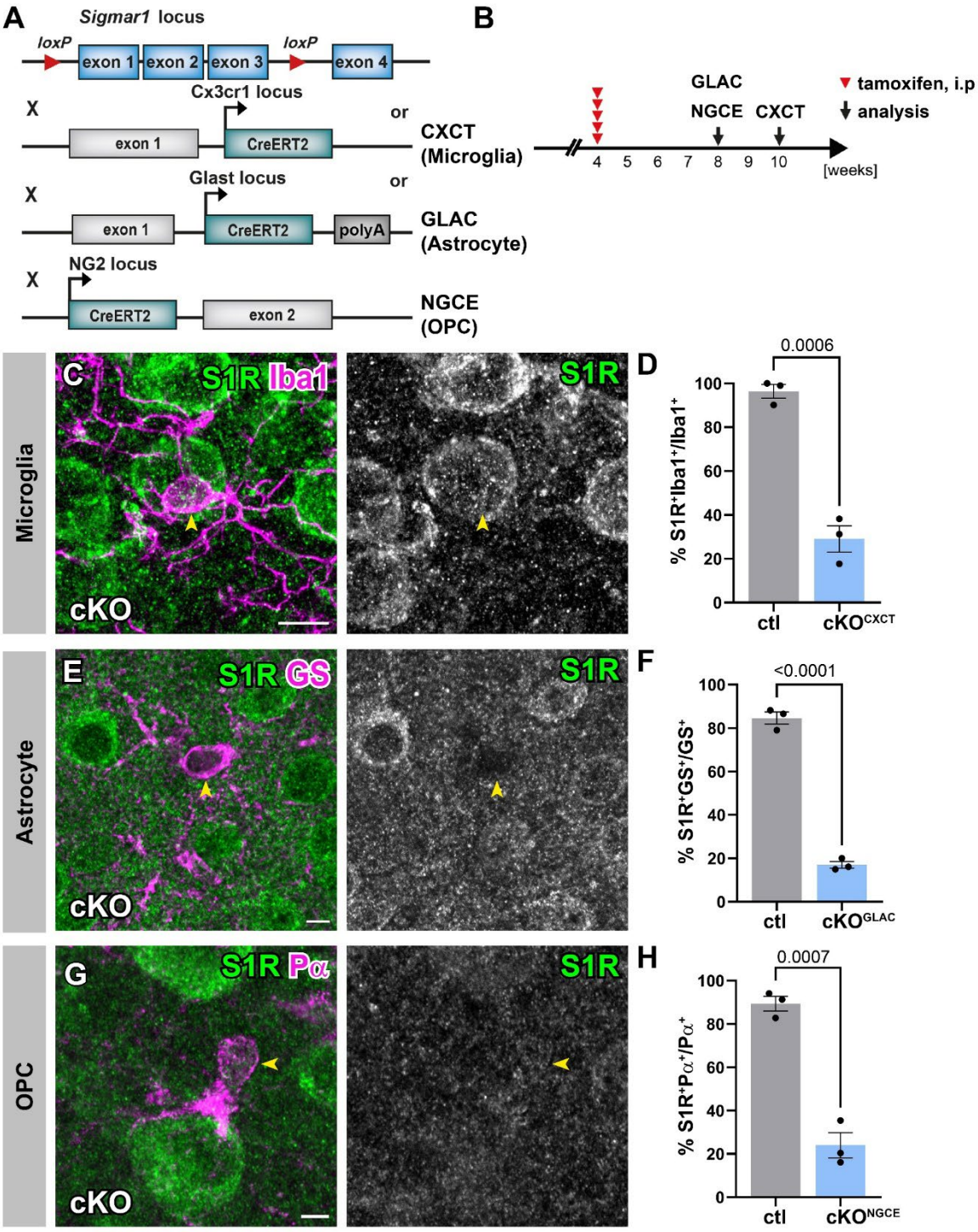

Figure 15. Successful deletion of S1Rs in different glial cells *in vivo*. A. Schematic representation of the double transgenic mice used for the conditional deletion of S1Rs in glial cells: CX3CR1-CreERT2 x S1R$^{fl/fl}$ for microglia, Glast-CreERT2 x S1R$^{fl/fl}$ for astrocyte, and Cspg4-CreERT2 x S1R$^{fl/fl}$ was used for OPC. **B.** Experimental plan. All mice were adiministrated with tamoxifen at 4w. The immunostaining of S1Rs was performed at 4w (for astrocyte and OPC) or 6w (for microglia) after the first tamoxifen injection. **C, E, G.** Confocal images showing the double-staining of S1R and Iba1, GS, and Pα in cKO mice. **D, F, H.** Quantification of S1R expression in Iba1$^+$ microglia, GS$^+$ astrocyte, and Pα$^+$ OPC in the ctx of ctl and cKO mice. The data for the ctl mice are the same as those in Figure 6. n=3 mice per group. Scale bars = 20 µm in C, E, G.

7.2.2 Conditional deletion of S1Rs in neurons *in vivo*

To generate S1R conditional knockout mice in neurons, we crossed $S1R^{fl/fl}$ mice to NEX-Cre knockin mice, where Cre is expressed in principal neurons (NEX-Cre x $S1R^{fl/fl}$) (Figure 14A). To detect the deletion of S1Rs in neurons, we performed co-immunostaining for S1R and NeuN. We observed a dramatic decreased expression of S1Rs in pyramidal neurons in the expected brain regions of cKO mice, such as neocortex and hips (Figure 14B-C). Quantification of S1R-expressing $NeuN^+$ cells in the dorsal ctx showed that both in the proportion (~96% in ctrl, ~5% in cKO) and density (2900 cells/mm^2 in ctrl, 156 cells/mm^2 in cKO) of S1R expression were largely reduced in the neuronal S1R cKO^{NEX} mice (Figure 14D-E).

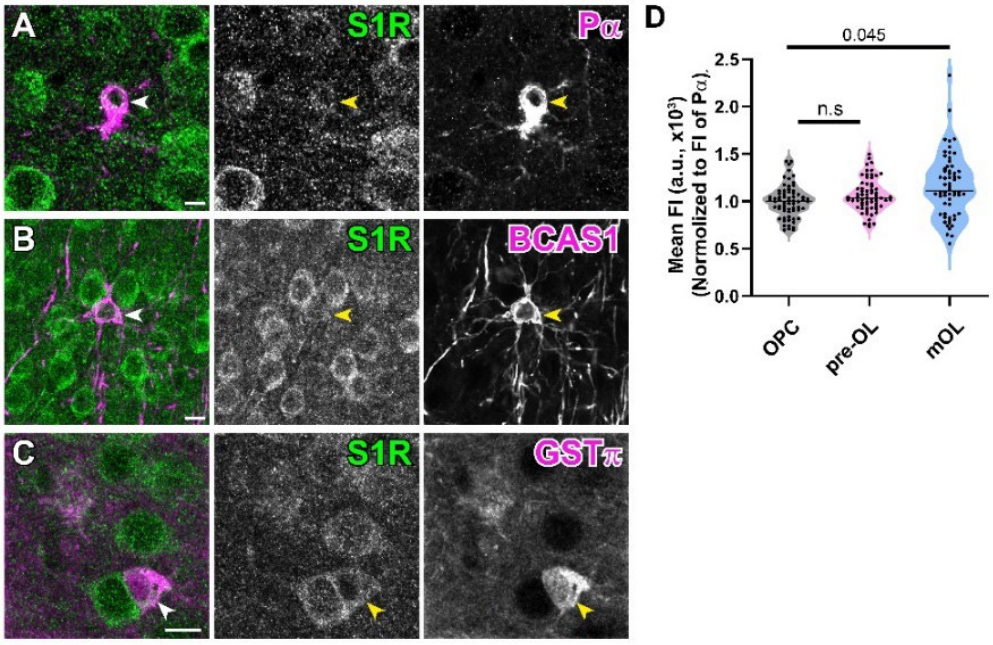

Figure 16. Increased expression of S1Rs in mOLs during OL development. A-C. Confocal images showing the specific immunostaining of S1Rs in $Pα^+$ OPC (**A**), $BCAS1^+$ premyelinating oligodendrocyte (preOL, **B**), and $GSTπ^+$ mature oligodendrocyte (mOL, **C**) at postnatal day 21 (P21). Arrowheads indicate the colocalization of S1R and Pα, BCAS1 and GSTπ co-immunostaining. **D.** Measurement of MFI of S1R immunostaining on individual marker-labelled cells in the ctx. Violin plots depict the relative expression levels of S1R in $BCAS1^+$ (preOL, n = 56 cells) and GST $π^+$ (mOL, n = 60 cells) cells compared to $Pα^+$ cells (OPC) on the same slide *in situ*. The dotted line indicates the Median of all values. Scale bars = 5 µm in A, 10 µm in B, C. n = 3 mice.

7.2.3 Conditional deletion of S1Rs in various glial cells *in vivo*

To assess the temporally controlled deletion of S1Rs in targeted cell types of $S1R^{fl/fl}$ mice, three different Cre-driven mouse lines for glia cells were introduced: CX3CR1-CreERT2 mice ($CXCT^{ct2/wt}$ x $S1R^{fl/fl}$, cKO^{CXCT}) for microglia, Glast-CreERT2 mice ($Glast^{ct2/wt}$ x $S1R^{fl/fl}$, cKO^{GLAC}) for astrocyte, and NG2-CreERT2 mice ($Cspg4^{ct2/wt}$ x $S1R^{fl/fl}$, cKO^{NGCE}) for OPC (Figure 15A). By crossbreeding $S1R^{fl/fl}$ mice with these Cre mice, we generated glial-specific S1R cKO mice. We injected mice with tamoxifen at 4 weeks (w) old and analysed them 4 or 6w post-injection (Figure 14B). We observed a significant decrease of the expression of S1Rs in $Iba1^+$ microglia (Figure 15C), GS^+ astrocyte (Figure 15E), and $Pα^+$ OPCs (Figure 15G) in different cKO mice. This was confirmed by the quantification results: the proportion of S1R-expressing $Iba1^+$ microglia was reduced to 29 ± 6% at 10 w compared to ctl (96.4 ± 3.2%) (Figure 15D); the proportion of GS^+ astrocytes expressing S1Rs was reduce

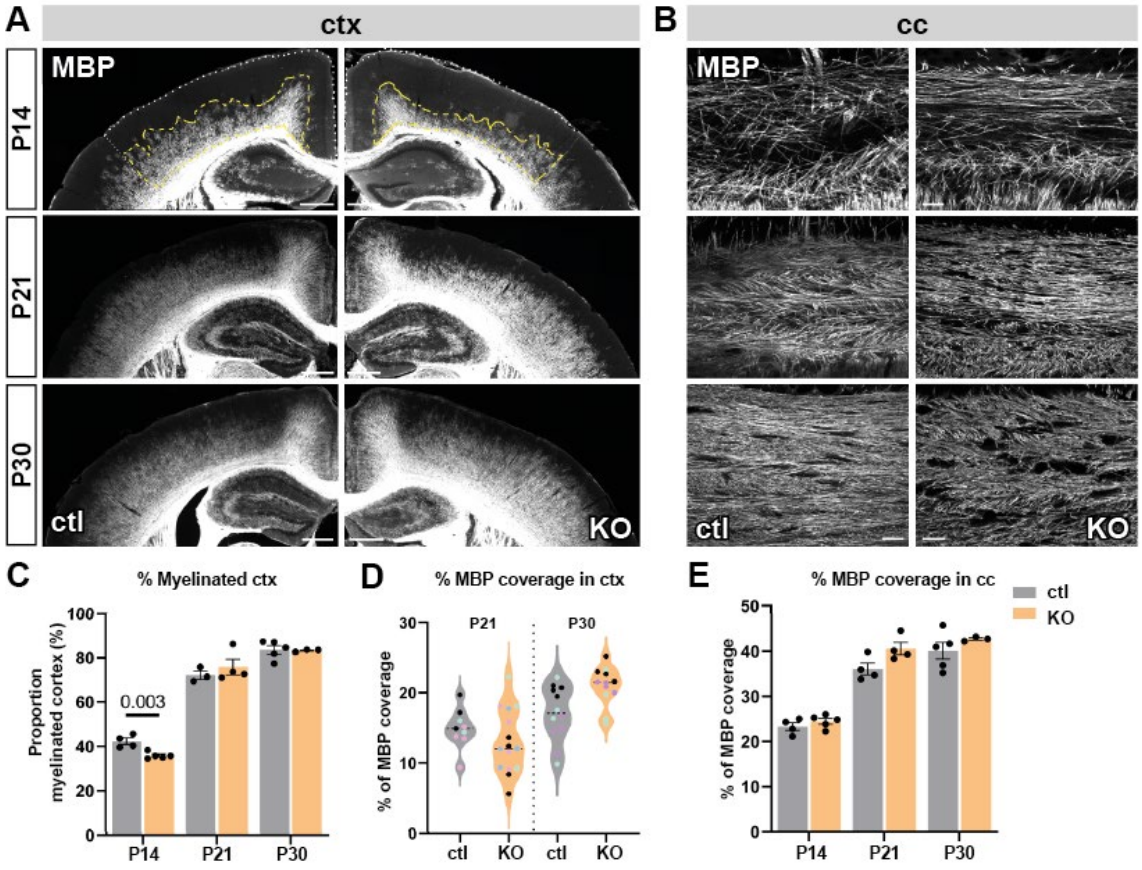

Figure 17. Transient reduction in myelination in the ctx of S1R KO mice at P14. A. Epifluorescent images of MBP staining in ctl and KO mice at P14, P21, and P30. Dotted lines indicate the representative areas of measurement. **B.** Confocal images showing MBP staining in cc of ctl and KO mice at different ages. **C.** The graphs show a reduced percentage of myelinated cortex in KO mice at P14, but no significant changes at P21 and P30. **D.** The percentage of MBP$^+$ occupied area in the whole image from ctx, show no significant differences between genotypes at P21 and P30. Each dot represents a slice, and different colours represent different mice. **E.** The percentage of MBP$^+$ occupied area in the cc, indicating no variation between ctl and KO mice at all analysed ages. Scale bar = 500 µm in A, 50 µm in B.

to 17.02 ± 1.5% compared to ctl (84.66 ± 2.8%) at 8 w (Figure 15F); the proportion of Pα$^+$ OPCs expressing S1Rs was 24.01 ± 5.8% in cKO mice and 89.39 ± 3.4% in ctl mice (Figure 15H). Therefore, we conclude that S1R expression can be substantially reduced in different glial cells within 4w after Cre induction in adult mice.

Overall, the S1R flox mice appear to be a powerful tool to efficiently delete S1Rs in neurons and glial cells in the CNS *in vivo*.

7.3 Functional analysis of S1Rs in OL lineage cells during development

Chaperone proteins assist in proper folding during the synthesis or proper function of other proteins. The S1Rs are ER chaperones mainly located at the MAM. Knockdown of S1Rs has been shown to inhibit lipid metabolism, as demonstrated by microarray analysis (Tsai et al., 2012). Previous studies have suggested that S1Rs could be crucial for the differentiation of OLs upon activation by S1R agonists under both physiological and pathological conditions (Hayashi and Su, 2004a; Song et al., 2023). We have demonstrated that S1Rs are widely expressed in OPCs (Pα$^+$) and OLs (CC1$^+$) in adult mice (8 w) *in situ* by using AR^{SDS} protocol. However, investigations into the biological functions of S1Rs in

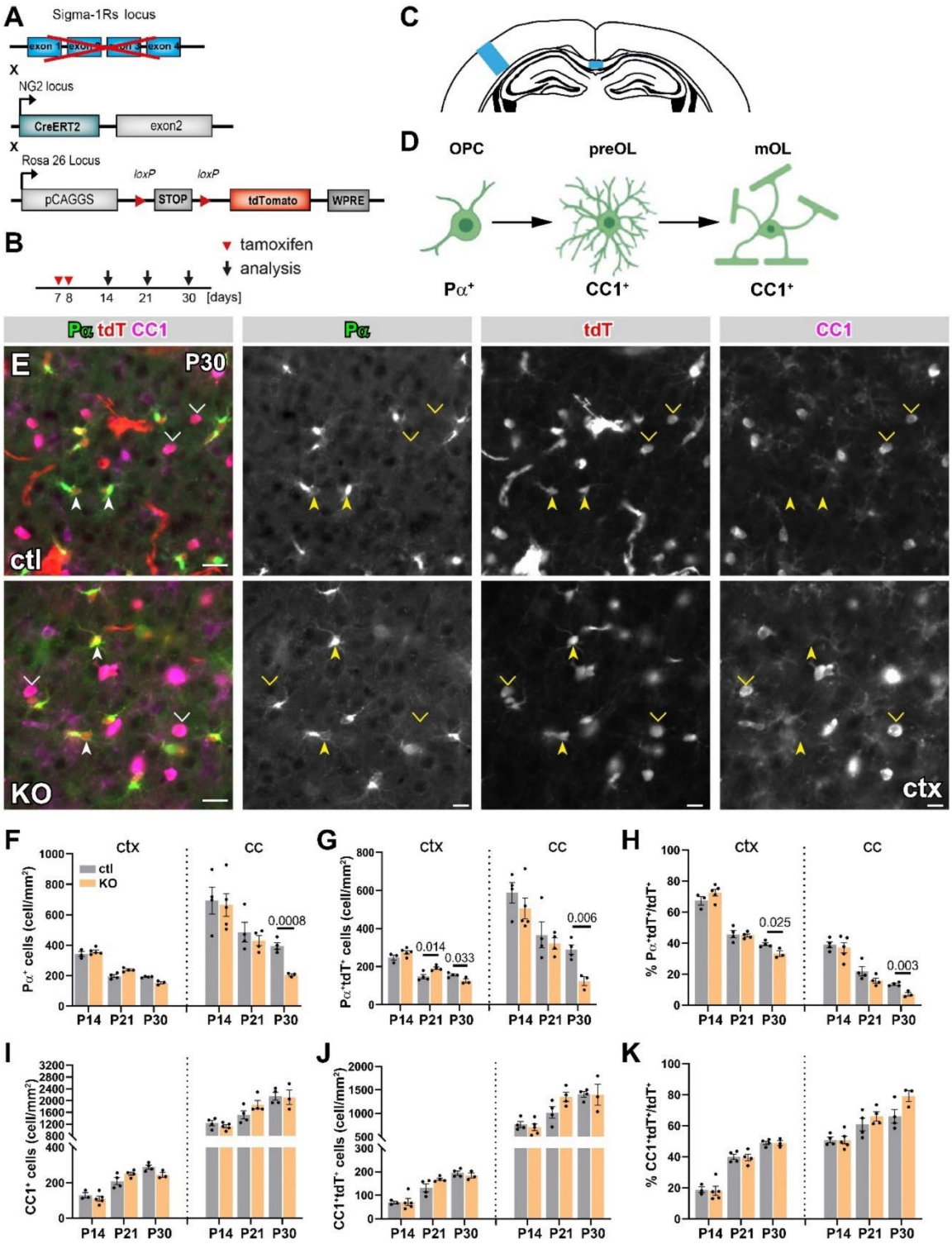

Figure 18. Decreased Pα⁺ OPCs in S1R KO mice at P30. A. Schematic representation of transgenic mice (S1R KO x NG2-CreERT2 x Rosa26-tdTomato) used to track the fate of OPCs in KO mice after tamoxifen induction. **B.** Experimental plan. All mice received tamoxifen injections at P7 and P8, and analysis was performed at P14, P21, and P30. **C.** The blue rectangles show the analyzed areas of ctx and cc. **D.** Schematic representation of the stages studied during OL development. **E.** Representative images of Pα (green) and CC1 (magenta) immunostaining and co-localization with tdTomato (tdT) in the ctx of WT and KO mice at P30. Arrowheads indicate Pα⁺tdT⁺ cells. Open triangles indicate CC1⁺tdT⁺ cells. **F-G.** Quantification of Pα⁺, Pα⁺tdT⁺ cells in ctx and cc of ctl and KO mice at different ages. **H.** The percentage of Pα⁺tdT⁺ cells in all tdT⁺ cells in ctx and cc of ctl and KO mice at different ages. **I-J.** Histograms showing the quantification results of CC1⁺,

CC1⁺tdT⁺ cell density in ctx and cc of ctl and KO mice. **K.** The percentage of CC1⁺tdT⁺ cells of all tdT⁺ in ctx and cc did not differ between ctl and KO mice. Each dot represents one mouse. Scale bar = 20 μm in E.

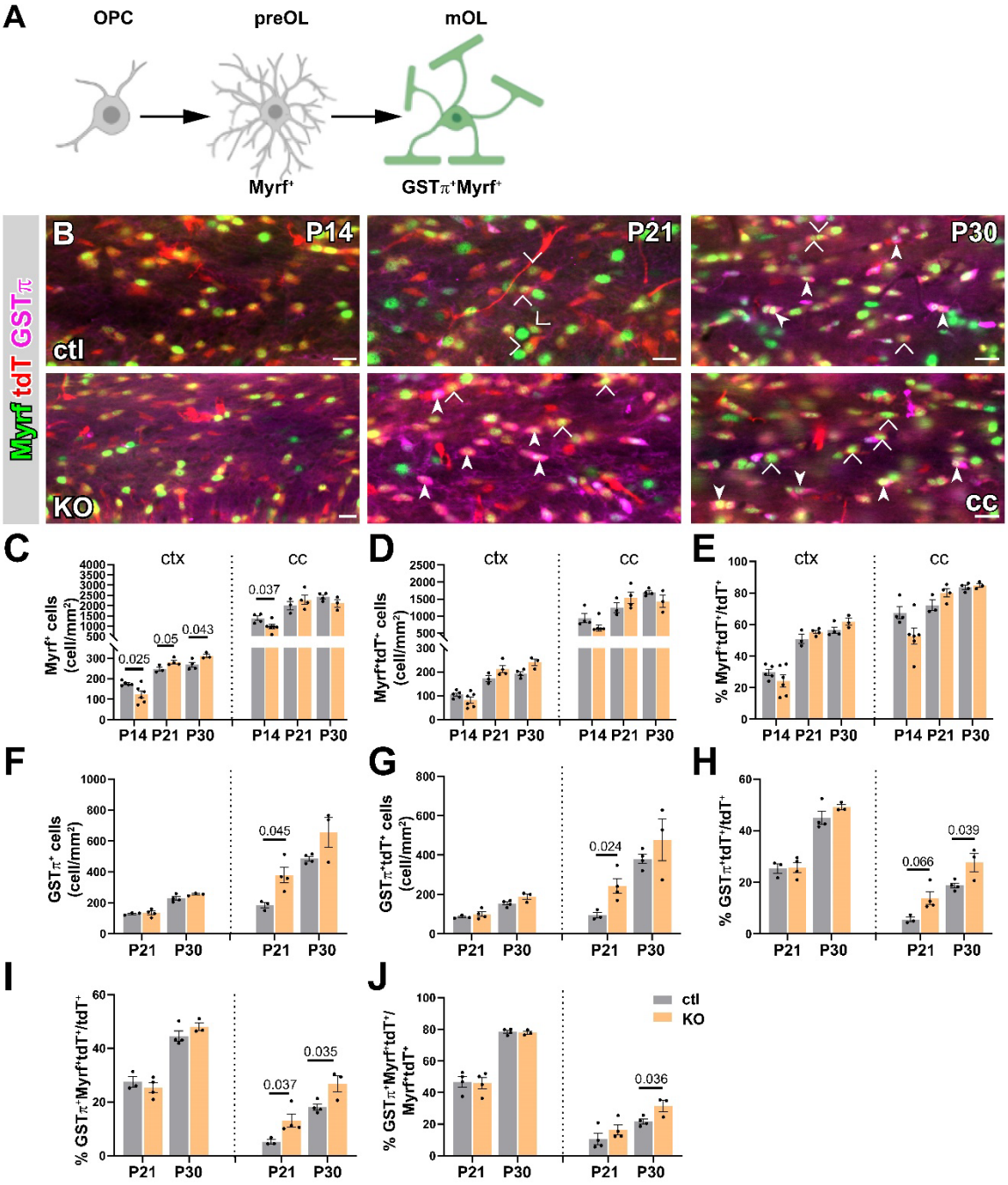

Figure 19. Increased GSTπ⁺ mOLs in cc of S1R KO mice. A. Schematic representation of the analysed stages of OL developmental (highlighted in colour), along with the corresponding markers. **B.** Fluorescent images showing the staining of OL markers (Myrf, GSTπ) in cc of ctl and KO mice. Arrowheads indicate triple positive (Myrf⁺GSTπ⁺tdT⁺) cells. Open triangles indicate Myrf⁺tdT⁺ cells. **C-E.** Quantification results showing the density of Myrf⁺, Myrf⁺tdT⁺ cells and the percentage of Myrf⁺tdT⁺ cells among all tdT⁺ cells in ctx and cc of ctl and KO mice. **F-H.** Quantitative bar graphs showing the density of GSTπ⁺, GSTπ⁺tdT⁺ cells, and the percentage of GSTπ⁺tdT⁺ among all tdT⁺ cells in ctx and cc of ctl and KO mice. **I-J.** Quantification results of the percentage Myrf⁺GSTπ⁺tdT⁺ among tdT⁺ or Myrf⁺tdT⁺ cells in ctx and cc of ctl and KO mice at P21 and P30. Each dot represents one mouse. Scale bar = 20 μm.

OL lineage cells are still lacking. In the current work, we investigated the biological functions of S1Rs in OLs during development and in adulthood by temporal control of *Sigma1r* gene expression using $S1R^{fl/fl}$ mice.

7.3.1 Increased S1R expression during OPC differentiation into OL

To specifically focus on developmental phases, we expanded our analysis to investigate the expression pattern of S1Rs during OL development at postnatal age. Co-immunostaining for S1R with Pα, BCAS1 (preOL marker) and GSTπ (mOL marker) was performed on brain slices obtained at postnatal day 21 (P21). Specific staining for S1R, identified by the ER-ring like structure, was observed in these three cell types at this age (Figure 16A-C). We further compared the relative expression levels of S1Rs in these cell types *in situ*. The MFI of S1Rs in individual cells was measured in the deep cortical layer. Using the S1R expression levels in $Pα^+$ cells as a control, the comparison result showed slightly higher expression of S1Rs in $GSTπ^+$ mOLs (1.16 ± 0.04%), while $BCAS1^+$ cells expressed comparable levels of S1R protein (1.06 ± 0.02%) compared to $Pα^+$ cells (Figure 16D). These results suggest that S1Rs are involved in the modulation of OL lineage cell maturation during OL development.

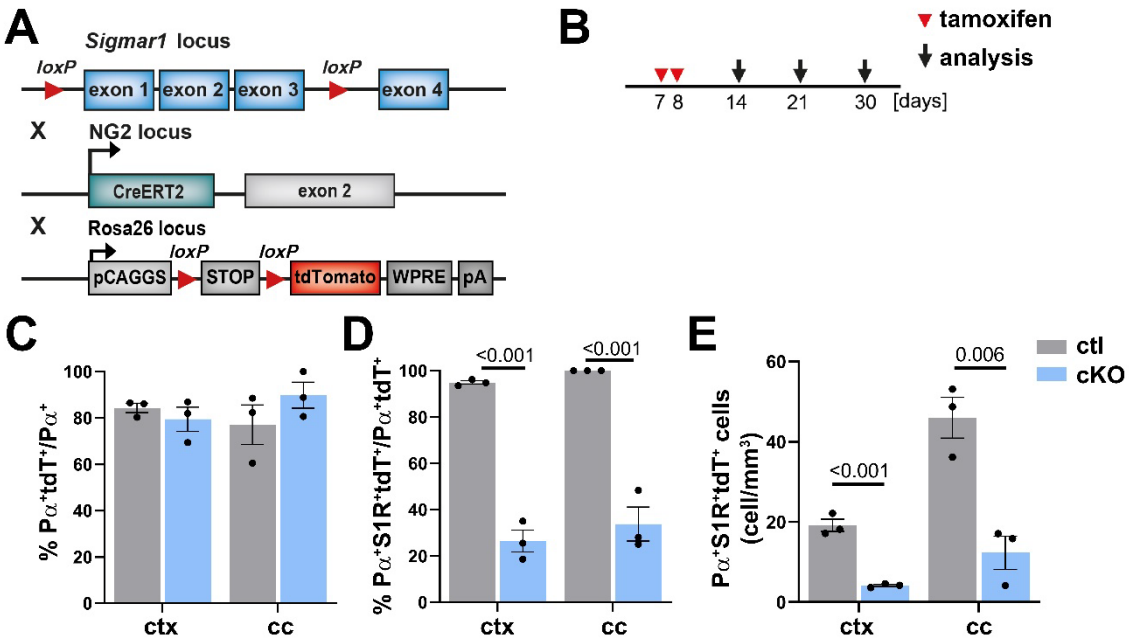

Figure 20. OPC-specific knockout of S1Rs in cKO mice at P21. A. Schematic diagram of the transgenic mice for conditional knockout of S1Rs in OPCs (S1R cKO) after tamoxifen injection, and the fate of OL lineage cells is tracked using reporter expression (Rosa26-tdTomato). **B.** The experimental plan, indicating the timing of tamoxifen injection and the analysis time points (P14, P21, and P30). **C.** Quantification of the percentage of $Pα^+tdT^+$ among $Pα^+$ cells, indicating the efficiency of recombination at P21. **D.** The percentage of $Pα^+tdT^+$ cells expressing S1Rs in $Pα^+tdT^+$ cells, demonstrating the significant deletion of S1Rs in OPCs both in the ctx and cc of ctl and cKO mice. **E.** Quantification analysis of $Pα^+S1R^+tdT^+$ cell density in the ctx and cc of ctl and cKO mice. Each dot represents one mouse.

7.3.2 Accelerated maturation of OLs in S1R KO mice during development

To investigate the potential biological functions of S1Rs in the OLs *in vivo*, we preliminarly analysed OL development in S1R KO mice, with a particular focus on the somatosensory ctx and cc. OLs are responsible for myelin formation of axons, which protects and provides nutritional support to neurons (Miller, 2002; Fünfschilling et al., 2012). We investigated the

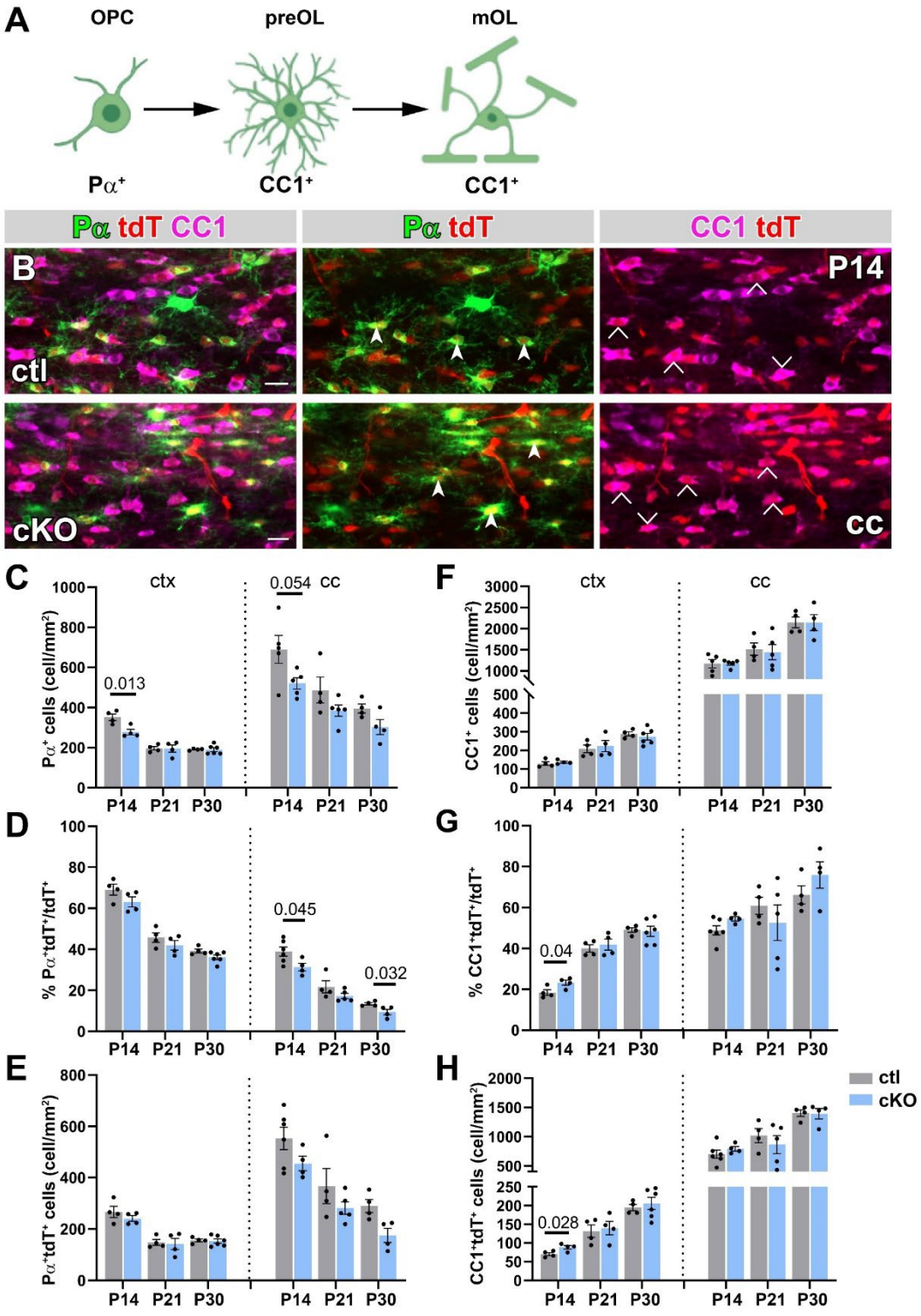

Figure 21. OL differentiation was unaltered in cKO mice. A. Schematic representation of the analysed stages of OL developmental (highlighted in colour) and the corresponding markers used for analysis. **B.** Representative immunohistochemical staining in the cc of ctl and cKO mice showing the co-localization of tdT with Pα (green) and CC1 (magenta) at P14. Arrowheads indicate double positive ($Pα^+tdT^+$) cells and open triangles indicate $CC1^+tdT^+$ cells. **C, F.** Quantitative analysis of $Pα^+$ OPCs in ctx and cc of ctl and cKO mice at different time points. **D, G.** The proportion of $Pα^+tdT^+$ or $CC1^+tdT^+$ cells among all tdT^+ cells in ctx and cc of ctl and cKO mice. **E, H.** Quantification of $Pα^+tdT^+$ or $CC1^+tdT^+$ cells in ctx and cc of ctl and cKO mice at different ages. Each dot represents one mouse. Scale bar = 20 μm.

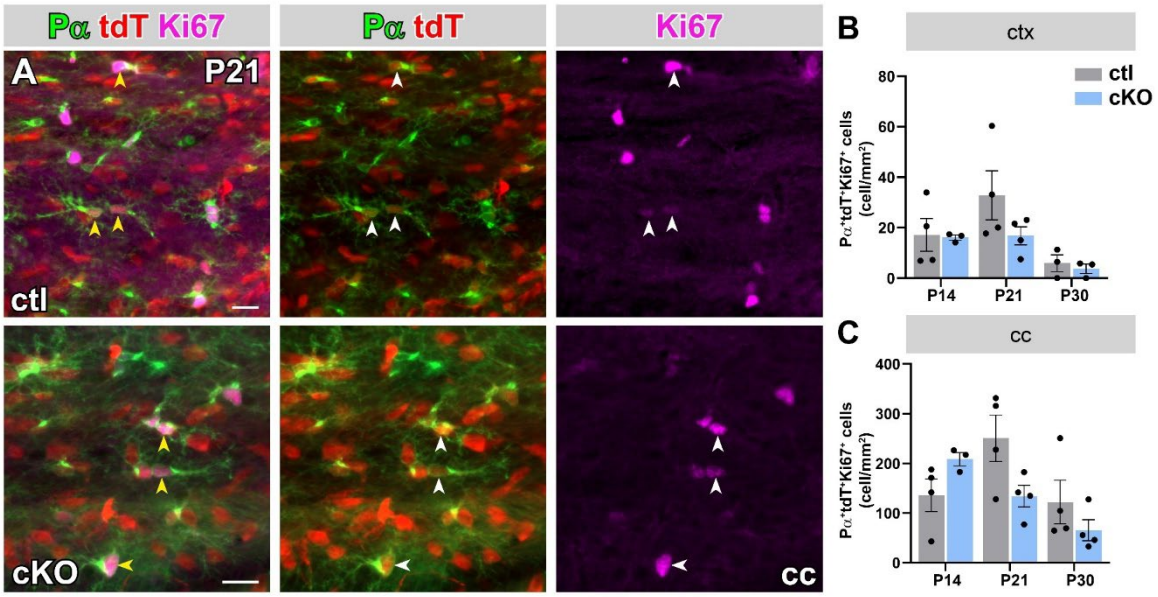

Figure 22. Conditional deletion of S1Rs in OPCs does not affect the proliferation of OPCs. A. Representative immunohistochemical images of Pα (green) and Ki67 (magenta) in the cc of ctl and cKO mice at P21. Arrowheads indicate the co-localization of Ki67 with $Pα^+tdT^+$ cells, indicating proliferating OPCs. **B-C.** Quantitative analysis of triple positive cell ($Pα^+tdT^+Ki67^+$) numbers in the ctx (**B**) and cc (**c**) of ctl and cKO mice at P14, P21 and P30. Each dot represents one mouse. Scale bar = 20 µm.

postnatal myelination of S1R KO mice by using IHC for MBP in the forebrain. Cortical myelination occurs from the deep cortical layer near the white matter to the upper cortical layer. We measured the proportion of ctx coverage with immunolabelling of MBP to assess the extent of cortical myelination at different ages (Figure 17A). Compared to ctl mice, we observed a reduced percentage of myelinated ctx in KO mice at P14 (P=0.003, Figure 17C). Additionally, we analysed myelination by measuring the MFI of MBP staining in specific regions (cortical L3-4) at P21 and P30. Compared to ctl mice, KO mice showed only a slight tendency toward an increased percentage of MBP coverage in the ctx (Figure 17D and Supplementary Figure 7A-B). We also examined the WM by measuring the percentage of MBP^+ area in all measured cc regions from P14 to P30 (Figure 17B). No significant changes in MBP coverage were observed at any time point (Figure 17E). These findings suggest that S1Rs may be involved in the initiation of myelin formation in the ctx during the early postnatal days (till P14).

In addition to myelination, we examined OL differentiation in S1R KO mice. To map the fate of OPCs, we crossbred S1R KO mice with NG2-CreERT2 mice and a reporter mouse line Rosa26-tdTomato (Figure 18A). Cre activity was induced at P7 and P8 by tamoxifen administration, and the analysis was conducted at different time points (P14, P21 and P30, Figure 18B). Similarly, we focused on the somatosensory ctx and cc in the forebrain (Figure 18C). Immunochemical staining was performed for the OPC marker Pα and OL marker CC1 on brain slices at different time points (Figure 18D-E). The total number of $Pα^+$ OPCs decreased with development in ctx and cc of ctl and KO mice. Moreover, in the cc of KO mice, $Pα^+$ cells decreased at P30 compared to ctl mice (P= 0.0008, Figure 18F). The $CC1^+$ OLs increased with development in both ctl and KO mice, but the number of $CC1^+$ cells were comparable between ctl and KO mice (Figure 18I). Moreover, among all tdTomato-

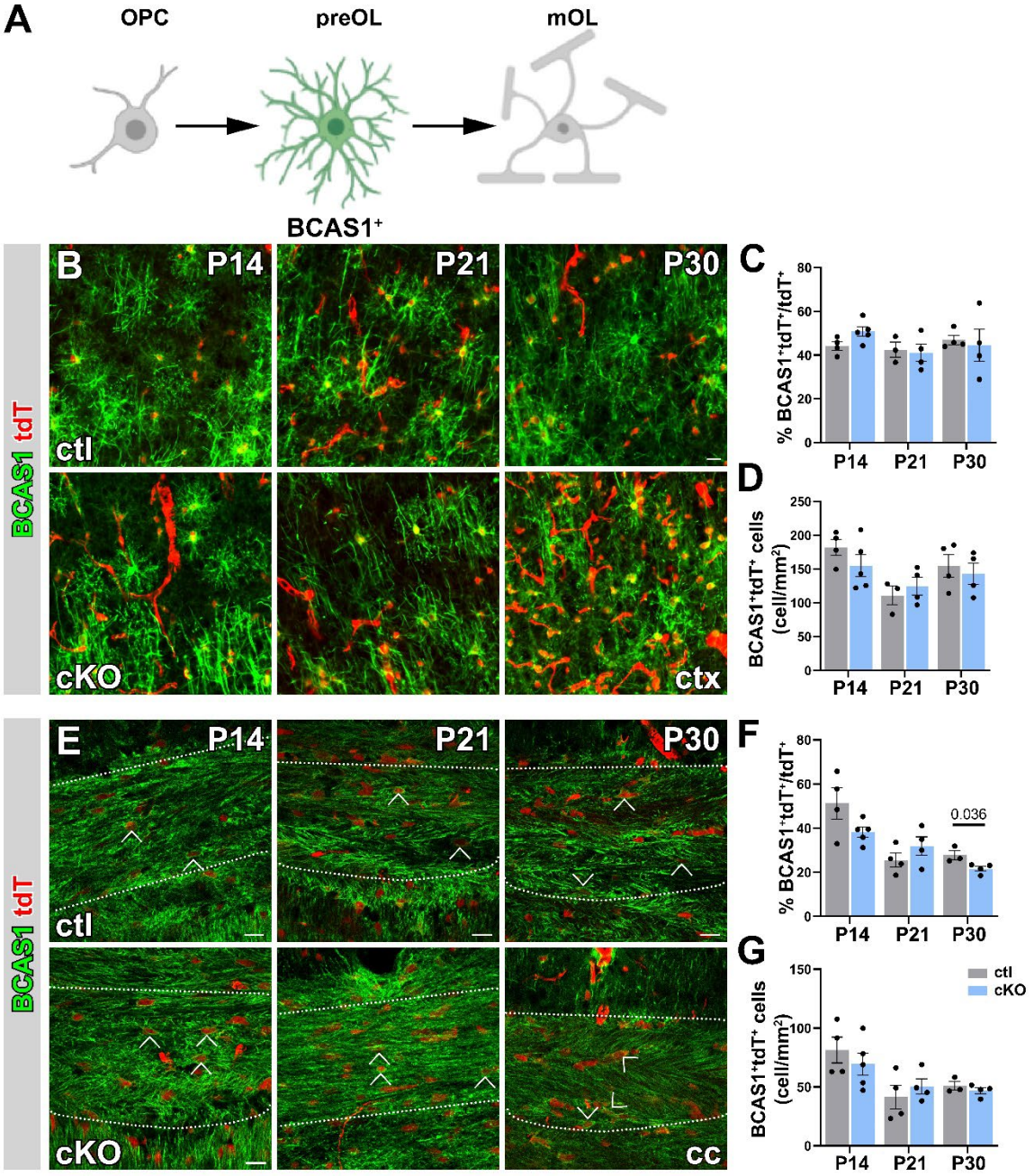

Figure 23. The amount of preOL was unchanged in cKO mouse brain. A. Schematic representation of the analysed OL developmental stages and the corresponding markers. **B.** Representative immunohistochemical staining in ctx of ctl and cKO mice, demonstrating the co-localization of tdT with BCAS1 at P14, P21, and P30. **C.** The percentage of BCAS1$^+$tdT$^+$ cells among all tdT$^+$ cells in ctx of ctl and cKO mice at different ages. **D.** Quantitative analysis of BCAS1$^+$tdT$^+$ cells in ctx of both genotypes. **E.** Confocal images showing the co-localization of tdT with BCAS1 in cc of ctl and cKO mice at different ages. Open arrows indicate BCAS1$^+$ cells. **F-G.** Quantitative analysis of the percentage of BCAS1$^+$tdT$^+$ cells in all tdT$^+$ cells and the total number of BCAS1$^+$tdT$^+$ cells in cc of ctl and cKO mice at P14, P21, and P30. Each dot represents one mouse. Scale bar = 20 μm.

positive (tdT$^+$) cells, we observed a decrease in the percentage and density of Pα$^+$tdT$^+$ cells, while the percentage and density of CC1$^+$tdT$^+$ cells increased in both genotypes with development (Figure 18G-H, J-K). Specifically, at P30, KO mice showed a significant decrease in the percentage or in density of Pα$^+$tdT$^+$ cells in both ctx (P=0.025) and cc (P=0.003) (Figure 18G-H). However, there was no significant increase in CC1$^+$tdT$^+$ cells in

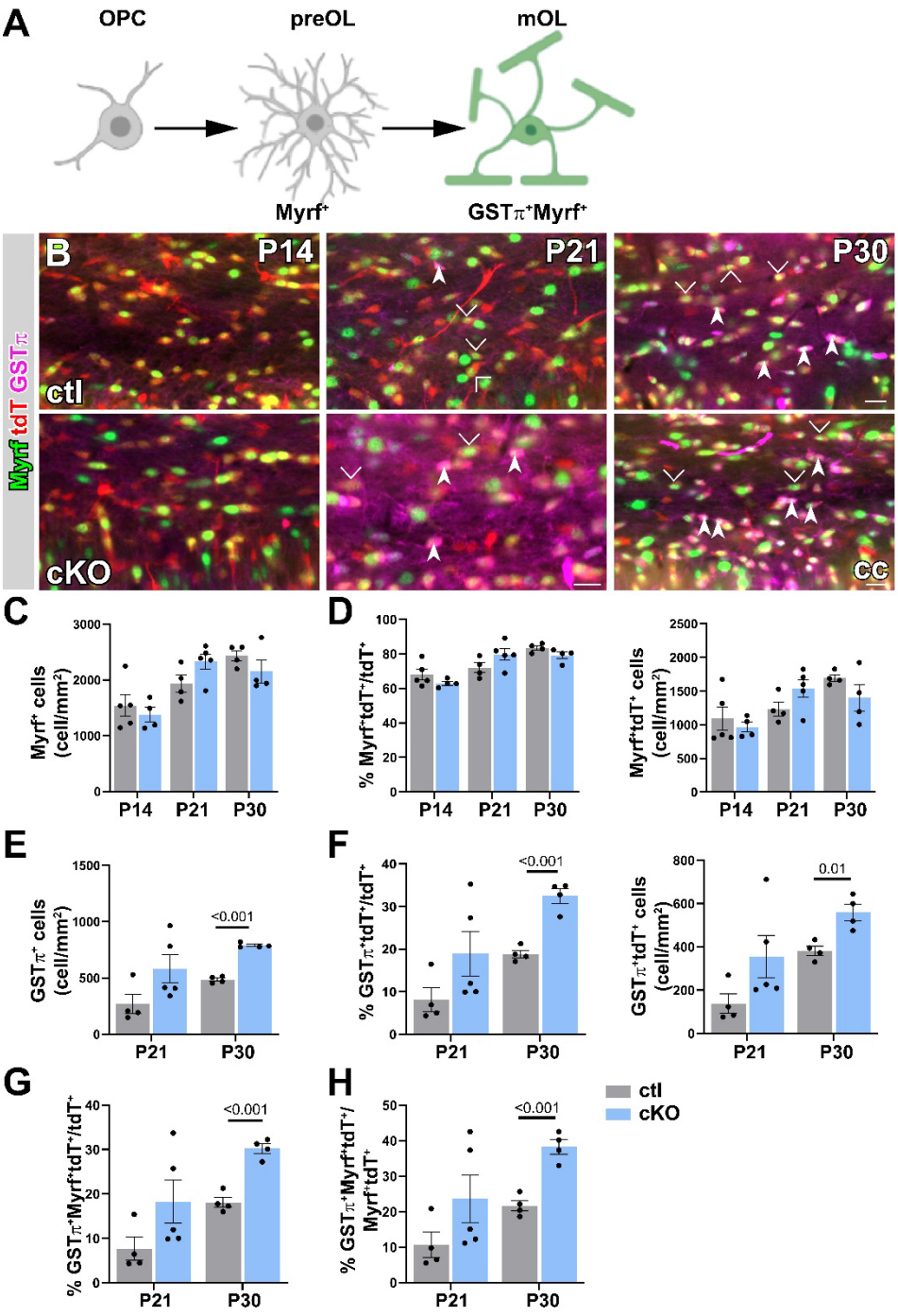

Figure 24. Increased GSTπ⁺ mOLs in cc of cKO mice. A. Schematic representation of the analysed OL developmental stages and the corresponding markers. **B.** Representative immunohistochemical images of OL markers (Myrf, GSTπ) in cc of ctl and cKO mice at P14, P21, and P30. Arrowheads indicate triple positive (Myrf⁺GSTπ⁺tdT⁺) cells. Open triangles indicate Myrf⁺tdT⁺ cells. **C.** Quantification of Myrf⁺ cell density in cc of ctl and cKO mice at different ages. **D.** Quantification of Myrf⁺tdT⁺ cells and the percentage of Myrf⁺tdT⁺ cells among all tdT⁺ cells in cc of ctl and cKO mice at different ages. **E.** Quantification of GSTπ⁺ cell density in cc of ctl and cKO mice. **F.** Histograms of GSTπ⁺tdT⁺ cells and percentage of Myrf⁺tdT⁺ cells among all tdT⁺ cells in cc from ctl and KO mice at P21 and P30. **G-H.** Quantitative analysis of the percentage of Myrf⁺GSTπ⁺tdT⁺ in tdT⁺ or Myrf⁺tdT⁺ cells in cc of ctl and cKO mice at P21 and P30. Each dot represents one mouse. Scale bar = 20 µm.

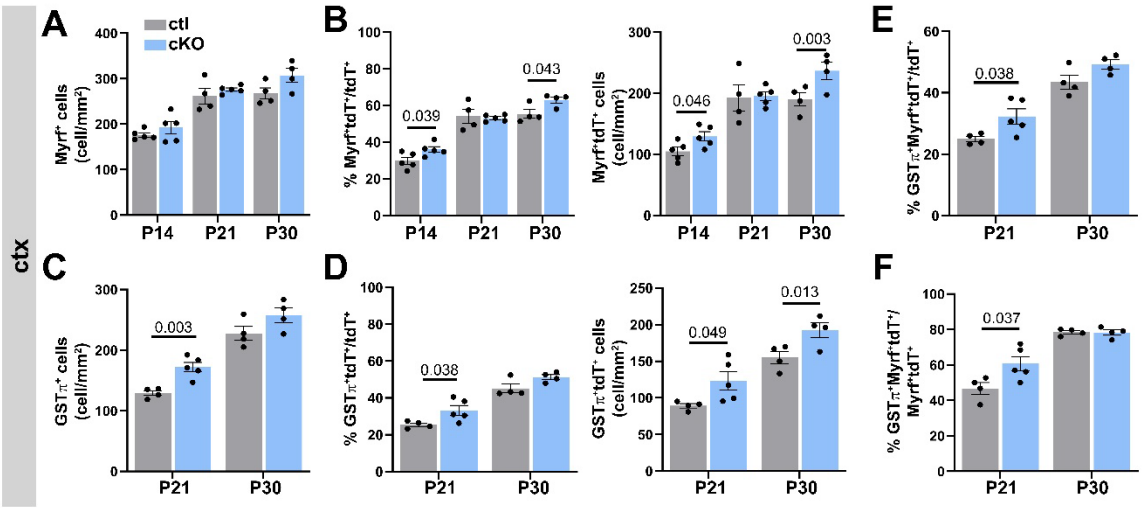

Figure 25. Increased GSTπ⁺ mOLs in ctx of cKO mice. A. Quantification of the number of Myrf⁺ cells in ctx of ctl and cKO mice at P14, P21, and P30. **B.** Quantification of Myrf⁺tdT⁺ cell density and percentage of Myrf⁺tdT⁺ cells among all tdT⁺ cells in ctx from ctl and cKO mice at different ages. **C.** Quantification of GSTπ⁺ cell density in ctx of ctl and cKO mice. **D.** Histograms of GSTπ⁺tdT⁺ cells and the percentage of GSTπ⁺tdT⁺ cells among all tdT⁺ cells in ctx of ctl and cKO mice at P21 and P30. **E-F.** Quantitative analysis of the percentage of Myrf⁺GSTπ⁺tdT⁺ cells among tdT⁺ or Myrf⁺tdT⁺ cells in ctx of ctl and cKO mice at P21 and P30. Each dot represents one mouse.

KO mice at this age, with only an increasing trend observed in cc (Figure 18J-K).

To analyze the expression of OL markers in S1R KO mice, we performed IHC staining for Myrf and GSTπ (Figure 19A-B). At P14, Myrf⁺ cells were reduced in both ctx (P=0.025) and cc (P= 0.037) (Figure 19C). The number of Myrf⁺tdT⁺ cells exhibited the same decreasing trend (Figure 19D). But there was only a decreasing trend in the percentage of Myrf⁺tdT⁺ among all tdT⁺ cells in both the ctx (ctl: 29.76 ± 1.96%, KO: 24.33 ± 3.76%) and the cc (ctl: 67.43 ± 3.85%, KO: 52.54 ± 5.08%) (Figure 19E). However, an increase in the number of Myrf⁺ cells was observed in ctx at P21 (P=0.05) and P30 (P=0.043), while the percentage and density of Myrf⁺tdT⁺ cells showed only a slight increasing trend (Figure 19C-E). Furthermore, there was a significant increase in the expression of GSTπ⁺ cells in the cc of KO mice at P21 (P=0.045), and a tend towards an increase at P30 (P= 0.098), but no change was observed in the ctx (Figure 19F). The same changes were observed for the percentage and density of GSTπ⁺tdT⁺ in KO mice (Figure 19G, H). We also analysed double positive cells for Myrf and GSTπ, which represent a cohort of late maturation OLs. In the cc, there was an increased percentage of GSTπ⁺Myrf⁺ cells in KO mice among all tdT⁺ (P21: ctl: 5.19 ± 0.77%, KO: 13.07 ± 2.45%; P30: ctl: 18.10 ± 1.12%, KO: 26.78 ± 3.08%; Figure 19I) or among Myrf⁺tdT⁺ cells (P21: ctl: 10.66 ± 3.52%, KO: 16.38 ± 3.11%; P30: ctl: 21.71 ± 1.49%, KO: 31.57 ± 3.57%) (Figure 19J) at both P21 and P30. These findings suggest that the deletion of S1Rs in OPCs leads to the early maturation of OLs during development.

7.3.3 Unaltered proliferation and differentiation of OPCs in S1R cKO mice during development

To elucidate the role of S1Rs in OL maturation in specific cell types, we took advantage of $S1R^{fl/fl}$ mice and crossbred with NG2-CreERT2 mice to generate S1R conditional deletion in OPCs (S1R cKO) mice. To follow the fate of OPCs, we further crossbred S1R cKO mice

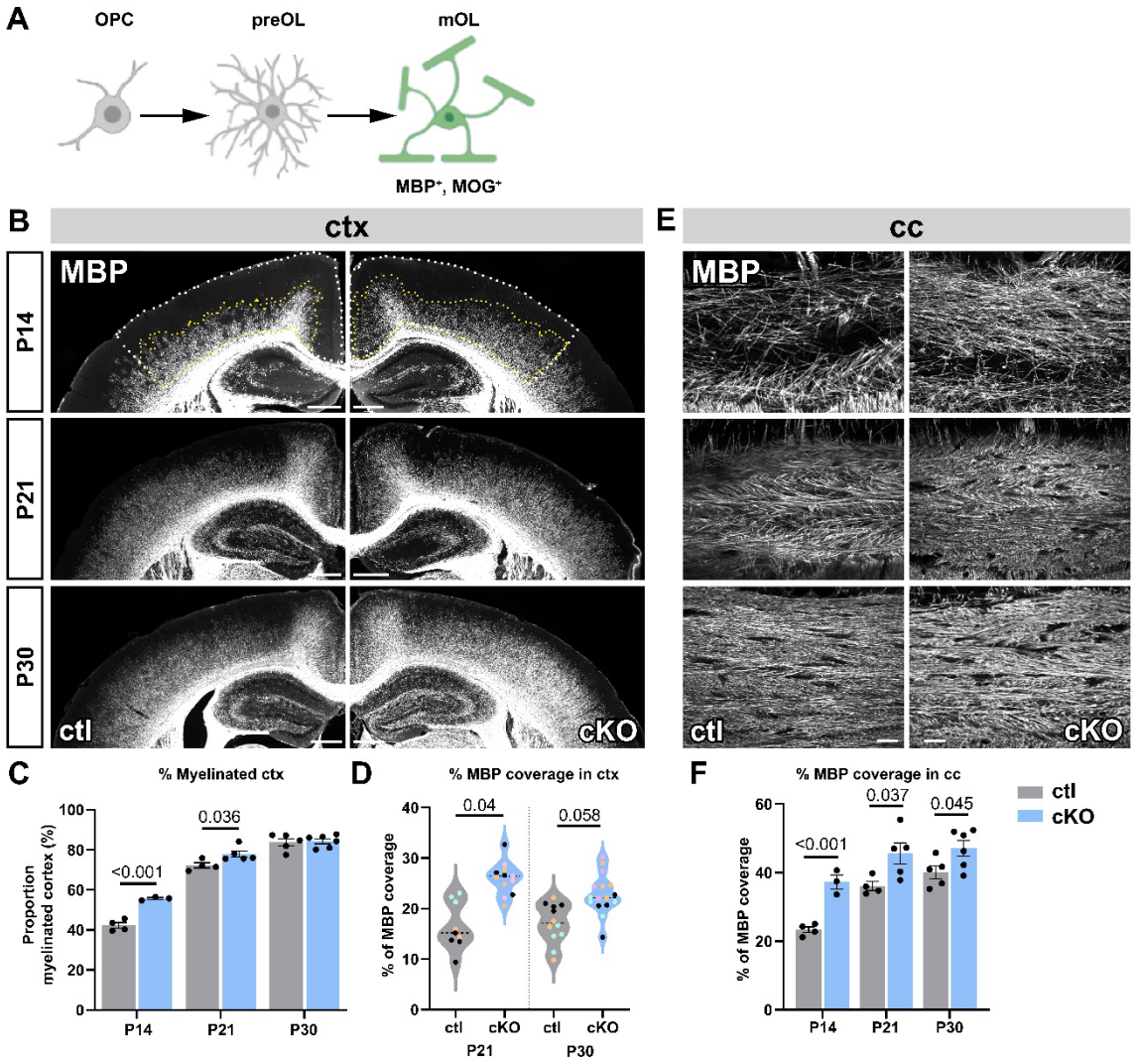

Figure 26. Increased myelination in cKO mouse brain during development. A. Schematic representation of the analysed OL developmental stages and the corresponding markers. **B.** Epifluorescent images of MBP staining on coronal brain sections of ctl and cKO mice at P14, P21, and P30. **C.** Histograms showing the percentage of myelinated ctx in the measured cortical area at P14, P21 and P30. **D.** The area occupied by MBP staining divided by the whole image area in ctl and cKO ctx at P21 and P30. Images were taken by confocal microscopy. Each dot represents a slice, and different colours represent different mice. **E.** Confocal images displaying MBP staining in the cc of ctl and cKO mice at different time points. **F.** The percentage of MBP$^+$ occupied area in all measured cc area of ctl and KO mice at P14, P21, and P30. Each dot represents one mouse in C and F. Scale bar = 500 µm in A, 50 µm in B.

with the Rosa26-tdTomato reporter mouse line (Figure 20A). Cre activity was induced by tamoxifen at P7 and P8, and the analysis was conducted at P14, P21, and P30 (Figure 20B). Meanwhile, we examined the deletion of S1Rs in OPCs two weeks (P21) after tamoxifen administration. The Cre recombination ratio, represented by the percentage of Pα$^+$tdT$^+$/Pα$^+$, was approximately 80% in both ctx and cc for both genotypes (Figure 20C). In cKO mice, S1R expression in Pα$^+$ OPCs was significantly reduced, as indicated by the decreased percentage (ctx and cc: P<0.001) and density (ctx: P<0.001; cc: P=0.006) (Figure 20D-E).

Next, we investigated the differentiation of OPCs during development in S1R cKO mice by immunostaining for Pα and CC1 (Figure 21A-B). In the ctx, the total number of Pα$^+$ OPCs

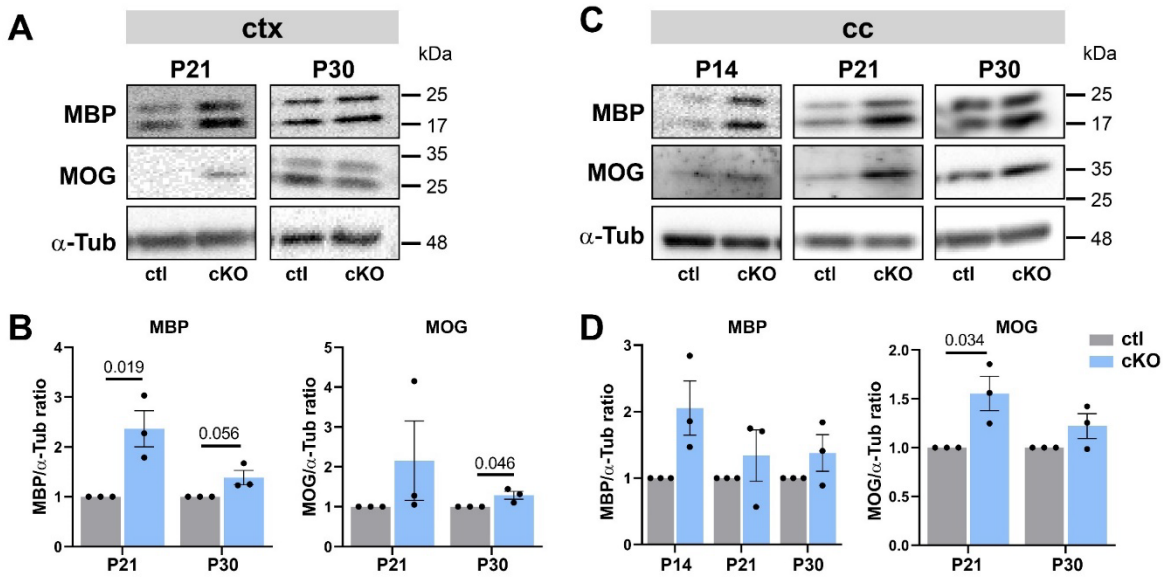

Figure 27. Increased expression of myelin-related genes in S1R cKO mice. A, C. Representative western blot images of MBP (16 and 18 kDa) and MOG (28 kDa) in protein lysates from the ctx (A) and cc (C) of ctl and cKO mice at different ages. **B, D.** Quantitative analysis of grayscale values of MBP and MOG protein levels, which were normalized to that of α-Tubulin used as a loading control. Each point represents one mouse.

decreased, while the expression of CC1⁺ OLs increased with development. However, there was no significant difference between ctl and cKO mice, except for a significant decreased expression of Pα⁺ cells at P14 (*P*=0.013). In the cc, we did not observe any significant changes in Pα⁺ and CC1⁺ cell density in cKO mice (Figure 21C and F). Focusing on tdT-labeled cells, we observed a decreasing trend of Pα⁺tdT⁺ cells and an increased number of CC1⁺tdT⁺ (*P*=0.04) cells in ctx at P14 (Figure 21D-G), while there was no significant difference in percentage and density at P21 and P30. In the cc, the percentage of Pα⁺tdT⁺ cells were decreased in cKO mice at all time points (P14: *P*=0.045; P21: *P*=0.17; P30: *P*= 0.032), but the density of Pα⁺tdT⁺ cells showed only a tendency in the same direction (Figure 21D-E). However, there was no alteration in CC1⁺tdT⁺ cells between ctl and cKO mice at all analysed ages (Figure 21G-H). With age, the decreased Pα⁺ OPCs and the increased CC1⁺ OLs suggest a normal progression of OL differentiation in cKO mice.

Furthermore, we examined the proliferation of OPCs by performing immunostaining for Pα and Ki67 on brain sections (Figure 22A). Both in ctx and cc; the Pα⁺tdT⁺Ki67⁺ cells did not differ between ctl and cKO mice (Figure 22B-C). This indicates that S1Rs do not affect the proliferation of OPCs during development.

OL development includes an intermediate state in which the preOLs are formed (Trapp et al., 1997; Hughes and Stockton, 2021). Previous studies have shown that BCAS1 expression serves as a marker for both preOLs and newly formed OLs (Fard et al., 2017). To investigate the changes of preOLs, we performed IHC for BCAS1 on brain slices and analysed them at different ages (Figure 23A, B and E). At all time points, we did not observe any significant difference in the percentage of BCAS1⁺tdT⁺ cells or the density in the ctx between ctl and cKO mice (Figure 23C-D). In the cc, we observed decreased BCAS1⁺tdT⁺ cells after P14 in both ctl and cKO mice, indicating the progression of OPCs to the OL stage. Compared to ctl mice, there was a decreased trend in the number of BCAS1⁺ tdT⁺ cells in cKO mice at P14 and a significant decrease in the percentage at P30 in cKO mice (*P*=0.036) (Figure 23F). However, the density of BCAS1⁺tdT⁺ cells showed no significant

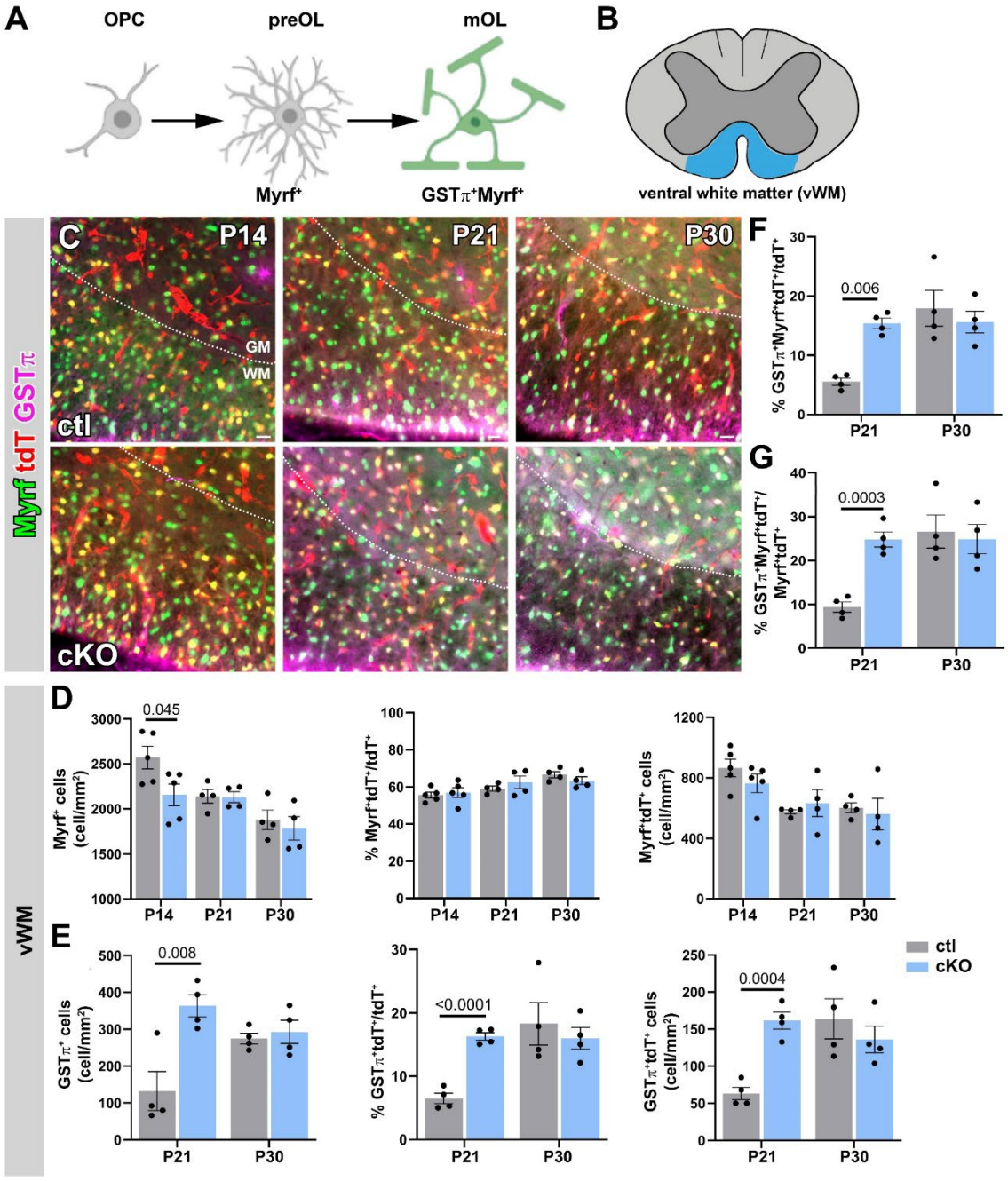

Figure 28. Conditional deletion of S1Rs in OPCs leads to precocious maturation of spinal OLs. A. Schematic representation of the analysed OL developmental stages and the corresponding markers. **B.** Schematic image of the spinal cord, highlighting the regions of the ventral white matter (vWM) that were analysed. **C.** Representative immunostaining images of Myrf and GSTπ in the spinal cord of ctl and cKO mice at different ages. **D.** Quantitative expression of Myrf$^+$, Myrf$^+$tdT$^+$ numbers, and the percentage of Myrf$^+$tdT$^+$ in all tdT$^+$ cells in vWM of ctl and cKO mice at different ages. **E.** Quantitative results of the density of GSTπ$^+$, GSTπ$^+$tdT$^+$ cells and the percentage of GSTπ$^+$tdT$^+$ cells in all tdT$^+$ cells in the vWM of ctl and cKO mice at P21 and P30. **F-G.** Quantitative analysis of the percentage of Myrf$^+$GSTπ$^+$tdT$^+$ cells among all tdT$^+$ or Myrf$^+$tdT$^+$ cells in the spinal vWM of ctl and cKO mice at P21 and P30. Each dot represents one mouse. Scale bar = 20 μm.

difference between ctl and cKO mice (Figure 23G). These findings suggest that OPCs in cKO mice retain the capacity to differentiate into preOLs and further progress into mOLs.

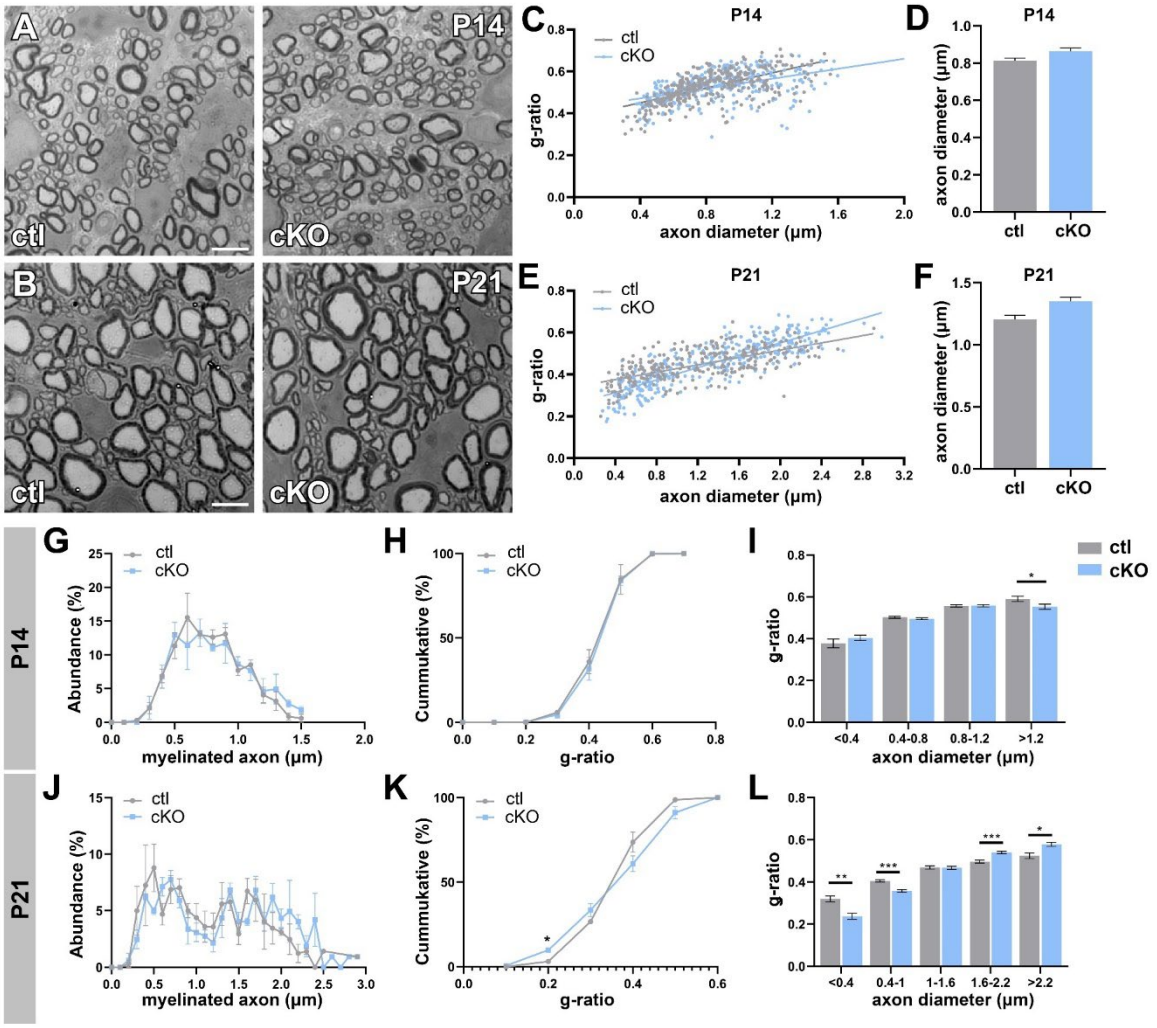

Figure 29. Altered myelination distribution of axons in the spinal vWM of cKO mice at P21. A-B. Representative confocal images for toluidine blue on semithin sections of spinal cord from ctl and cKO mice at P14 and P21. **C, E.** Scatter plot showing the g-ratio for individual axons in the spinal vWM of ctl and cKO at P14 (C) and P21 (E). The linear regression analysis of slope was performed: F= 13.04, *P*=0.0003 of P14 mice; F= 56.47, *P*< 0.0001 of P21 mice. **D, F.** Histograms showing the mean diameter of myelinated axon of ctl and cKO mice at P14 (D) and P21 (F). **G, J.** The axon size distribution is represented by the accumulation ratio of ctl and cKO mice at P14 (G) and P21 (J). **H, K.** Cumulative frequency of g-ratio measured for single axons in ctl and cKO mice at P14 (H) and P21 (K). **I, L.** Mean g-ratio grouped by different axon size were calculated for ctl and cKO mice at P14 and P21. At P14, 337 myelinated axons of ctl group and 324 myelinated axons of cKO group were measured. At P21, 285 myelinated axons of ctl group and 323 myelinated axons of cKO group were measured. **P*<0.05; ***P*<0.001; ****P*< 0.0001. N = 3 mice per genotype. Scale bar = 5 μm.

7.3.4 Earlier maturation of OLs in the brain of S1R cKO mice during development

We further investigated the expression of OL markers (Myrf, GSTπ) in S1R cKO mice during development (Figure 24A-B). In the cc, the expression levels of Myrf protein was comparable between ctl and cKO mice at all analysed ages (Figure 24C-D). In addition, we observed an increase in the number of GSTπ$^+$ mOLs in cKO mice from P21 to P30 (*P*<0.001) (Figure 24E). Among all tdT$^+$ cells, the increase in GSTπ$^+$tdT$^+$ cells was indicated both by percentage and density at P21 and P30 (Figure 24E). We further confirmed this by quantifying the percentage of GSTπ$^+$Myrf$^+$ cells among all tdT$^+$ or Myrf$^+$tdT$^+$ cells. As shown in Figure 24 G and H, more GSTπ$^+$Myrf$^+$tdT$^+$ cells were detected in cKO mice from P21

onwards, which indicates there are more OLs in late maturation stage in cKO mice (Figure 24G, H). Meanwhile, we also analysed the expression of OL markers in the ctx. Consistent with the changes in the cc, we observed an increase in GSTπ$^+$ cells in cKO mice both at P21 (P= 0.003) and a tendency towards an increase at P30 (Figure 25C), while there was no significant changes in Myrf$^+$ cell density (Figure 25A). Regarding the percentage of tdT$^+$ cells, cKO mice exhibited a higher percentage of Myrf$^+$tdT$^+$ cells compared to ctl mice at P14 (P=0.039) and P30 (P=0.043) (Figure 25B). This finding was supported by the increased density of Myrf$^+$tdT$^+$ cells in cKO mice at P14 (P=0.046) and P30 (P=0.003) (Figure 25B). Although there was no significant difference in Myrf$^+$tdT$^+$ cells at P21 between the genotypes (Figure 25B), we observed a high percentage (P=0.038) and density (P= 0.049) of GSTπ$^+$tdT$^+$ cells in cKO mice at P21 (Figure 25D). This was further confirmed by analyzing the proportion of GSTπ$^+$Myrf$^+$tdT$^+$ among tdT$^+$ cells, showing a higher percentage in cKO mice at P21 (P=0.038) and a tendency towards an increase at P30 (Figure 25E). The proportion of GSTπ$^+$Myrf$^+$tdT$^+$ cells among Myrf$^+$tdT$^+$ cells increased only at P21 but not at P30 in cKO mice, which may be due to an increase in Myrf$^+$tdT$^+$ cells at P30. Collectively, these findings suggest that the deletion of S1Rs in OPCs leads to the earlier maturation of OLs during development.

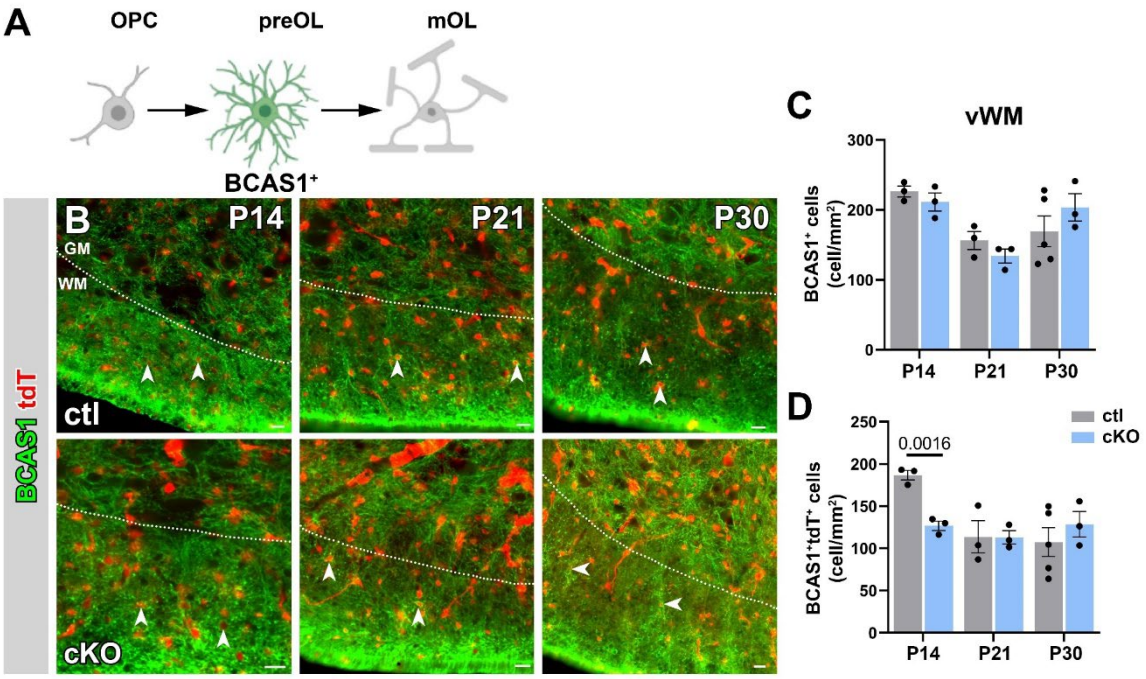

Figure 30. BCAS1 immunolabelled preOLs was unaltered in the spinal vWM of S1R cKO mice. **A.** Schematic representation of the analysed OL developmental stages (highlighted in colour) and the corresponding markers. **B.** Representative immunohistochemical staining images in the spinal cord of ctl and cKO mice, demonstrating the co-localization of tdT with BCAS1 (green) in the WM at P14, P21, and P30. Arrowheads indicate BCAS1$^+$tdT$^+$ cells. **C-D.** Quantification of BCAS1$^+$, BCAS1$^+$tdT$^+$ cells in the spinal WM of ctl and cKO mice at different ages. Each dot represents one mouse. Scale bar = 20 µm.

7.3.5 Increased expression of myelin proteins in the forebrain of S1R cKO mice

We examined the expression of myelin-related proteins in S1R cKO mice during development. We performed IHC for MBP on brain slices. Firstly, we assessed the extension of myelin formation in the ctx during development (Figure 26B). We observed a

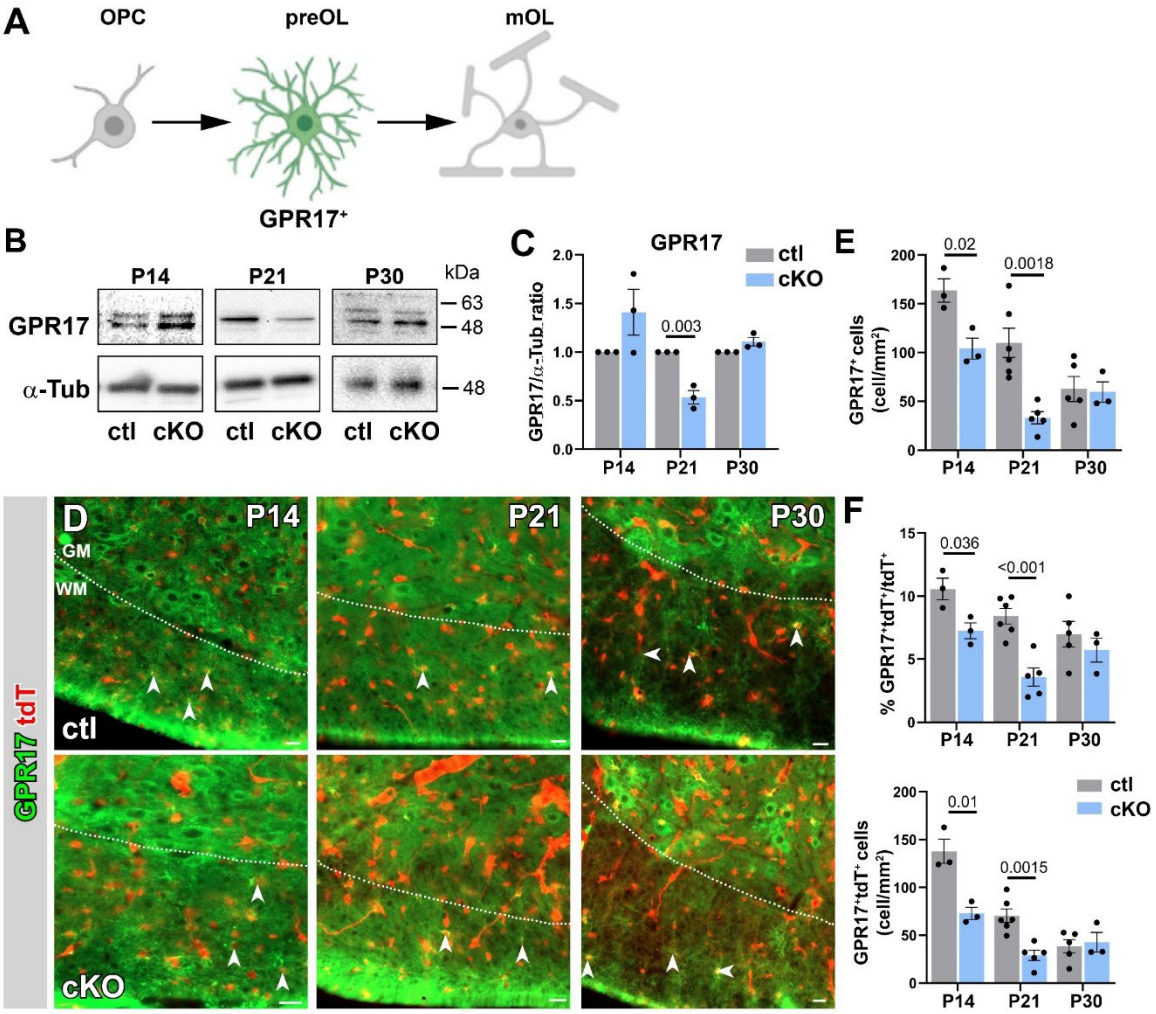

Figure 31. Reduced GPR17 immunolabelled preOLs in the spinal vWM of S1R cKO mice. A. Schematic representation of the analysed OL developmental stages and the corresponding markers. **B.** Western blot of GPR17 (50 kDa) in cervical spinal cord lysates from ctl and cKO mice at different ages. **C.** Quantitative analysis of grayscale values of GPR17 protein levels normalized to that of α-Tubulin used as a loading control. **D.** Representative immunohistochemical staining in the spinal cord of ctl and cKO mice, showing co-localization of tdT with GPR17 (green) in the spinal WM at P14, P21, and P30. Arrowheads indicate GPR17$^+$tdT$^+$ cells. **E.** Quantitative analysis of GPR17$^+$ cells in the spinal WM of ctl and cKO mice at different ages. **F.** Quantitative analysis of the percentage of GPR17$^+$tdT$^+$ among all tdT$^+$ cells and the density of GPR17$^+$tdT$^+$ cells in the WM of ctl and cKO mice at different ages. Each dot represents one mouse. Scale bar = 20 μm

higher proportion of myelinated ctx in cKO mice compared to ctl mice at both P14 (P<0.001) and P21 (P=0.036), while was caught up at P30 (Figure 26C). In addition, we compared the MBP$^+$ occupied area in the same region of ctx (L2-4) at P21 and P30 (Supplementary Figure 7A, C). The violin plots showed a relatively higher proportion of MBP$^+$ occupied area across the measured region in cKO mice compared to ctl mice at P21 (P=0.04) and P30 (P=0.058) (Figure 26D). In the cc, we measured the MBP$^+$ occupied area in single z-stack images (Figure 26E) of MBP immunostaining. We observed a higher proportion of MBP$^+$ area in cKO mice compared to ctl mice at all analysed ages (P14: P<0.001; P21: P=0.037; P30: P=0.045; Figure 26F). Furthermore, we measured the expression of myelin proteins (MBP and MOG) by immunoblotting using total proteins collected from the ctx and cc. Consistent with the results of immunostaining, the protein expression levels of MBP and

MOG were increased in cKO mice in both ctx (Figure 27A-B) and cc (Figure 27C-D) at all analysed ages.

These findings suggest that there may be an early onset of myelination in OLs of S1R cKO mice. However, it remains unclear whether the myelin formation in cKO mice is affected by the early maturation of OLs. Therefore, further detailed analysis of myelination is needed to better understand the impact of S1R cKO mice.

7.4 Precocious maturation of OLs in the spinal cord of S1R cKO mice

To extend our findings, we investigated the role of S1Rs in spinal cord OL development. Based on the results from the forebrain, we first examined the expression of OL markers in the spinal cord during development (Figure 28A). Immunostaining for Myrf and GSTπ was performed on coronal sections of spinal cord at different developmental stages (Figure 28C). In the ventral white matter of spinal cord (vWM, Figure 28B), we did not observe comparable differences in $Myrf^+tdT^+$ cells between ctl and cKO at P21 and P30, whereas the number of $Myrf^+$ cell was significantly decreased in cKO mice at P14 (P=0.03) (Figure 28D). Meanwhile, we observed an increase in $GST\pi^+$ cells in cKO mice at P21 (Figure 28E). The proportion (P<0.001) and density (P=0.0004) for $GST\pi^+tdT^+$ cells were also significantly increased in cKO mice at P21, while no change at P30 was detected (Figure 28E). This was further confirmed by a significant increase in the proportion of $GST\pi^+Myrf^+$ tdT^+ cells among all tdT^+ (Figure 28F) or $Myrf^+tdT^+$ (Figure 28G) cells at P21. In addition, we analysed the immunostaining results from the ventral grey matter of spinal cord (vGM, Supplementary Figure 8B). From the analysis results, we did not observe any significant changes in Myrf immunostaining in cKO mice. However, we observed an increase of $GST\pi^+$ cells in vGM of cKO mice, and an increased proportion in all tdT^+ cells and density of $GST\pi^+tdT^+$ cells was only present at P21 (Figure S8D). In addition, the proportion of $GST\pi^+Myrf^+tdT^+$ among all tdT^+ or $Myrf^+tdT^+$ cells were also increased in cKO mice at P21, but were not different at P30 (Figure S8E, F). These findings indicate that OLs in the spinal cord show transient precocious maturation during development as a result of S1R deletion.

Furthermore, the myelination status of the spinal cord was also detected. Total proteins from the cervical spinal cord were used to measure myelin proteins by western blotting (Supplementary Figure 9A). However, unlike the brain, we did not observe significant differences in the expression levels of MBP and MOG at P21 and P30. At P14, we observed an increased protein level of MBP but no change of MOG level in cKO mice. (Figure S9B). To assess changes in the structure of myelin in the spinal cord, we further prepared semithin sections and performed toluidine blue staining at P14 and P21 (Figure 29A-B). To compare differences in myelin thickness, we measured the g-ratio (the ratio of the axon caliber to the fiber caliber) of individual axons in the spinal vWM. Scatter plots of the g-ratio showed the relative myelin thickness for a given axon diameter. The linear regression analysis of slopes of cKO mice were significantly different from those of ctl mice at P14 (F=13.05, P=0.0003) and P21 (F=56.47, P<0.0001) (Figure 29C, E). However, the average g-ratio per mouse showed no significant difference between ctl and cKO at P14 and P21 (data not shown). In addition, we did not observe any significant changes in myelinated axon diameters both at P14 (P=0.5147) and P21(P=0.1642) (Figure 29D, F). For the

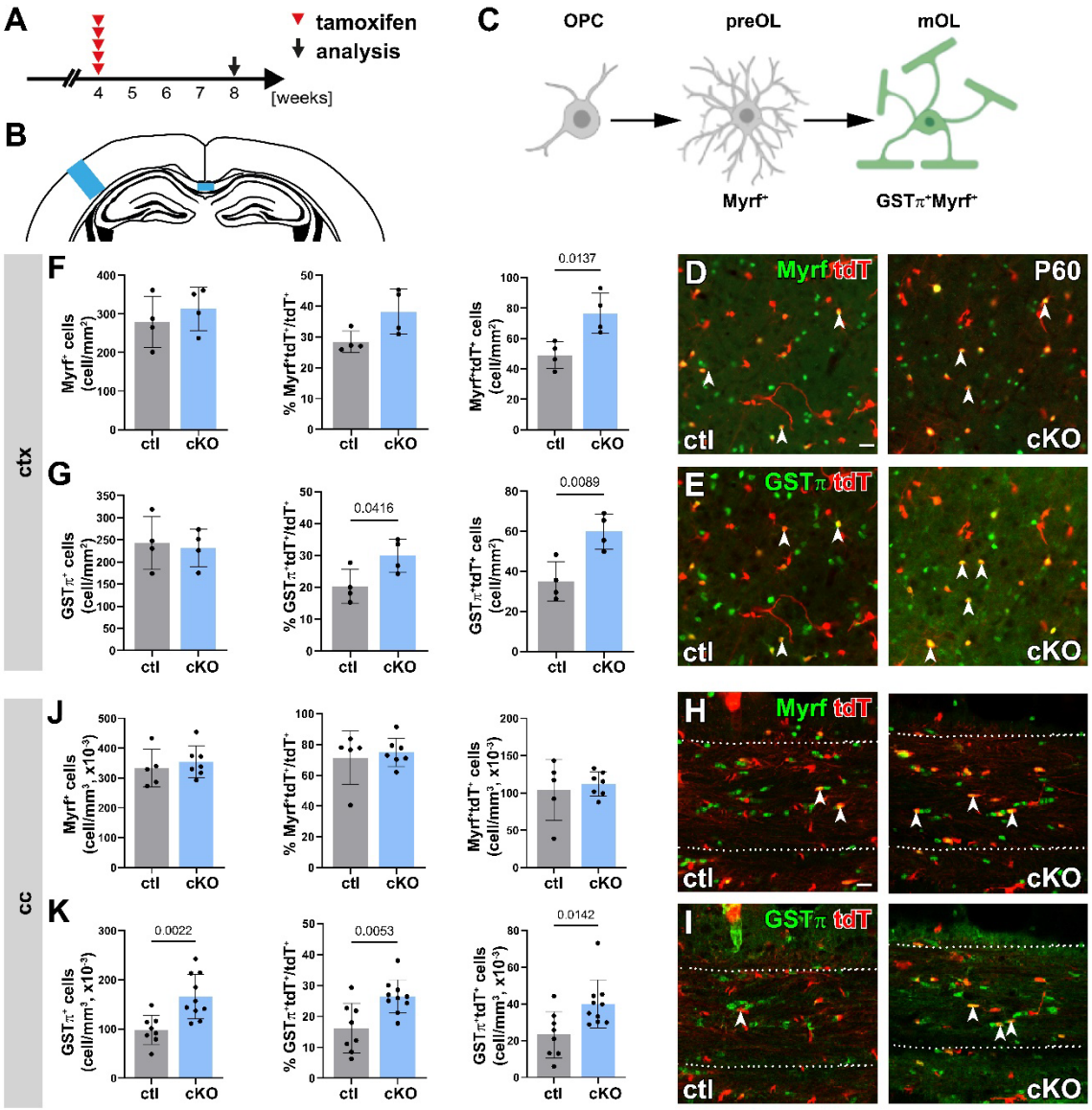

Figure 32. Deletion of S1Rs in adult OPCs leads to increased GSTπ⁺ cells in adult mouse brain. A. Experimental plan. All mice were injected with tamoxifen at 4w old and analysed at 8w (P60). **B.** Highlighted regions of ctx and cc that were analysed. **C.** Schematic representation of the analysed OL developmental stages and the corresponding markers. **D, H.** Representative immunohistochemical images showing the staining for Myrf in the ctx (D) and cc (H) of ctl and cKO mice at P60. Arrowheads indicate double positive (Myrf⁺tdT⁺) cells. **E, I.** Representative immunostaining images of mOL marker GSTπ in the ctx (E) and cc (I) of ctl and cKO mice at P60. Arrowheads indicate double positive (GSTπ⁺tdT⁺) cells. **F, J.** Quantification of the density of Myrf⁺, Myrf⁺tdT⁺ cells and the percentage of Myrf⁺tdT⁺ cells among tdT⁺ cells in ctx and cc of ctl and cKO mice at P60. **G, K.** Quantitation of GSTπ⁺, GSTπ⁺tdT⁺ cell number and percentage of GSTπ⁺tdT⁺ in tdT⁺ cells in ctx (G) and cc (K) of ctl and cKO mice at P60. Each point represents one mouse. Scale bar = 20 μm.

distribution of myelinated axon size, there was no significant difference between ctl and cKO at P14 (Figure 29G) and P21 (Figure 29J). The cumulative percentage of myelinated axons of different thickness (indicated by g-ratio) showed that cKO mice had more small-sized axons with myelin at P21 (Figure 29K), but no change at P14 (Figure 29H). The quantitative results according to different diameter groupings showed that at P14, large size axons (>1.2) had thicker myelin in cKO mice (Figure 29I), whereas at P21, smaller size

axons had thicker myelin and large size axons had thinner myelin in cKO mice (Figure 29L). Collectively, these results further might indicate a potential role of S1Rs in the regulation of OL myelination during development in the spinal cord.

In addition, we investigated the potential changes of preOLs in cKO mice in the spinal WM. We performed immunostaining of BCAS1 on the spinal cord sections (Figure 30B). At P14, the density of $BCAS1^+tdT^+$ cells was decreased in cKO mice (Figure 30D), while $BCAS1^+$ cells showed no significant difference between genotypes (Figure 30C). For the other analyzed ages (P21 and P30), we did not observe any significant differences between ctl and cKO in the number of $BCAS1^+$ cells or $BCAS1^+tdT^+$ cells in the vWM (Figure 30C-D). We further examined this stage using another preOL marker, GPR17 (Figure 31A). Western blotting results showed a decreased level of GPR17 protein in cKO mice at P21 compared to ctl, and an increased tendency of GPR17 level at P14 in cKO mice (Figure 31B-C). We also performed immunostaining for GPR17 on spinal cord slices (Figure 31D). From quantification results, we observed a decrease in the number of $GPR17^+$ preOLs in cKO mice at P14 (P=0.02) and P21 (P=0.0018) (Figure 31E). Moreover, among all tdT^+ cells, cKO mice showed a decrease in the proportion (P14: P=0.036; P21: P<0.001) or density (P14: P=0.01; P21: P=0.0015) of $GPR17^+tdT^+$ cells at P14 and P21, but not at P30 (Figure 31F). Downregulation of GPR17 expression has been shown to promote the progression of OL maturation, serving as an intrinsic timer of myelination (Chen et. al., 2009; Rivera et. al., 2021). Therefore, S1R deletion in OPCs induces an early onset of OL maturation during development, which may be related to the regulation of GPR17 expression in the spinal cord. However, further studies on its molecular mechanism are still needed.

7.5 Functional analysis of S1Rs in adult OPCs

To elucidate whether the role of S1Rs in OL maturation is also required in adult CNS, we investigated oligodendrogenesis of adult OPCs upon S1R deletion under physiological conditions. We induced Cre activity in 4w old mice and analysed them 4w after induction (~around P60; Figure 32A). Next, we examined the expression of OL markers in the adult brain (Figure 32C, D, E, H, I). In cKO mice, we observed increased density of $Myrf^+tdT^+$ cells only in ctx (P= 0.0137; Figure 32F), but not in cc (Figure 32J). For myelinating OLs immuno-labeled by GSTπ, only the cc of cKO mice showed an increased cell density (P= 0.0022) (Figure 32G, K). For $GST\pi^+tdT^+$ cells, we observed an increase in the percentage (ctx: P=0.0416; cc: P=0.0053) and density (ctx: P=0.0089; cc: P=0.0142) of all tdT^+ cells in both ctx and cc of cKO mice compared to ctl mice (Figure 32 G, K). This suggests that S1Rs deletion in adult OPCs affects OL maturation during oligodendrogenesis. In addition, the proportion of $GST\pi^+tdT^+$ cells among all $GST\pi^+$ cells in cc was unaltered (ctl: 23.33±3.020; cKO: 24.66±1.94). Thus, we found that the density of $GST\pi^+tdT^-$ cells was also increased in cKO mice compared to ctl (ctl: 75.11± 7.75; cKO: 126.1±12.15; P=0.0042). This suggests that deletion of S1R in adult OPCs affects not only affect the lineage cells we tracked, but also the pre-existing OLs in that environment. Further studies are needed to investigate functional changes, such as locomotor or cognitive alterations, in adult mice lacking S1Rs in OPCs.

8 Discussion

8.1 Specific detection of S1Rs reveal their wide expression pattern in the CNS

8.1.1 A reliable antibody for specific detection of S1R

Antibodies are a pivotal tool in biomedical research, but the specificity of commercial antibodies is inconsistent. Validation in KO animals is a golden standard for validating the specificity of antibodies for immunoblot and immuno-labelling (Laflamme et al., 2019). In this study, we screened six commercial S1R antibodies using S1R KO mice and found that one antibody from Cell Signaling ($Ab^{\#61994}$) could be used to specifically detect S1R using immunoblot. $Ab^{\#61994}$ is a newly produced rabbit monoclonal antibody, which has been used only in a few studies so far (six publications according to the Cell Signaling website). A recent study by Abdullah et al. verified the specificity of $Ab^{\#61994}$ for detecting S1Rs in tissue lysate from mouse heart, but without showing the complete protein separation range of the immunoblot (Abdullah et al., 2020). Therefore, the current work provides further evidence that $Ab^{\#61994}$ is a reliable antibody that specifically recognizes S1Rs in immunoblot without generating any unspecific bands at any other molecular weight. However, the other four S1R antibodies showed bands in protein samples from both WT and KO mice, indicating that they are not working specifically for immunoblotting. For example, one of these antibodies from Santa Cruz ($Ab^{sc\text{-}137075}$), which is widely used in the study of S1R, showed both bands of the expected size and other unspecific binding of different sizes.

Furthermore, some studies on S1Rs were performed using custom-made antibodies. However, to date, only one antibody from Arnold Ruoho group (Ab^{Ruoho}) has been validated with S1R KO mice, although it did not work well in immunoblots (Mavlyutov et al., 2010; Mavlyutov et al., 2016; Nakamura et al., 2019). In addition, custom-made antibodies have limited availability to the research community.

Indeed, the detection of S1R expression in different cell types *in vivo* is limited by the absence of specific antibody. Among them, Ab^{Ruoho} showed specific immunostaining of S1R by IHC in the brain and spinal cord. However, they observed the expression of S1Rs only in neurons (Alonso et al., 2000). Ab^{Rouho} did not provide a clear S1R expression pattern at the (sub)cellular level in the CNS *in vivo*. Another antibody generated by Palacios et al. showed expression of S1Rs in OLs (Palacios et al., 2003). Ruscher et al. performed IHC with a commercial antibody and showed the increased expression of S1Rs in astrocytes after stroke (Ruscher et al., 2011). It has been shown that S1Rs are expressed at the RNA and protein level in microglia of brain tissue, whereas the expression pattern of S1Rs in microglia *in situ* has not been shown (Gekker et al., 2006; Zhao et al., 2014).

Here, considering that $Ab^{\#61994}$ can recognizes denatured S1R proteins, we modified the IHC protocol involving the antigen retrieval process with 1%SDS (AR^{SDS}) and observed specific immunostaining of S1Rs *in situ* by using $Ab^{\#61994}$ only in WT mice but not S1R KO mice. As S1Rs are mainly localized at the ER lumen, we tested the cellular distribution of S1Rs by performing IHC of $Ab^{\#61994}$ and ER marker (calnexin). With the AR^{SDS} protocol, we observed the specific immunolabeling of S1Rs with ER-like structure as suggested by *in vitro* studies. Unlike the result by using one of commercial antibody, we did not observe the co-immunolabeling of S1R with GFAP (Ruscher et al., 2011), even under pathological

conditions (data not shown). In addition, we tested the other S1R antibodies with our modified IHC protocol. However, all of these antibodies failed to generate specific immunostaining *in vivo* under the current testing conditions. Therefore, our results suggest that cautious re-evaluation of previous studies using those antibodies for immunoblot, immunoprecipitation and/or immunohistochemistry of S1Rs may be considered.

Several AR methods such as heating with citrate buffer and microwave treatment have been tested to improve the immunostaining quality for the S1R in cultured cells (Hayashi et al., 2011). In the current study, 1% SDS was used for the AR of the formaldehyde-fixed CNS tissue, substantially improving the S1R immunostaining. However, no AR was performed in studies using Ab^{Rouho} (Mavlyutov et al., 2016; Nakamura et al., 2019), which may explain their relatively fainter staining of S1Rs in the CNS compared to the results of the current protocol.

Although $Ab^{\#61994}$ displayed a very good capacity to specifically detect S1Rs in immunoblot and IHC, some drawbacks of using this antibody have to be considered. First, regarding the punctate background signal in S1R KO brain, the signal-to-noise ratio of the current IHC protocol is not satisfactory to identify potential S1R expressions in fine structures such as the plasma membrane *in vivo*. Second, $Ab^{\#61994}$ binds non-specifically to myelin-like structures in the WM of spinal cord, brain stem and cerebellar, thus limiting its application in white matter studies in certain CNS regions. Third, $Ab^{\#61994}$ does not work for IHC in brain tissues without SDS treatment, suggesting that $Ab^{\#61994}$ may only recognize denatured S1R proteins. Therefore, it would be difficult to immunoprecipitate naïve S1Rs using $Ab^{\#61994}$. Further optimization of the AR protocols for $Ab^{\#61994}$ as well as newly designed S1R antibodies will help to solve such problems.

8.1.2 The broad expression of S1Rs in CNS cells

Some transcriptome profiling studies have shown that *sigma1r* is widely expressed in CNS cells (OPCs > Microglia > Astrocyte) of the cerebral cortex (Zhang et al., 2014a; Marques et al., 2016). In the current study, we observed variable protein levels of S1Rs in MAC-sorted glial cells by western blotting (Astrocyte>Microglia>OPCs), which may be affected by the expression of house-keeping genes. Moreover, our established IHC protocol (AR^{SDS} protocol) using $Ab^{\#61994}$ clearly displays that S1Rs are mainly localized in ER-like structures of CNS cells. Notably, unlike studies using Ab^{Rouho} (Mavlyutov et al., 2010; Mavlyutov et al., 2016), the current protocol demonstrated high levels of S1R expression in the olfactory bulb, cerebral cortex, hippocampus, and thalamus. Combining immunostaining with cell type-specific markers, we were able to show that in addition to neurons suggested by using Ab^{Rouho} (Mavlyutov et al., 2010), S1Rs are widely expressed in various glial cells in the CNS including astrocytes, OPCs, OLs, and microglia. By comparing the mean fluorescent intensity of S1R in the individual cells, we observed high expression of S1Rs in microglia and oligodendrocyte lineage cells in adult. In addition, we showed high expression of S1R in neurons, which were less expressed in neurons than glial cells in the transcriptome profiling results. As showed by both studies, the expression of S1Rs was also high in the OPCs and OLs.

8.2 A powerful tool for studying cell-specific S1R functions *in vivo*

The pharmacological effects of S1Rs have been intensively studied, and they are considered a therapeutic target for many neurological and psychiatric disorders. S1Rs are ER chaperon proteins that form a complex with Bip under physiological situation. Agonists of S1Rs disrupt the binding of S1Rs and Bip, resulting in calcium efflux to the mitochondria

via IP_3R3. Activation of S1Rs by agonists not only leads to the dissociation of Bip, but also triggers downstream signalling cascades to exert neuroprotective functions. For example, treatment with S1R agonist PRE-084 promoted the ER stress response through EIF2α/ATF4 and NRF2 signalling, improving locomotor performance in a zebrafish model of TDP43 mutant ALS (Lasbleiz et al., 2022). In addition, *in vivo* studies of S1R biological functions may pave the way for innovative treatments and therapies.

Loss-of-function experiments would be an ideal strategy to study the biological function of S1Rs. However, previous studies using S1R KO mice have shown variable and mild phenotypes in aging-related memory loss, cognitive impairments, and motor defects (Couly et al., 2022). In this project, we observed earlier maturation of OLs in the cc of S1R KO mice during development, but not in the ctx. However, we did not observe alterations in myelin protein expression in the S1R KO mice. One possible explanation for this difference is that the observed changes are transient and may involve compensatory genetic mechanisms established during embryonic development, which rescue the loss of S1R function in global KO mice (El-Brolosy and Stainier, 2017). For example, hepatocyte-specific SIRT1 cKO mice develop a fatty liver which was not seen in global SIRT1 KO mice (Wang et al., 2010). Additionally, OLs may exhibit regional heterogeneity and show different functional characteristics in different brain regions. In addition, the neural circuits are maintained through interactions between neurons and glial cells, whereas global knockout of S1Rs in all cell types can have multifactorial effects. Indeed, neither pharmacological intervention nor constitutive deletion of S1Rs could exclusively study S1R functions in specified cell types.

To address such questions, we generated a Cre-dependant S1R conditional KO mouse (S1R flox). As proof of concept, we showed that S1Rs could be successfully deleted in neurons and different glial cells (microglia, astrocytes, and OPCs) mediated by Cre or CreER/tamoxifen systems *in viv*o. Regarding the broad expression of S1Rs in various cell types in and outside of the CNS, this newly generated S1R flox mouse will be a powerful tool to study cell-type specific functions of the S1R *in vivo*.

8.3 S1Rs are involved in regulating OL maturation rather than differentiation

It has been previously demonstrated that S1Rs are located at the lipid rafts which was showed in rat OL progenitors (CG-4 cells) (Hayashi and Su, 2004a). Hayashi and Su showed an increase in S1R expression in OLs and myelin during development in the rat brain (Hayashi and Su, 2004a). However, using our AR^{SDS} protocol, we did not observe the expression of S1Rs in myelin, except for some unspecific labelling of myelin-like structure in adult mice. Nevertheless, we detected increased expression of S1Rs following OPC differentiation into OLs, suggesting that S1Rs are involved in regulating OL development.

Indeed, *in vitro* study showed that activation of S1Rs by agonist PRE-084 contributes to OL differentiation, while S1R siRNA inhibits differentiation (Hayashi and Su, 2004a). However, the *in vivo* investigation of OL development regulated by S1Rs was still missing. In the current study, we observed that the myelination was either transiently delayed and increased in the ctx of S1R KO and OPC-S1R cKO mice at P14, respectively, indicating that rather than in OPCs alone, the S1Rs in other CNS cells may contribute to regulate myelination. Therefore, it is important to dissect the cell-specific functions of S1Rs to fully understand its molecular mechanism regulating myelin development.

In the current study, we aim to unravel the role of OL-lineage cell-specific S1Rs in regulating OL development by studying the OPC-specific S1R cKO mice during development. Different OL markers are used to identify OLs at different stages of OL development. However, some markers can be found at multiple stages. For example, APC CC1 is a marker for mature OLs but can be observed in both immature and mature OLs. BCAS1 is a marker for pre-myelinating OLs and de novo myelinating OLs. In our study, we combined different stage markers and reporter expression to obtain accurate results and characterize the maturation status of OLs. Although, we did not observe changes in OPC proliferation and differentiation into OLs in cKO mice during development, the loss of S1Rs led to early maturation of OLs, as indicated by increased amount of mOLs (immunolabeled with GSTπ) in the mouse brain and spinal cord.

8.3.1 Potential intracellular mechanisms of S1Rs regulating OL development

It has been shown that two types of GSTπ cells are present in the adult rat ctx: C-type cells in the cytoplasm (co-immunostained with 2',3'-cyclic nucleotide 3'-phosphodiesterase, CNPase), and N-type cells in the nucleus (expressing NG2). During OL maturation, GSTπ translocates from the nucleus to the cytoplasm (Tamura et al., 2007). In our study, we used three OL markers to immunolabel OL with varying results: $CC1^+$ and $Myrf^+$ cells were not significantly altered in cKO mice while $GST\pi^+$ cells were increased. Activated S1Rs have been shown to be involved in regulating the autophagy process under pathological conditions (Weng et al., 2017; Zhao et al., 2019). Activation of S1Rs promotes nuclear translocation of TFEB, which in turn affects autophagy (Wang et al., 2023). Therefore, S1Rs may play a role in the nuclear translocation of nuclear proteins such as GSTπ and/or other transcription factors, leading to increased $GST\pi^+$ mOLs during OL development. Further studies are needed to investigate the specific mechanisms involved in this process.

We found precocious maturation of OLs in the spinal cord of cKO mice as well. Particularly, we observed decreased expression of GPR17 in cKO mice at P21. GPR17 is a preOL marker that is mainly expressed at the onset of differentiation of OPCs and decreases as these cells mature into myelinating OLs (Chen et al., 2009). Several extracellular signals and intracellular timers play important roles in regulating OL maturation, such as the helix-loop-helix protein ID2 and ID4 which have been identified as differentiation inhibitors. It has been shown that the ID2 is translocated out of the nucleus at the onset of OL differentiation (Kondo and Raff, 2000; Wang et al., 2001). Overexpression of GPR17 increases expression of ID2 and promotes nuclear translocation of ID2/4, thereby inhibiting OL maturation (Chen et al., 2009). Therefore, further investigation is needed to determine if the changes in GPR17 expression upon S1R deletion are linked to altered intracellular mechanisms affecting OL maturation.

In addition, preOLs undergo a selection process during development, which results in a significant percentage of these cells undergoing cell death following differentiation (Barres et al., 1992; Hughes et al., 2018). Therefore, only surviving preOLs form mOLs, which is the checkpoint in the formation process of newly formed OLs (Hughes and Stockton, 2021). It has been shown that S1Rs are involved in regulating apoptosis under pathological conditions (Weng et al., 2017; Zhao et al., 2019). For example, activation of S1Rs by ANAVEX2-73 and dextromethorphan (DM) (both are S1R agonist) protect neuron from cytotoxic and apoptosis (Lisak et al., 2020). It is possible that S1Rs promote the survival of preOLs during OL development. Further experiments, such as assessing OL apoptosis in the context of S1R deletion, are required.

In the present study, we also detected elevated levels of MBP and MOG protein in mouse brain of cKO mice. Meanwhile, in the spinal cord, we observed changes in the distribution of axonal myelin thickness in cKO mice. This suggests that the absence of S1Rs may lead to changes in myelin formation or maintenance. Previous studies have demonstrated that S1Rs are localized to specific lipid microdomains on the ER, which are enriched in GalCer and cholesterol. S1Rs are involved in the transport of Gal and cholesterol from the ER to the plasma membrane (Hayashi and Su, 2007). We deleted S1Rs in OPCs at P7 and 8, which subsequently leads to the absence of S1R expression in differentiated mOLs. During the differentiation of OPCs into OLs, various molecular and cellular processes are involved in myelin formation. The absence of S1Rs in mOLs may disrupt these processes and interfere with the proper formation and maintenance of myelin. Further research is required to investigate the underlying mechanisms by which S1Rs influence myelination and to elucidate the consequences of their absence in mOLs.

8.3.2 Can OPCs regulate OL maturation via S1R signaling?

OPCs are a type of multitasking glial cell in the CNS that not only differentiate into OLs, but also interact with other cell types to regulate their functional behaviour (Fang and Bai, 2023). OPC responses to synaptic activity have been proven to take an important part in OPC proliferation and differentiation into OLs. Synaptic activity can influence the release of signaling molecules, such as neurotransmitters, that can impact OPC behaviour and promote their maturation (Bergles et al., 2010; Moura et al., 2021). In addition, the release of factors from axons and their interaction with OPCs are critical for the initiation and progression of myelination (Michailov et al., 2004; Nave and Werner, 2014). A study by using neuron-OL coculture showed that the activation of S1Rs with an agonist promotes myelination (Demerens et al., 1999), which suggests that S1Rs play a role on OL maturation. The deletion of S1Rs in OPCs may disrupt this axon-OPC communication, leading to alterations in the release of axonal factors and affecting the maturation of OLs and myelin formation. In our study, GSTπ$^+$ OL population includes tdT$^+$ and tdT$^-$ cells. We found that not only the recombined GSTπ$^+$tdT$^+$ but also GSTπ$^+$tdT$^-$ OLs in cKO mice were increased in the cc of mice when Cre activity was induced at P30. Therefore, the deletion of S1Rs in OPCs may lead to alterations in neuronal activity, which in turn promote OL (irrespective tdT$^+$ or tdT$^-$) maturation.

The phagocytic and pruning functions of microglia are important for forming neuronal circuits. They have also been shown to be involved in myelination during development by providing trophic factors (e.g., IGF) that support OPC proliferation and differentiation (Miron, 2017). The intricate interplay between microglia and OPCs further extends to immune homeostasis maintenance, as activated microglia can release cytokines such as IL-6, IL-1β, and TNFα, which can promote OL development (Shigemoto-Mogami et al., 2014). Furthermore, Zhang et al. showed that TGF-β2 released from NG2 glia (a type of OPC) can target its receptor TGFBR2 in microglia and regulate neuroinflammation (Zhang et al., 2019). Therefore, it is plausible to hypothesize that the premature maturation of OLs in S1R cKO mice is downstream cascade effect of the S1Rs deletion in OPCs that modulates microglial functions. Nevertheless, the comprehensive understanding of the impact of S1R deletion in OPCs on other cell types such as microglia would require further investigation.

9 Conclusion and Outlook

In this study, we conducted a comprehensive investigation of S1R expression and function in the CNS. We initially screened six commercial antibodies and identified one specific antibody from Cell Signaling ($Ab^{\#61994}$) for immunoblotting. In addition, we established a modified immunohistochemical staining protocol involving an antigen retrieval with 1% SDS (AR^{SDS}) against S1R antibody ($Ab^{\#61994}$) to specifically immunolabel S1Rs in brain and spinal cord. By using different brain cell markers and S1R $Ab^{\#61994}$, we found that S1Rs are widely expressed in different CNS cells *in situ*. Particularly, we displayed the expression pattern of S1Rs in OPCs with the AR^{SDS} protocol. In addition, we provided a powerful tool for studying the specific functions of S1Rs in different cell populations *in vivo* which using tamoxifen inducible S1R flox mouse lines. This part of work has been published in Liu et al., 2023 (Liu et al., 2023).

We further investigated the function of S1Rs in OL lineage cells by using both S1R KO and cKO mice. Deletion of S1Rs in global or specific in OPCs did not affect their proliferation or differentiation but resulted in an increased amount of mOLs during development. This was accompanied by elevated levels of myelin-related proteins in the brain of cKO mice. Collectively, these findings suggest that S1Rs are involved in the regulating of OL maturation during development.

The early onset of OL maturation in OPC-S1R cKO mice raises questions about the long-term effects and potential changes in myelin structure. Future studies should investigate whether these alterations persist into adulthood and whether they have functional consequences. In addition, to elucidate the potential mechanisms by which S1Rs regulate OL maturation, the role of S1Rs in different cell types of the CNS needs to be clarified. We will investigate the potential changes in OL development in mice with different cell type-specific S1R deletions such as microglia, astrocyte, and neuron.

Furthermore, adult oligodendrogenesis is a key process in maintaining the required cell number under physiological and pathological conditions. Deletion of S1Rs in adult OPCs led to an increase in mOL number. However, further studies of OPC-specific S1Rs on the proliferation and differentiation of OLs are required. In addition, motor training accelerates OPCs differentiation. Xiao et al. found that $Enpp6^{+}$ newly formed oligodendrocytes were rapidly increased during motor skill training (Xiao et al., 2017). Therefore, taking advantage of this model, the role of S1Rs on the oligodendrogenesis in adult mice will be further investigated.

Understanding the roles of S1Rs in different cell populations, particularly in OL lineage cells, may have implications for the development of therapeutic strategies targeting demyelination-related diseases and maintaining proper myelin function in the CNS.

10 Appendix

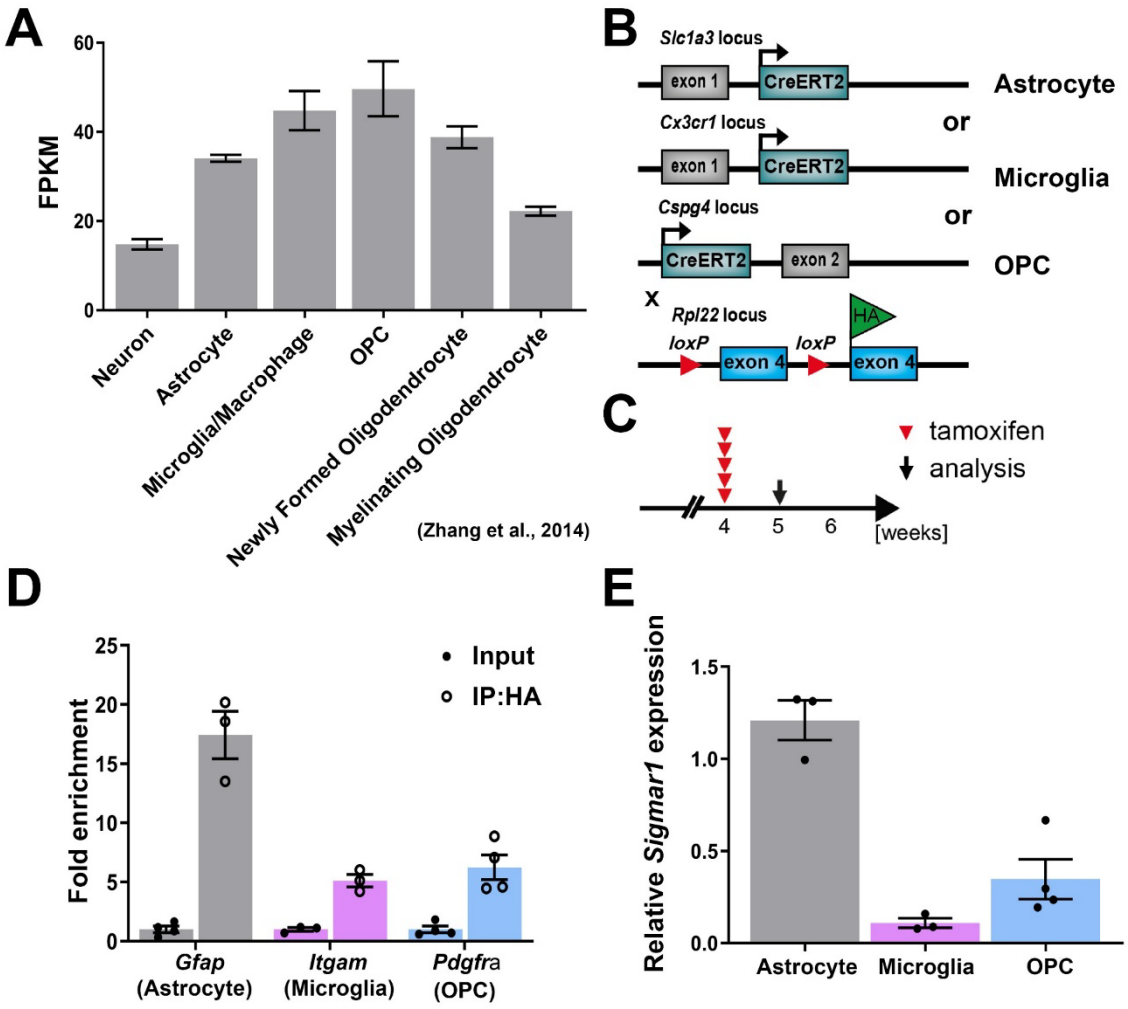

Supplementary Figure 1. mRNA expression of S1Rs in different glial cells in mouse brain.

A. Results from Brainrnaseq database (Zhang et al., 2014a) show *sigmar1* mRNA levels in different types of purified brain cells from pups at postnatal day 7 or 17 (only for OLs). FPKM: Fragments per kilo base of transcript per million mapped reads. **B.** Transgenic schemes of three glial-specific CreERT2-expressing mouse lines crossbred with RiboTag mice to purify translated mRNA in astrocytes, microglia and OPCs. **C.** Experimental plan. Mice were injected with tamoxifen at 4w and analysed 1 w after injection. **D.** Enrichment of different glial cells were detected using the expression levels of specific marker genes of input control and immunoprecipitated RNA by qPCR. **E.** qPCR analysis comparing the relative translated *sigmar1* mRNA expression level in astrocytes, microglia and OPCs, with normalization to input control. Each point represents one mouse.

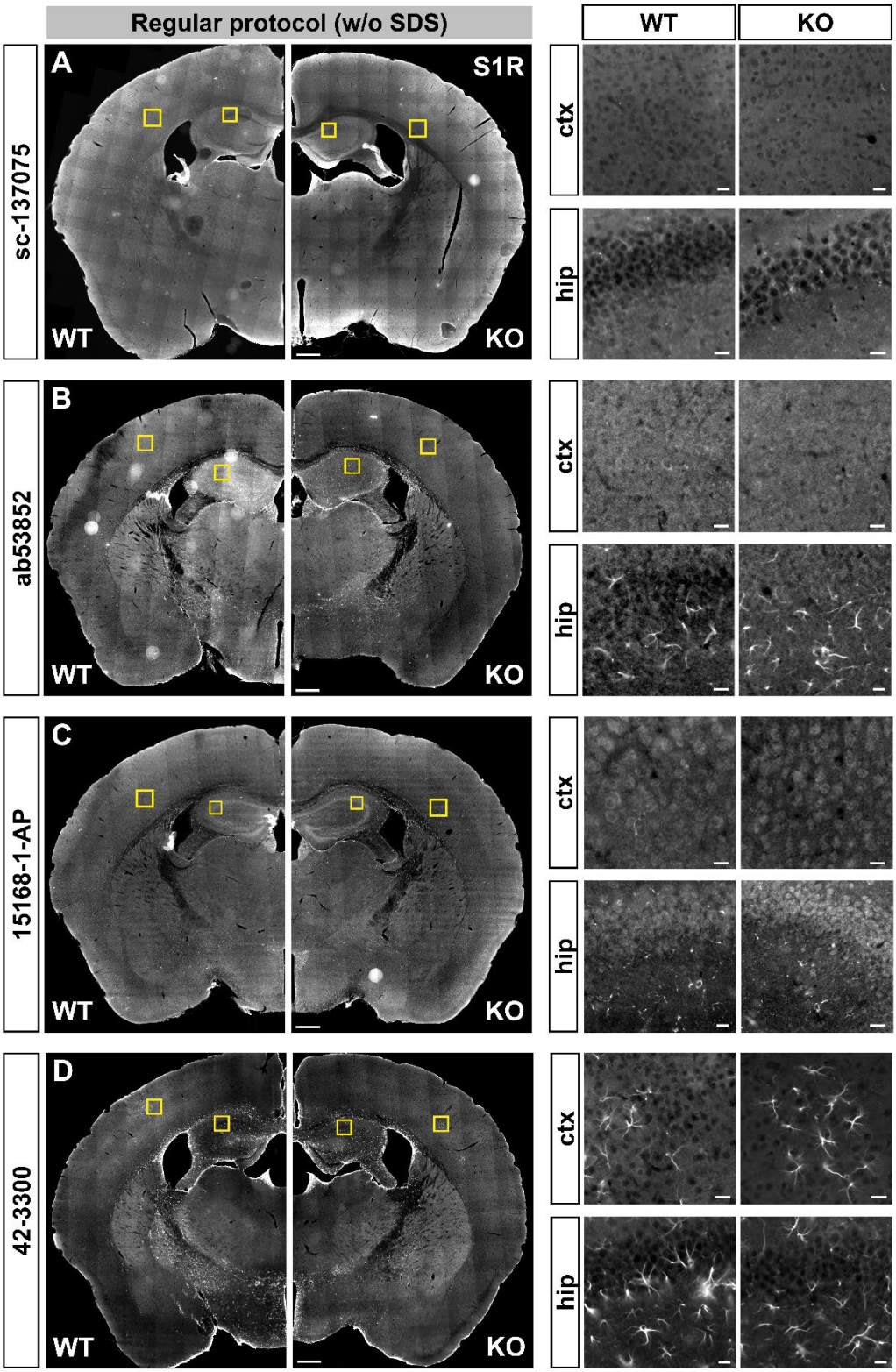

Supplementary Figure 2. Immunostaining using the regular IHC protocol with various commercial S1R antibodies in mouse brain.

A-D. Overviews of brain sections from WT and S1R KO mice immunostained with S1R Abs from Santa Cruz (sc-137075), Invitrogen (42-3300), Abcam (ab53852) and Proteintech (15168-1-AP), respectively. Representative images for boxed regions in the cortex (ctx) and hippocampus (hip) are listed on the right side. Scale bars = 200 µm in A-D, 5 µm in magnified images.

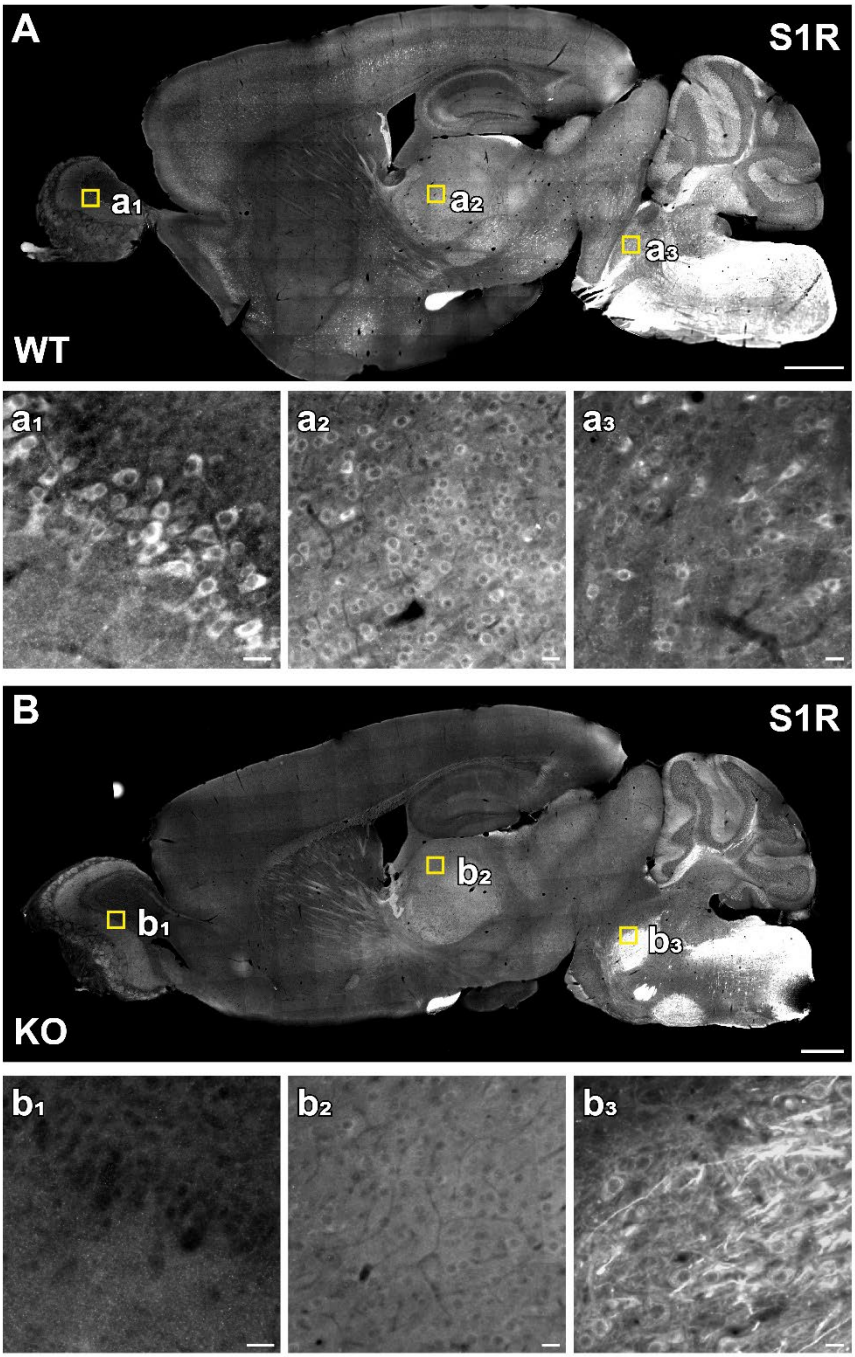

Supplementary Figure 3. Overview of S1R immunolabelling in the brain using the AR^{SDS} protocol.

A-B. Overviews of S1R immunostaining in sagittal mouse brain sections. Images showing a broad distribution of S1R from rostral to caudal in WT mice (**A**) which were largely absent in S1R KO mice (**B**). Some unspecific signal could be observed mainly in myelin tracts in the brain stem and spinal cord. **a_1-a_3**, **b_1-b_3**. Magnified views showing representative images of olfactory bulb (a_1, b_1), thalamus (a_2, b_2) and medulla (a_3, b_3) from WT and KO mice. Scale bars = 1000 µm in A-B and 20 µm in a_1-a_3 and b_1-b_3.

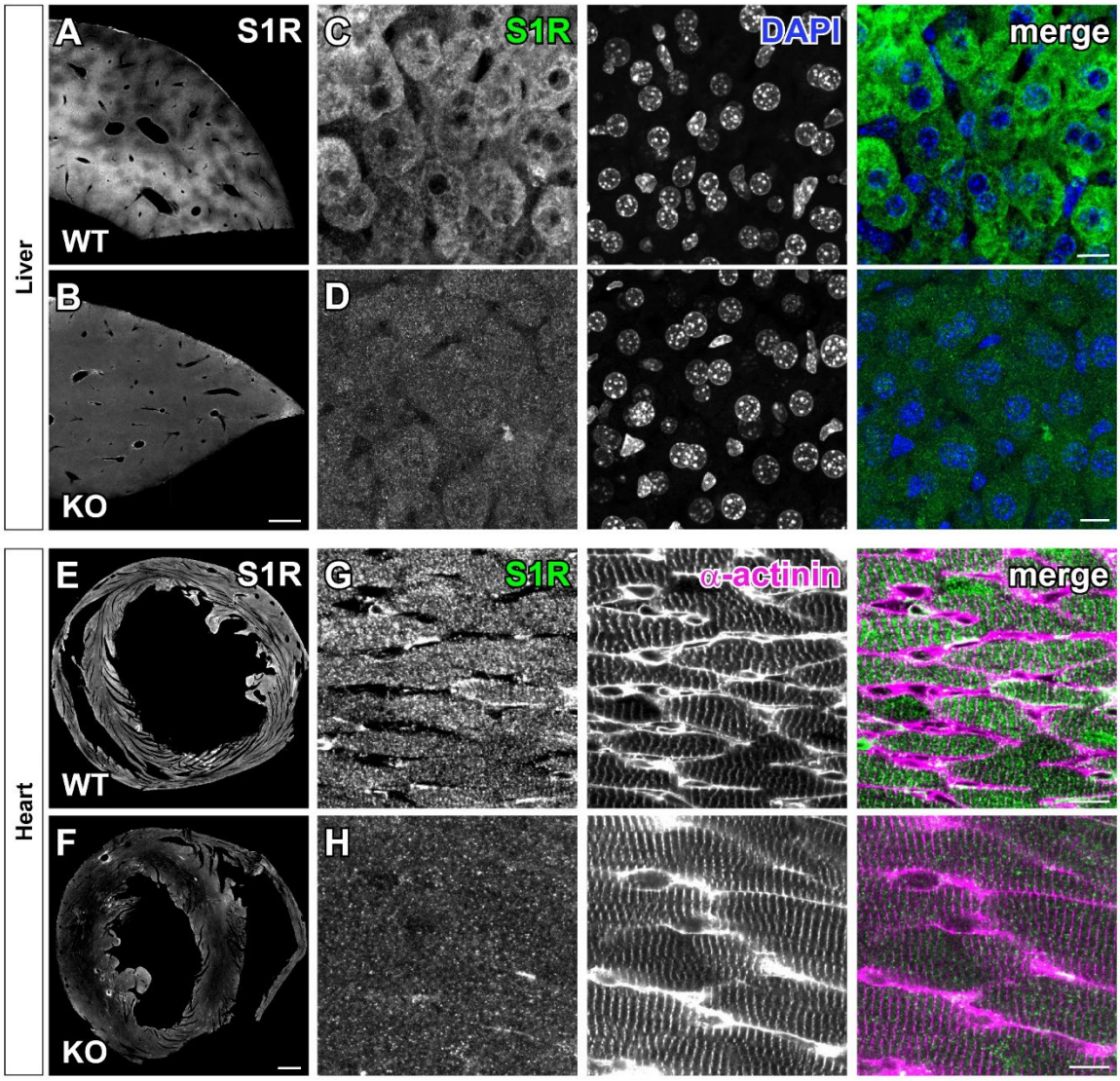

Supplementary Figure 4. Specific detection of S1Rs in liver and heart.
With AR^{SDS} protocol, we performed S1R staining on liver (**A-D**) and heart (**E-H**) from WT and S1R KO mice. α-actinin was used as the marker of cardiomyocytes. S1R immunostainings images with lower magnifications show clearly contract of WT and S1R KO mice. Scale bars = 500 μm in A, B, E, F, 10 μm in c, d, g, h.

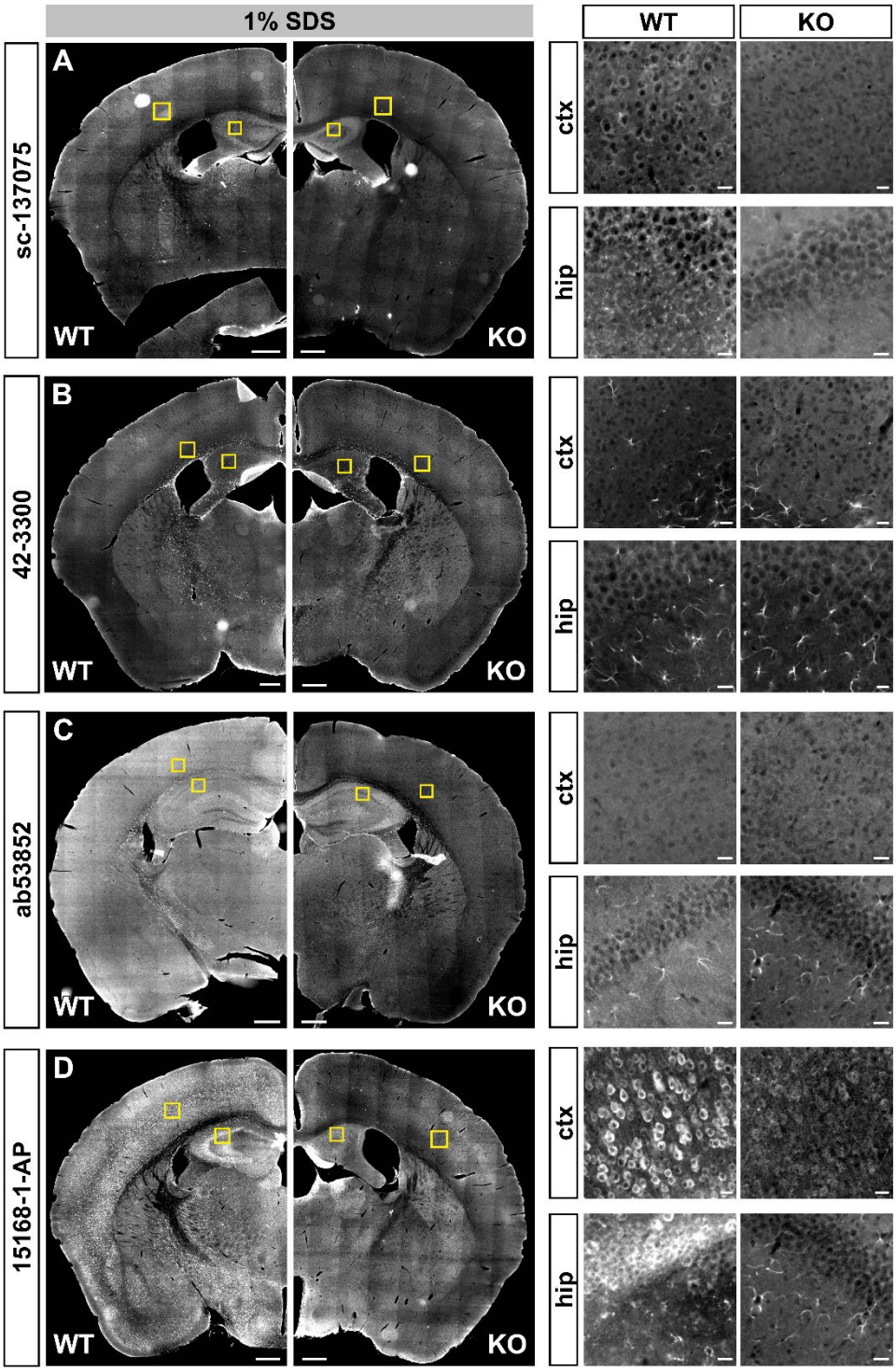

Supplementary Figure 5. Performances of various commercial S1R antibodies in IHC with SDS-antigen retrieval.

A-D. Brain sections from WT and S1R KO mice were pre-treated with 1% SDS and immune-stained by various S1R antibodies from Santa Cruz (sc-137075), Invitrogen (42-3300), Abcam (ab53852) and Proteintech (15168-1-AP), respectively. Magnified images on the right side correspond to boxed regions from ctx and hip in a-d. Scale bars = 200 μm in a-d and 5 μm in magnified images.

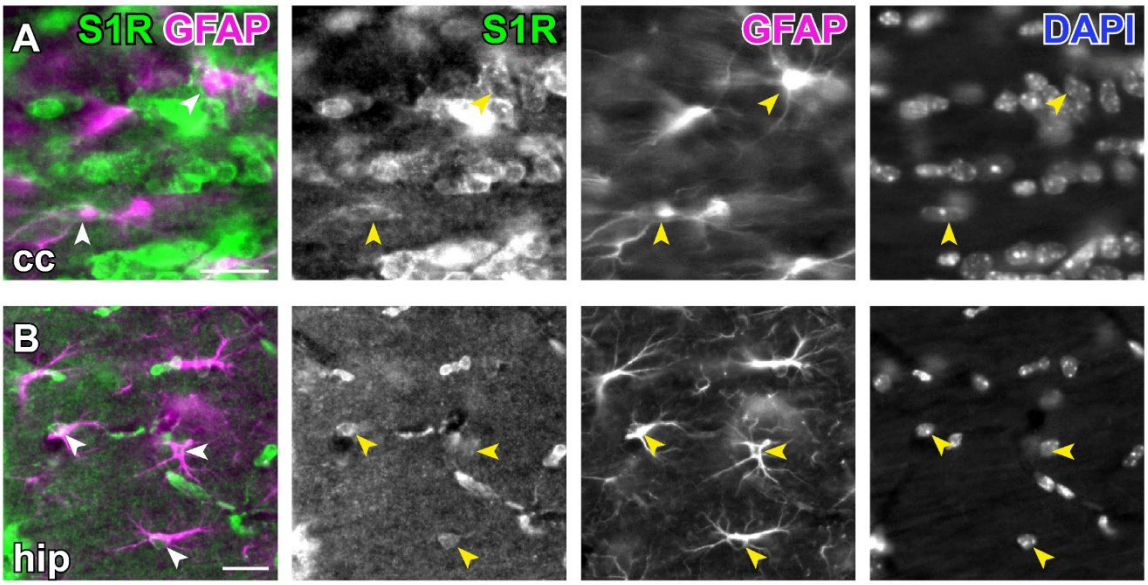

Supplementary Figure 6. Expression pattern of S1Rs in astrocytes *in situ*.
A-B. Axioscan images showing the ring-like structure of S1R staining in GFAP$^+$ astrocytes in the corpus callosum (cc, **A**), hippocampus (hip, **B**).

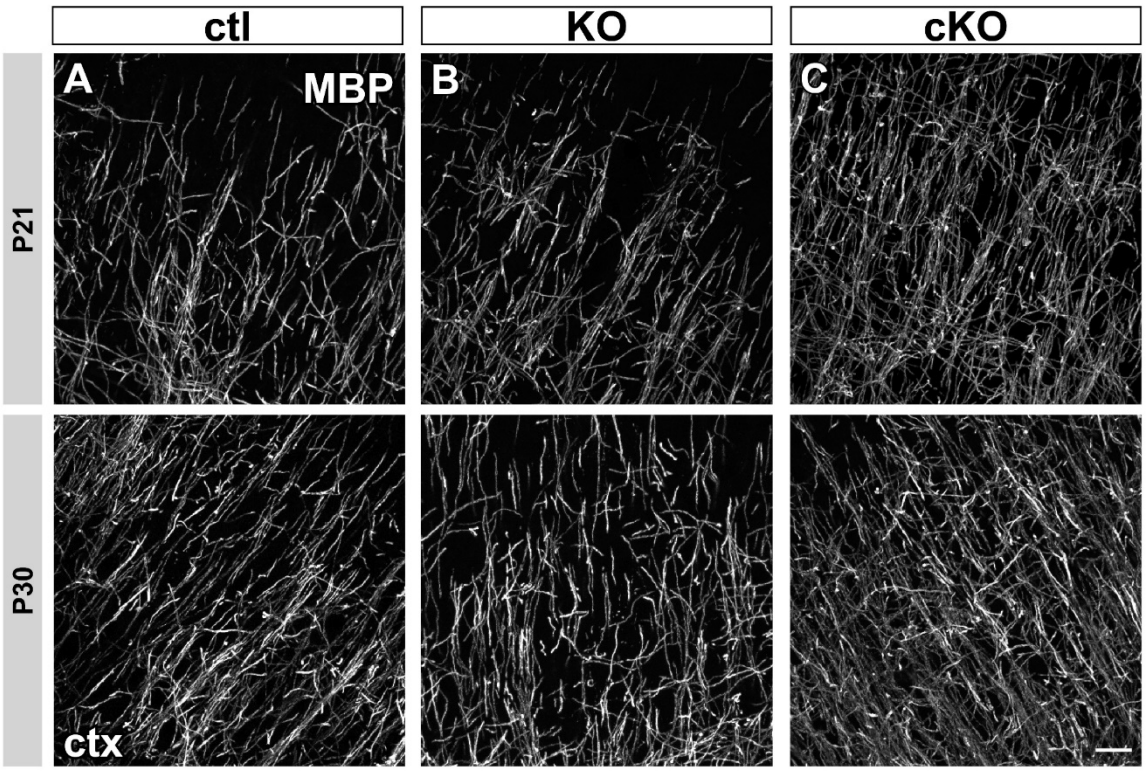

Supplementary Figure 7. Myelination of cortex in S1R KO and S1R cKO mice at P21 and P30.

A-C. Representative confocal images showing MBP staining in the ctx of ctl (**A**), KO (**B**) and cKO (**C**) mice at P21 and P30. Scale bars = 20 µm.

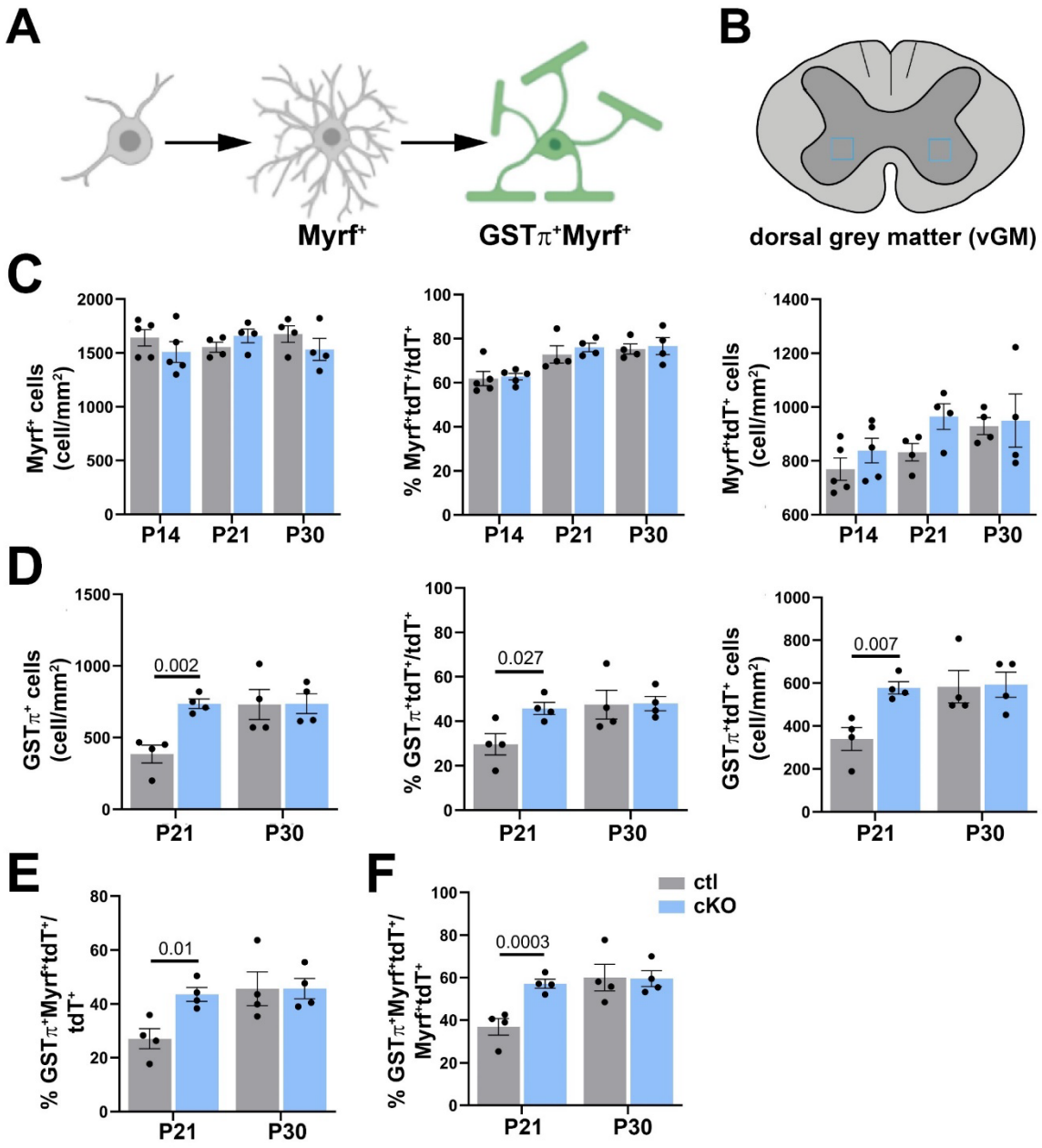

Supplementary Figure 8. Conditional deletion of S1Rs in OPCs leads to precocious maturation of OLs in spinal vGM during development.

A. Schematic representation of the analysed OL developmental stages and the corresponding markers. **B.** Schematic image of the spinal cord, indicating the regions of interest in the ventral grey matter (vGM) using blue squares. **C.** Quantitative expression analysis of Myrf$^+$, Myrf$^+$tdT$^+$ numbers, and the percentage of Myrf$^+$tdT$^+$ among all tdT$^+$ cells in the spinal vGM of ctl and cKO mice at different ages. **D.** Quantitative results of the density of GSTπ$^+$, GSTπ$^+$tdT$^+$ cells and the percentage of GSTπ$^+$tdT$^+$ cells in all tdT$^+$ cells in the spinal vGM of ctl and cKO mice at P21 and P30. **F-G.** Quantitative analysis of the percentage of Myrf$^+$GSTπ$^+$tdT$^+$ cells among all tdT$^+$ or Myrf$^+$tdT$^+$ cells in the spinal vGM of ctl and cKO mice at P21 and P30. Each dot represents one mouse. Scale bar = 20 μm.

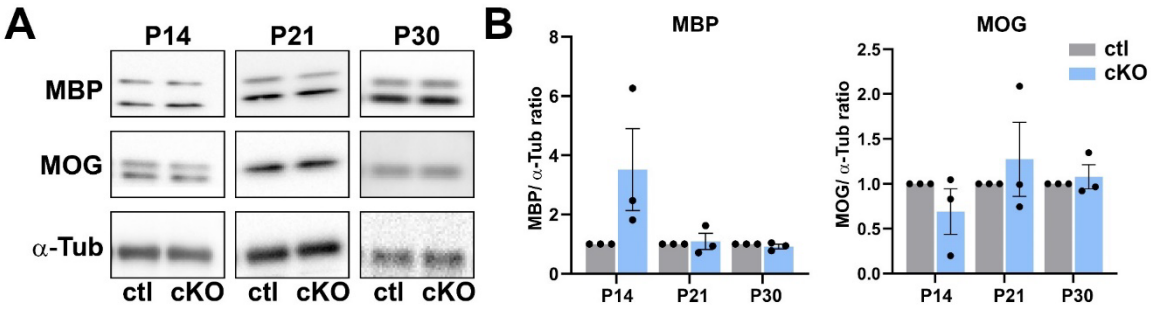

Supplementary Figure 9. Unaltered myelin-related genes in the spinal cord of S1R cKO mice.

A. Western blot images of MBP (16 and 18 kDa) and MOG (28 kDa) in protein lysates from the cervical spinal cord of ctl and cKO mice at different ages. **B.** Quantitative analysis of grayscale values of MBP and MOG protein levels, which were normalized to that of α-Tubulin used as loading control. Each dot represents one mouse.

11 References

Abdullah CS et al. (2020) Methamphetamine induces cardiomyopathy by Sigmar1 inhibition-dependent impairment of mitochondrial dynamics and function. Commun Biol 3:682.

Abraham MJ, Fleming KL, Raymond S, Wong AYC, Bergeron R (2019) The sigma-1 receptor behaves as an atypical auxiliary subunit to modulate the functional characteristics of Kv1.2 channels expressed in HEK293 cells. Physiol Rep 7:e14147.

Allahtavakoli M, Jarrott B (2011) Sigma-1 receptor ligand PRE-084 reduced infarct volume, neurological deficits, pro-inflammatory cytokines and enhanced anti-inflammatory cytokines after embolic stroke in rats. Brain Res Bull 85:219-224.

Almeida RG (2018) The Rules of Attraction in Central Nervous System Myelination. Front Cell Neurosci 12:367.

Alonso G, Phan V, Guillemain I, Saunier M, Legrand A, Anoal M, Maurice T (2000) Immunocytochemical localization of the sigma(1) receptor in the adult rat central nervous system. Neuroscience 97:155-170.

Aprato J, Sock E, Weider M, Elsesser O, Fröb F, Wegner M (2020) Myrf guides target gene selection of transcription factor Sox10 during oligodendroglial development. Nucleic Acids Res 48:1254-1270.

Bacon C, Lakics V, Machesky L, Rumsby M (2007) N-WASP regulates extension of filopodia and processes by oligodendrocyte progenitors, oligodendrocytes, and Schwann cells-implications for axon ensheathment at myelination. Glia 55:844-858.

Balasuriya D, Stewart AP, Crottès D, Borgese F, Soriani O, Edwardson JM (2012) The sigma-1 receptor binds to the Nav1.5 voltage-gated Na+ channel with 4-fold symmetry. J Biol Chem 287:37021-37029.

Barres BA, Raff MC (1993) Proliferation of oligodendrocyte precursor cells depends on electrical activity in axons. Nature 361:258-260.

Barres BA, Hart IK, Coles HS, Burne JF, Voyvodic JT, Richardson WD, Raff MC (1992) Cell death and control of cell survival in the oligodendrocyte lineage. Cell 70:31-46.

Bauer NG, Richter-Landsberg C, Ffrench-Constant C (2009) Role of the oligodendroglial cytoskeleton in differentiation and myelination. Glia 57:1691-1705.

Bechler ME, Byrne L, Ffrench-Constant C (2015) CNS Myelin Sheath Lengths Are an Intrinsic Property of Oligodendrocytes. Curr Biol 25:2411-2416.

Bergles DE, Jabs R, Steinhäuser C (2010) Neuron-glia synapses in the brain. Brain Res Rev 63:130-137.

Boiko T, Winckler B (2006) Myelin under construction -- teamwork required. J Cell Biol 172:799-801.

Borbély E, Varga V, Szögi T, Schuster I, Bozsó Z, Penke B, Fülöp L (2022) Impact of Two Neuronal Sigma-1 Receptor Modulators, PRE084 and DMT, on Neurogenesis and Neuroinflammation in an Aβ. Int J Mol Sci 23.

Brown D, Lydon J, McLaughlin M, Stuart-Tilley A, Tyszkowski R, Alper S (1996) Antigen retrieval in cryostat tissue sections and cultured cells by treatment with sodium dodecyl sulfate (SDS). Histochem Cell Biol 105:261-267.

Bujalka H, Koenning M, Jackson S, Perreau VM, Pope B, Hay CM, Mitew S, Hill AF, Lu QR, Wegner M, Srinivasan R, Svaren J, Willingham M, Barres BA, Emery B (2013) MYRF is a membrane-associated transcription factor that autoproteolytically cleaves to directly activate myelin genes. PLoS Biol 11:e1001625.

Cellerino A, Carroll P, Thoenen H, Barde YA (1997) Reduced size of retinal ganglion cell axons and hypomyelination in mice lacking brain-derived neurotrophic factor. Mol Cell Neurosci 9:397-408.

Cheli VT, Santiago González DA, Namgyal Lama T, Spreuer V, Handley V, Murphy GG, Paez PM (2016) Conditional Deletion of the L-Type Calcium Channel Cav1.2 in Oligodendrocyte Progenitor Cells Affects Postnatal Myelination in Mice. J Neurosci 36:10853-10869.

Chen Y, Wu H, Wang S, Koito H, Li J, Ye F, Hoang J, Escobar SS, Gow A, Arnett HA, Trapp BD, Karandikar NJ, Hsieh J, Lu QR (2009) The oligodendrocyte-specific G protein-coupled receptor GPR17 is a cell-intrinsic timer of myelination. Nat Neurosci 12:1398-1406.

Chevallier N, Keller E, Maurice T (2011) Behavioural phenotyping of knockout mice for the sigma-1 (σ_1) chaperone protein revealed gender-related anxiety, depressive-like and memory alterations. J Psychopharmacol 25:960-975.

Chew LJ, King WC, Kennedy A, Gallo V (2005) Interferon-gamma inhibits cell cycle exit in differentiating oligodendrocyte progenitor cells. Glia 52:127-143.

Christ MG, Huesmann H, Nagel H, Kern A, Behl C (2019) Sigma-1 Receptor Activation Induces Autophagy and Increases Proteostasis Capacity In Vitro and In Vivo. Cells 8.

Cobos EJ, Entrena JM, Nieto FR, Cendán CM, Del Pozo E (2008) Pharmacology and therapeutic potential of sigma(1) receptor ligands. Curr Neuropharmacol 6:344-366.

Couly S, Goguadze N, Yasui Y, Kimura Y, Wang SM, Sharikadze N, Wu HE, Su TP (2022) Knocking Out Sigma-1 Receptors Reveals Diverse Health Problems. Cell Mol Neurobiol 42:597-620.

Dai J, Bercury KK, Ahrendsen JT, Macklin WB (2015) Olig1 function is required for oligodendrocyte differentiation in the mouse brain. J Neurosci 35:4386-4402.

Demerens C, Stankoff B, Zalc B, Lubetzki C (1999) Eliprodil stimulates CNS myelination: new prospects for multiple sclerosis? Neurology 52:346-350.

Demerens C, Stankoff B, Logak M, Anglade P, Allinquant B, Couraud F, Zalc B, Lubetzki C (1996) Induction of myelination in the central nervous system by electrical activity. Proc Natl Acad Sci U S A 93:9887-9892.

Dimou L, Gallo V (2015) NG2-glia and their functions in the central nervous system. Glia 63:1429-1451.

Djalali S, Höltje M, Grosse G, Rothe T, Stroh T, Grosse J, Deng DR, Hellweg R, Grantyn R, Hörtnagl H, Ahnert-Hilger G (2005) Effects of brain-derived neurotrophic factor (BDNF) on glial cells and serotonergic neurones during development. J Neurochem 92:616-627.

Díez-Revuelta N, Higuero AM, Velasco S, Peñas-de-la-Iglesia M, Gabius HJ, Abad-Rodríguez J (2017) Neurons define non-myelinated axon segments by the regulation of galectin-4-containing axon membrane domains. Sci Rep 7:12246.

El Waly B, Macchi M, Cayre M, Durbec P (2014) Oligodendrogenesis in the normal and pathological central nervous system. Front Neurosci 8:145.

El-Brolosy MA, Stainier DYR (2017) Genetic compensation: A phenomenon in search of mechanisms. PLoS Genet 13:e1006780.

Elbaz B, Popko B (2019) Molecular Control of Oligodendrocyte Development. Trends Neurosci 42:263-277.

Fang LP, Bai X (2023) Oligodendrocyte precursor cells: the multitaskers in the brain. Pflugers Arch.

Fang LP, Zhao N, Caudal LC, Chang HF, Zhao R, Lin CH, Hainz N, Meier C, Bettler B, Huang W, Scheller A, Kirchhoff F, Bai X (2022) Impaired bidirectional communication between interneurons and oligodendrocyte precursor cells affects social cognitive behavior. Nat Commun 13:1394.

Fard MK, van der Meer F, Sánchez P, Cantuti-Castelvetri L, Mandad S, Jäkel S, Fornasiero EF, Schmitt S, Ehrlich M, Starost L, Kuhlmann T, Sergiou C, Schultz V, Wrzos C, Brück W, Urlaub H, Dimou L, Stadelmann C, Simons M (2017) BCAS1 expression defines a population of early myelinating oligodendrocytes in multiple sclerosis lesions. Sci Transl Med 9.

Fernandez PA, Tang DG, Cheng L, Prochiantz A, Mudge AW, Raff MC (2000) Evidence that axon-derived neuregulin promotes oligodendrocyte survival in the developing rat optic nerve. Neuron 28:81-90.

Fontanilla D, Johannessen M, Hajipour AR, Cozzi NV, Jackson MB, Ruoho AE (2009) The hallucinogen N,N-dimethyltryptamine (DMT) is an endogenous sigma-1 receptor regulator. Science 323:934-937.

Francardo V, Bez F, Wieloch T, Nissbrandt H, Ruscher K, Cenci MA (2014) Pharmacological stimulation of sigma-1 receptors has neurorestorative effects in experimental parkinsonism. Brain 137:1998-2014.

Friede RL (1972) Control of myelin formation by axon caliber (with a model of the control mechanism). J Comp Neurol 144:233-252.

Fünfschilling U, Supplie LM, Mahad D, Boretius S, Saab AS, Edgar J, Brinkmann BG, Kassmann CM, Tzvetanova ID, Möbius W, Diaz F, Meijer D, Suter U, Hamprecht B, Sereda MW, Moraes CT, Frahm J, Goebbels S, Nave KA (2012) Glycolytic oligodendrocytes maintain myelin and long-term axonal integrity. Nature 485:517-521.

Gaja-Capdevila N, Hernández N, Navarro X, Herrando-Grabulosa M (2021) Sigma-1 Receptor is a Pharmacological Target to Promote Neuroprotection in the SOD1. Front Pharmacol 12:780588.

Gao XF, Yao JJ, He YL, Hu C, Mei YA (2012) Sigma-1 receptor agonists directly inhibit Nav1.2/1.4 channels. PLoS One 7:e49384.

Gard AL, Burrell MR, Pfeiffer SE, Rudge JS, Williams WC (1995) Astroglial control of oligodendrocyte survival mediated by PDGF and leukemia inhibitory factor-like protein. Development 121:2187-2197.

Gekker G, Hu S, Sheng WS, Rock RB, Lokensgard JR, Peterson PK (2006) Cocaine-induced HIV-1 expression in microglia involves sigma-1 receptors and transforming growth factor-beta1. Int Immunopharmacol 6:1029-1033.

Gibson EM, Purger D, Mount CW, Goldstein AK, Lin GL, Wood LS, Inema I, Miller SE, Bieri G, Zuchero JB, Barres BA, Woo PJ, Vogel H, Monje M (2014) Neuronal activity promotes oligodendrogenesis and adaptive myelination in the mammalian brain. Science 344:1252304.

Goebbels S, Wieser GL, Pieper A, Spitzer S, Weege B, Yan K, Edgar JM, Yagensky O, Wichert SP, Agarwal A, Karram K, Renier N, Tessier-Lavigne M, Rossner MJ, Káradóttir RT, Nave KA (2017) A neuronal PI(3,4,5)P. Nat Neurosci 20:10-15.

Gromek KA, Suchy FP, Meddaugh HR, Wrobel RL, LaPointe LM, Chu UB, Primm JG, Ruoho AE, Senes A, Fox BG (2014) The oligomeric states of the purified sigma-1 receptor are stabilized by ligands. J Biol Chem 289:20333-20344.

Gundlach AL, Largent BL, Snyder SH (1986) Autoradiographic localization of sigma receptor binding sites in guinea pig and rat central nervous system with (+)3H-3-(3-hydroxyphenyl)-N-(1-propyl)piperidine. J Neurosci 6:1757-1770.

Guo F, Wang Y (2023) TCF7l2, a nuclear marker that labels premyelinating oligodendrocytes and promotes oligodendroglial lineage progression. Glia 71:143-154.

Guo Q, Scheller A, Huang W (2021) Progenies of NG2 glia: what do we learn from transgenic mouse models ? Neural Regen Res 16:43-48.

Haak LL, Song LS, Molinski TF, Pessah IN, Cheng H, Russell JT (2001) Sparks and puffs in oligodendrocyte progenitors: cross talk between ryanodine receptors and inositol trisphosphate receptors. J Neurosci 21:3860-3870.

Hanner M, Moebius FF, Flandorfer A, Knaus HG, Striessnig J, Kempner E, Glossmann H (1996) Purification, molecular cloning, and expression of the mammalian sigma1-binding site. Proc Natl Acad Sci U S A 93:8072-8077.

Hayashi T (2015) Sigma-1 receptor: the novel intracellular target of neuropsychotherapeutic drugs. J Pharmacol Sci 127:2-5.

Hayashi T, Su TP (2004a) Sigma-1 receptors at galactosylceramide-enriched lipid microdomains regulate oligodendrocyte differentiation. Proc Natl Acad Sci U S A 101:14949-14954.

Hayashi T, Su TP (2004b) Sigma-1 receptor ligands: potential in the treatment of neuropsychiatric disorders. CNS Drugs 18:269-284.

Hayashi T, Su TP (2007) Sigma-1 receptor chaperones at the ER-mitochondrion interface regulate Ca(2+) signaling and cell survival. Cell 131:596-610.

Hayashi T, Su TP (2010) Cholesterol at the endoplasmic reticulum: roles of the sigma-1 receptor chaperone and implications thereof in human diseases. Subcell Biochem 51:381-398.

Hayashi T, Lewis A, Hayashi E, Betenbaugh MJ, Su TP (2011) Antigen retrieval to improve the immunocytochemistry detection of sigma-1 receptors and ER chaperones. Histochem Cell Biol 135:627-637.

Hellewell SB, Bowen WD (1990) A sigma-like binding site in rat pheochromocytoma (PC12) cells: decreased affinity for (+)-benzomorphans and lower molecular weight suggest a different sigma receptor form from that of guinea pig brain. Brain Res 527:244-253.

Hetz C (2012) The unfolded protein response: controlling cell fate decisions under ER stress and beyond. Nat Rev Mol Cell Biol 13:89-102.

Hildebrand C, Waxman SG (1984) Postnatal differentiation of rat optic nerve fibers: electron microscopic observations on the development of nodes of Ranvier and axoglial relations. J Comp Neurol 224:25-37.

Hines JH, Ravanelli AM, Schwindt R, Scott EK, Appel B (2015) Neuronal activity biases axon selection for myelination in vivo. Nat Neurosci 18:683-689.

Hirrlinger PG, Scheller A, Braun C, Quintela-Schneider M, Fuss B, Hirrlinger J, Kirchhoff F (2005) Expression of reef coral fluorescent proteins in the central nervous system of transgenic mice. Mol Cell Neurosci 30:291-303.

Hong W, Nuwayhid SJ, Werling LL (2004) Modulation of bradykinin-induced calcium changes in SH-SY5Y cells by neurosteroids and sigma receptor ligands via a shared mechanism. Synapse 54:102-110.

Hornig J, Fröb F, Vogl MR, Hermans-Borgmeyer I, Tamm ER, Wegner M (2013) The transcription factors Sox10 and Myrf define an essential regulatory network module in differentiating oligodendrocytes. PLoS Genet 9:e1003907.

Huang W, Bai X, Meyer E, Scheller A (2020) Acute brain injuries trigger microglia as an additional source of the proteoglycan NG2. Acta Neuropathol Commun 8:146.

Huang W, Guo Q, Bai X, Scheller A, Kirchhoff F (2019) Early embryonic NG2 glia are exclusively gliogenic and do not generate neurons in the brain. Glia.

Huang W, Zhao N, Bai X, Karram K, Trotter J, Goebbels S, Scheller A, Kirchhoff F (2014) Novel NG2-CreERT2 knock-in mice demonstrate heterogeneous differentiation potential of NG2 glia during development. Glia 62:896-913.

Hughes EG, Stockton ME (2021) Premyelinating Oligodendrocytes: Mechanisms Underlying Cell Survival and Integration. Front Cell Dev Biol 9:714169.

Hughes EG, Orthmann-Murphy JL, Langseth AJ, Bergles DE (2018) Myelin remodeling through experience-dependent oligodendrogenesis in the adult somatosensory cortex. Nat Neurosci 21:696-706.

Jakovcevski I, Mo Z, Zecevic N (2007) Down-regulation of the axonal polysialic acid-neural cell adhesion molecule expression coincides with the onset of myelination in the human fetal forebrain. Neuroscience 149:328-337.

Jepson S, Vought B, Gross CH, Gan L, Austen D, Frantz JD, Zwahlen J, Lowe D, Markland W, Krauss R (2012) LINGO-1, a transmembrane signaling protein, inhibits oligodendrocyte differentiation and myelination through intercellular self-interactions. J Biol Chem 287:22184-22195.

Kargbo RB (2021) Sigma-1 and Sigma-2 Receptor Modulators as Potential Therapeutics for Alzheimer's Disease. ACS Med Chem Lett 12:178-179.

Kessaris N, Fogarty M, Iannarelli P, Grist M, Wegner M, Richardson WD (2006) Competing waves of oligodendrocytes in the forebrain and postnatal elimination of an embryonic lineage. Nat Neurosci 9:173-179.

Kiefer JC (2007) Back to basics: Sox genes. Dev Dyn 236:2356-2366.

Kirischuk S, Scherer J, Möller T, Verkhratsky A, Kettenmann H (1995) Subcellular heterogeneity of voltage-gated Ca2+ channels in cells of the oligodendrocyte lineage. Glia 13:1-12.

Koenning M, Jackson S, Hay CM, Faux C, Kilpatrick TJ, Willingham M, Emery B (2012) Myelin gene regulatory factor is required for maintenance of myelin and mature oligodendrocyte identity in the adult CNS. J Neurosci 32:12528-12542.

Kondo T, Raff M (2000) The Id4 HLH protein and the timing of oligodendrocyte differentiation. EMBO J 19:1998-2007.

Kordes U, Cheng YC, Scotting PJ (2005) Sox group E gene expression distinguishes different types and maturational stages of glial cells in developing chick and mouse. Brain Res Dev Brain Res 157:209-213.

Kourrich S, Hayashi T, Chuang JY, Tsai SY, Su TP, Bonci A (2013) Dynamic interaction between sigma-1 receptor and Kv1.2 shapes neuronal and behavioral responses to cocaine. Cell 152:236-247.

Laflamme C, McKeever PM, Kumar R, Schwartz J, Kolahdouzan M, Chen CX, You Z, Benaliouad F, Gileadi O, McBride HM, Durcan TM, Edwards AM, Healy LM, Robertson J, McPherson PS (2019) Implementation of an antibody characterization procedure and application to the major ALS/FTD disease gene C9ORF72. Elife 8.

Lasbleiz C, Peyrel A, Tarot P, Sarniguet J, Crouzier L, Cubedo N, Delprat B, Rossel M, Maurice T, Liévens JC (2022) Sigma-1 receptor agonist PRE-084 confers protection against TAR DNA-binding protein-43 toxicity through NRF2 signalling. Redox Biol 58:102542.

Laursen LS, Chan CW, ffrench-Constant C (2009) An integrin-contactin complex regulates CNS myelination by differential Fyn phosphorylation. J Neurosci 29:9174-9185.

Lee X, Yang Z, Shao Z, Rosenberg SS, Levesque M, Pepinsky RB, Qiu M, Miller RH, Chan JR, Mi S (2007) NGF regulates the expression of axonal LINGO-1 to inhibit oligodendrocyte differentiation and myelination. J Neurosci 27:220-225.

Li T, Wang L, Ma T, Wang S, Niu J, Li H, Xiao L (2018) Dynamic Calcium Release From Endoplasmic Reticulum Mediated by Ryanodine Receptor 3 Is Crucial for Oligodendroglial Differentiation. Front Mol Neurosci 11:162.

Li Y, Tennekoon GI, Birnbaum M, Marchionni MA, Rutkowski JL (2001) Neuregulin signaling through a PI3K/Akt/Bad pathway in Schwann cell survival. Mol Cell Neurosci 17:761-767.

Liang X, Draghi NA, Resh MD (2004) Signaling from integrins to Fyn to Rho family GTPases regulates morphologic differentiation of oligodendrocytes. J Neurosci 24:7140-7149.

Ligon KL, Fancy SP, Franklin RJ, Rowitch DH (2006) Olig gene function in CNS development and disease. Glia 54:1-10.

Linneberg C, Harboe M, Laursen LS (2015) Axo-Glia Interaction Preceding CNS Myelination Is Regulated by Bidirectional Eph-Ephrin Signaling. ASN Neuro 7.

Lisak RP, Nedelkoska L, Benjamins JA (2020) Sigma-1 receptor agonists as potential protective therapies in multiple sclerosis. J Neuroimmunol 342:577188.

Liu Q, Guo Q, Fang LP, Yao H, Scheller A, Kirchhoff F, Huang W (2023) Specific detection and deletion of the sigma-1 receptor widely expressed in neurons and glial cells in vivo. J Neurochem 164:764-785.

Lu QR, Sun T, Zhu Z, Ma N, Garcia M, Stiles CD, Rowitch DH (2002) Common developmental requirement for Olig function indicates a motor neuron/oligodendrocyte connection. Cell 109:75-86.

Lu QR, Yuk D, Alberta JA, Zhu Z, Pawlitzky I, Chan J, McMahon AP, Stiles CD, Rowitch DH (2000) Sonic hedgehog--regulated oligodendrocyte lineage genes encoding bHLH proteins in the mammalian central nervous system. Neuron 25:317-329.

Lunn KF, Baas PW, Duncan ID (1997) Microtubule organization and stability in the oligodendrocyte. J Neurosci 17:4921-4932.

Mancuso R, Oliván S, Rando A, Casas C, Osta R, Navarro X (2012) Sigma-1R agonist improves motor function and motoneuron survival in ALS mice. Neurotherapeutics 9:814-826.

Marques S et al. (2016) Oligodendrocyte heterogeneity in the mouse juvenile and adult central nervous system. Science 352:1326-1329.

Martin WR, Eades CG, Thompson JA, Huppler RE, Gilbert PE (1976) The effects of morphine- and nalorphine-like drugs in the nondependent and morphine-dependent chronic spinal dog. J Pharmacol Exp Ther 197:517-532.

Matsumoto RR, McCracken KA, Pouw B, Zhang Y, Bowen WD (2002) Involvement of sigma receptors in the behavioral effects of cocaine: evidence from novel ligands and antisense oligodeoxynucleotides. Neuropharmacology 42:1043-1055.

Matsumoto RR, Bowen WD, Tom MA, Vo VN, Truong DD, De Costa BR (1995) Characterization of two novel sigma receptor ligands: antidystonic effects in rats suggest sigma receptor antagonism. Eur J Pharmacol 280:301-310.

Maurice T (2016) Protection by sigma-1 receptor agonists is synergic with donepezil, but not with memantine, in a mouse model of amyloid-induced memory impairments. Behav Brain Res 296:270-278.

Maurice T, Privat A (1997) SA4503, a novel cognitive enhancer with sigma1 receptor agonist properties, facilitates NMDA receptor-dependent learning in mice. Eur J Pharmacol 328:9-18.

Maurice T, Su TP (2009) The pharmacology of sigma-1 receptors. Pharmacol Ther 124:195-206.

Maurice T, Urani A, Phan VL, Romieu P (2001) The interaction between neuroactive steroids and the sigma1 receptor function: behavioral consequences and therapeutic opportunities. Brain Res Brain Res Rev 37:116-132.

Maurice T, Su TP, Parish DW, Nabeshima T, Privat A (1994) PRE-084, a sigma selective PCP derivative, attenuates MK-801-induced impairment of learning in mice. Pharmacol Biochem Behav 49:859-869.

Mavlyutov TA, Epstein ML, Andersen KA, Ziskind-Conhaim L, Ruoho AE (2010) The sigma-1 receptor is enriched in postsynaptic sites of C-terminals in mouse motoneurons. An anatomical and behavioral study. Neuroscience 167:247-255.

Mavlyutov TA, Epstein ML, Verbny YI, Huerta MS, Zaitoun I, Ziskind-Conhaim L, Ruoho AE (2013) Lack of sigma-1 receptor exacerbates ALS progression in mice. Neuroscience 240:129-134.

Mavlyutov TA, Duellman T, Kim HT, Epstein ML, Leese C, Davletov BA, Yang J (2016) Sigma-1 receptor expression in the dorsal root ganglion: Reexamination using a highly specific antibody. Neuroscience 331:148-157.

McKinnon RD, Waldron S, Kiel ME (2005) PDGF alpha-receptor signal strength controls an RTK rheostat that integrates phosphoinositol 3'-kinase and phospholipase Cgamma pathways during oligodendrocyte maturation. J Neurosci 25:3499-3508.

Mei F, Wang H, Liu S, Niu J, Wang L, He Y, Etxeberria A, Chan JR, Xiao L (2013) Stage-specific deletion of Olig2 conveys opposing functions on differentiation and maturation of oligodendrocytes. J Neurosci 33:8454-8462.

Mei J, Pasternak GW (2001) Molecular cloning and pharmacological characterization of the rat sigma1 receptor. Biochem Pharmacol 62:349-355.

Meng F, Xiao Y, Ji Y, Sun Z, Zhou X (2022) An open-like conformation of the sigma-1 receptor reveals its ligand entry pathway. Nat Commun 13:1267.

Michailov GV, Sereda MW, Brinkmann BG, Fischer TM, Haug B, Birchmeier C, Role L, Lai C, Schwab MH, Nave KA (2004) Axonal neuregulin-1 regulates myelin sheath thickness. Science 304:700-703.

Miller RH (2002) Regulation of oligodendrocyte development in the vertebrate CNS. Prog Neurobiol 67:451-467.

Miron VE (2017) Microglia-driven regulation of oligodendrocyte lineage cells, myelination, and remyelination. J Leukoc Biol 101:1103-1108.

Mishina M, Ohyama M, Ishii K, Kitamura S, Kimura Y, Oda K, Kawamura K, Sasaki T, Kobayashi S, Katayama Y, Ishiwata K (2008) Low density of sigma1 receptors in early Alzheimer's disease. Ann Nucl Med 22:151-156.

Mishra AK, Mavlyutov T, Singh DR, Biener G, Yang J, Oliver JA, Ruoho A, Raicu V (2015) The sigma-1 receptors are present in monomeric and oligomeric forms in living cells in the presence and absence of ligands. Biochem J 466:263-271.

Monnet FP, Debonnel G, Junien JL, De Montigny C (1990) N-methyl-D-aspartate-induced neuronal activation is selectively modulated by sigma receptors. Eur J Pharmacol 179:441-445.

Mori T, Hayashi T, Hayashi E, Su TP (2013) Sigma-1 receptor chaperone at the ER-mitochondrion interface mediates the mitochondrion-ER-nucleus signaling for cellular survival. PLoS One 8:e76941.

Mori T, Tanaka K, Buffo A, Wurst W, Kühn R, Götz M (2006) Inducible gene deletion in astroglia and radial glia--a valuable tool for functional and lineage analysis. Glia 54:21-34.

Motawe ZY, Abdelmaboud SS, Cuevas J, Breslin JW (2020) PRE-084 as a tool to uncover potential therapeutic applications for selective sigma-1 receptor activation. Int J Biochem Cell Biol 126:105803.

Moura DMS, Brennan EJ, Brock R, Cocas LA (2021) Neuron to Oligodendrocyte Precursor Cell Synapses: Protagonists in Oligodendrocyte Development and Myelination, and Targets for Therapeutics. Front Neurosci 15:779125.

Nakamura Y, Dryanovski DI, Kimura Y, Jackson SN, Woods AS, Yasui Y, Tsai SY, Patel S, Covey DP, Su TP, Lupica CR (2019) Cocaine-induced endocannabinoid signaling mediated by sigma-1 receptors and extracellular vesicle secretion. Elife 8.

Narita N, Hashimoto K, Tomitaka S, Minabe Y (1996) Interactions of selective serotonin reuptake inhibitors with subtypes of sigma receptors in rat brain. Eur J Pharmacol 307:117-119.

Nash B, Thomson CE, Linington C, Arthur AT, McClure JD, McBride MW, Barnett SC (2011) Functional duality of astrocytes in myelination. J Neurosci 31:13028-13038.

Nave KA, Werner HB (2014) Myelination of the nervous system: mechanisms and functions. Annu Rev Cell Dev Biol 30:503-533.

Nguyen EC, McCracken KA, Liu Y, Pouw B, Matsumoto RR (2005) Involvement of sigma (sigma) receptors in the acute actions of methamphetamine: receptor binding and behavioral studies. Neuropharmacology 49:638-645.

Nicholas RS, Stevens S, Wing MG, Compston DA (2002) Microglia-derived IGF-2 prevents TNFalpha induced death of mature oligodendrocytes in vitro. J Neuroimmunol 124:36-44.

Nishiyama A, Komitova M, Suzuki R, Zhu X (2009) Polydendrocytes (NG2 cells): multifunctional cells with lineage plasticity. Nat Rev Neurosci 10:9-22.

Okuyama S, Imagawa Y, Ogawa S, Araki H, Ajima A, Tanaka M, Muramatsu M, Nakazato A, Yamaguchi K, Yoshida M (1993) NE-100, a novel sigma receptor ligand: in vivo tests. Life Sci 53:PL285-290.

Ono Y, Tanaka H, Takata M, Nagahara Y, Noda Y, Tsuruma K, Shimazawa M, Hozumi I, Hara H (2014) SA4503, a sigma-1 receptor agonist, suppresses motor neuron damage in in vitro and in vivo amyotrophic lateral sclerosis models. Neurosci Lett 559:174-178.

Palacios G, Muro A, Vela JM, Molina-Holgado E, Guitart X, Ovalle S, Zamanillo D (2003) Immunohistochemical localization of the sigma1-receptor in oligodendrocytes in the rat central nervous system. Brain Res 961:92-99.

Park J, Liu B, Chen T, Li H, Hu X, Gao J, Zhu Y, Zhu Q, Qiang B, Yuan J, Peng X, Qiu M (2008) Disruption of Nectin-like 1 cell adhesion molecule leads to delayed axonal myelination in the CNS. J Neurosci 28:12815-12819.

Park SK, Miller R, Krane I, Vartanian T (2001) The erbB2 gene is required for the development of terminally differentiated spinal cord oligodendrocytes. J Cell Biol 154:1245-1258.

Pasquale EB (2008) Eph-ephrin bidirectional signaling in physiology and disease. Cell 133:38-52.

Prasanth MI, Malar DS, Tencomnao T, Brimson JM (2021) The emerging role of the sigma-1 receptor in autophagy: hand-in-hand targets for the treatment of Alzheimer's. Expert Opin Ther Targets 25:401-414.

Redmond SA, Mei F, Eshed-Eisenbach Y, Osso LA, Leshkowitz D, Shen YA, Kay JN, Aurrand-Lions M, Lyons DA, Peles E, Chan JR (2016) Somatodendritic Expression of JAM2 Inhibits Oligodendrocyte Myelination. Neuron 91:824-836.

Richardson WD, Kessaris N, Pringle N (2006) Oligodendrocyte wars. Nat Rev Neurosci 7:11-18.

Rinholm JE, Hamilton NB, Kessaris N, Richardson WD, Bergersen LH, Attwell D (2011) Regulation of oligodendrocyte development and myelination by glucose and lactate. J Neurosci 31:538-548.

Rosen DA, Seki SM, Fernández-Castañeda A, Beiter RM, Eccles JD, Woodfolk JA, Gaultier A (2019) Modulation of the sigma-1 receptor-IRE1 pathway is beneficial in preclinical models of inflammation and sepsis. Sci Transl Med 11.

Rossino G, Orellana I, Caballero J, Schepmann D, Wünsch B, Rui M, Rossi D, González-Avendaño M, Collina S, Vergara-Jaque A (2020) New Insights into the Opening of the Occluded Ligand-Binding Pocket of Sigma1 Receptor: Binding of a Novel Bivalent RC-33 Derivative. J Chem Inf Model 60:756-765.

Rumsby M, Afsari F, Stark M, Hughson E (2003) Microfilament and microtubule organization and dynamics in process extension by central glia-4 oligodendrocytes: evidence for a microtubule organizing center. Glia 42:118-129.

Ruscher K, Shamloo M, Rickhag M, Ladunga I, Soriano L, Gisselsson L, Toresson H, Ruslim-Litrus L, Oksenberg D, Urfer R, Johansson BB, Nikolich K, Wieloch T (2011) The sigma-1 receptor enhances brain plasticity and functional recovery after experimental stroke. Brain 134:732-746.

Sabeti J, Nelson TE, Purdy RH, Gruol DL (2007) Steroid pregnenolone sulfate enhances NMDA-receptor-independent long-term potentiation at hippocampal CA1 synapses: role for L-type calcium channels and sigma-receptors. Hippocampus 17:349-369.

Sabino V, Cottone P, Parylak SL, Steardo L, Zorrilla EP (2009) Sigma-1 receptor knockout mice display a depressive-like phenotype. Behav Brain Res 198:472-476.

Sanz E, Yang L, Su T, Morris DR, McKnight GS, Amieux PS (2009) Cell-type-specific isolation of ribosome-associated mRNA from complex tissues. Proc Natl Acad Sci U S A 106:13939-13944.

Sałaciak K, Pytka K (2022) Revisiting the sigma-1 receptor as a biological target to treat affective and cognitive disorders. Neurosci Biobehav Rev 132:1114-1136.

Schmidt HR, Betz RM, Dror RO, Kruse AC (2018) Structural basis for σ. Nat Struct Mol Biol 25:981-987.

Schmidt HR, Zheng S, Gurpinar E, Koehl A, Manglik A, Kruse AC (2016) Crystal structure of the human σ1 receptor. Nature 532:527-530.

Schnädelbach O, Ozen I, Blaschuk OW, Meyer RL, Fawcett JW (2001) N-cadherin is involved in axon-oligodendrocyte contact and myelination. Mol Cell Neurosci 17:1084-1093.

Shigemoto-Mogami Y, Hoshikawa K, Goldman JE, Sekino Y, Sato K (2014) Microglia enhance neurogenesis and oligodendrogenesis in the early postnatal subventricular zone. J Neurosci 34:2231-2243.

Skuza G, Rogóz Z (2006) Effect of BD 1047, a sigma1 receptor antagonist, in the animal models predictive of antipsychotic activity. Pharmacol Rep 58:626-635.

Soliven B (2001) Calcium signalling in cells of oligodendroglial lineage. Microsc Res Tech 52:672-679.

Song J, Goetz BD, Baas PW, Duncan ID (2001) Cytoskeletal reorganization during the formation of oligodendrocyte processes and branches. Mol Cell Neurosci 17:624-636.

Song W, Yao Y, Zhang H, Hao X, Zhou L, Song Z, Wei T, Chi T, Liu P, Ji X, Zou L (2023) Sigma-1 Receptor Activation Improves Oligodendrogenesis and Promotes White-Matter Integrity after Stroke in Mice with Diabetic Mellitus. Molecules 28.

Stankoff B, Aigrot MS, Noël F, Wattilliaux A, Zalc B, Lubetzki C (2002) Ciliary neurotrophic factor (CNTF) enhances myelin formation: a novel role for CNTF and CNTF-related molecules. J Neurosci 22:9221-9227.

Stelfa G, Vavers E, Svalbe B, Serzants R, Miteniece A, Lauberte L, Grinberga S, Gukalova B, Dambrova M, Zvejniece L (2021) Reduced GFAP Expression in Bergmann Glial Cells in the Cerebellum of Sigma-1

Receptor Knockout Mice Determines the Neurobehavioral Outcomes after Traumatic Brain Injury. Int J Mol Sci 22.

Stevens B, Porta S, Haak LL, Gallo V, Fields RD (2002) Adenosine: a neuron-glial transmitter promoting myelination in the CNS in response to action potentials. Neuron 36:855-868.

Su TP (1982) Evidence for sigma opioid receptor: binding of [3H]SKF-10047 to etorphine-inaccessible sites in guinea-pig brain. J Pharmacol Exp Ther 223:284-290.

Su TP, London ED, Jaffe JH (1988) Steroid binding at sigma receptors suggests a link between endocrine, nervous, and immune systems. Science 240:219-221.

Su TP, Su TC, Nakamura Y, Tsai SY (2016) The Sigma-1 Receptor as a Pluripotent Modulator in Living Systems. Trends Pharmacol Sci 37:262-278.

Takebayashi H, Nabeshima Y, Yoshida S, Chisaka O, Ikenaka K (2002) The basic helix-loop-helix factor olig2 is essential for the development of motoneuron and oligodendrocyte lineages. Curr Biol 12:1157-1163.

Tamura Y, Kataoka Y, Cui Y, Takamori Y, Watanabe Y, Yamada H (2007) Intracellular translocation of glutathione S-transferase pi during oligodendrocyte differentiation in adult rat cerebral cortex in vivo. Neuroscience 148:535-540.

Tansey FA, Cammer W (1991) A pi form of glutathione-S-transferase is a myelin- and oligodendrocyte-associated enzyme in mouse brain. J Neurochem 57:95-102.

Taveggia C, Thaker P, Petrylak A, Caporaso GL, Toews A, Falls DL, Einheber S, Salzer JL (2008) Type III neuregulin-1 promotes oligodendrocyte myelination. Glia 56:284-293.

Taveggia C, Zanazzi G, Petrylak A, Yano H, Rosenbluth J, Einheber S, Xu X, Esper RM, Loeb JA, Shrager P, Chao MV, Falls DL, Role L, Salzer JL (2005) Neuregulin-1 type III determines the ensheathment fate of axons. Neuron 47:681-694.

Terada N, Kidd GJ, Kinter M, Bjartmar C, Moran-Jones K, Trapp BD (2005) Beta IV tubulin is selectively expressed by oligodendrocytes in the central nervous system. Glia 50:212-222.

Trapp BD, Nishiyama A, Cheng D, Macklin W (1997) Differentiation and death of premyelinating oligodendrocytes in developing rodent brain. J Cell Biol 137:459-468.

Tsai HH, Frost E, To V, Robinson S, Ffrench-Constant C, Geertman R, Ransohoff RM, Miller RH (2002) The chemokine receptor CXCR2 controls positioning of oligodendrocyte precursors in developing spinal cord by arresting their migration. Cell 110:373-383.

Tsai SY, Rothman RK, Su TP (2012) Insights into the Sigma-1 receptor chaperone's cellular functions: a microarray report. Synapse 66:42-51.

Tsai SY, Chuang JY, Tsai MS, Wang XF, Xi ZX, Hung JJ, Chang WC, Bonci A, Su TP (2015) Sigma-1 receptor mediates cocaine-induced transcriptional regulation by recruiting chromatin-remodeling factors at the nuclear envelope. Proc Natl Acad Sci U S A 112:E6562-6570.

Turnescu T, Arter J, Reiprich S, Tamm ER, Waisman A, Wegner M (2018) Sox8 and Sox10 jointly maintain myelin gene expression in oligodendrocytes. Glia 66:279-294.

van Tilborg E, de Theije CGM, van Hal M, Wagenaar N, de Vries LS, Benders MJ, Rowitch DH, Nijboer CH (2018) Origin and dynamics of oligodendrocytes in the developing brain: Implications for perinatal white matter injury. Glia 66:221-238.

Voyvodic JT (1989) Target size regulates calibre and myelination of sympathetic axons. Nature 342:430-433.

Wang RH, Li C, Deng CX (2010) Liver steatosis and increased ChREBP expression in mice carrying a liver specific SIRT1 null mutation under a normal feeding condition. Int J Biol Sci 6:682-690.

Wang S, Sdrulla A, Johnson JE, Yokota Y, Barres BA (2001) A role for the helix-loop-helix protein Id2 in the control of oligodendrocyte development. Neuron 29:603-614.

Wang S, Sdrulla AD, diSibio G, Bush G, Nofziger D, Hicks C, Weinmaster G, Barres BA (1998) Notch receptor activation inhibits oligodendrocyte differentiation. Neuron 21:63-75.

Wang SM, Wu HE, Yasui Y, Geva M, Hayden M, Maurice T, Cozzolino M, Su TP (2023) Nucleoporin POM121 signals TFEB-mediated autophagy via activation of SIGMAR1/sigma-1 receptor chaperone by pridopidine. Autophagy 19:126-151.

Wang Y, Zhao CS (2019) Sigma-1 receptor activation ameliorates LPS-induced NO production and ROS formation through the Nrf2/HO-1 signaling pathway in cultured astrocytes. Neurosci Lett 711:134387.

Weng TY, Tsai SA, Su TP (2017) Roles of sigma-1 receptors on mitochondrial functions relevant to neurodegenerative diseases. J Biomed Sci 24:74.

Wilson DM, Bianchi C (1999) Improved immunodetection of nuclear antigens after sodium dodecyl sulfate treatment of formaldehyde-fixed cells. J Histochem Cytochem 47:1095-1100.

Wolf RM, Wilkes JJ, Chao MV, Resh MD (2001) Tyrosine phosphorylation of p190 RhoGAP by Fyn regulates oligodendrocyte differentiation. J Neurobiol 49:62-78.

Wu Z, Li L, Zheng LT, Xu Z, Guo L, Zhen X (2015) Allosteric modulation of sigma-1 receptors by SKF83959 inhibits microglia-mediated inflammation. J Neurochem 134:904-914.

Xiao L, Ohayon D, McKenzie IA, Sinclair-Wilson A, Wright JL, Fudge AD, Emery B, Li H, Richardson WD (2016) Rapid production of new oligodendrocytes is required in the earliest stages of motor-skill learning. Nat Neurosci 19:1210-1217.

Ximerakis M, Lipnick SL, Innes BT, Simmons SK, Adiconis X, Dionne D, Mayweather BA, Nguyen L, Niziolek Z, Ozek C, Butty VL, Isserlin R, Buchanan SM, Levine SS, Regev A, Bader GD, Levin JZ, Rubin LL (2019) Single-cell transcriptomic profiling of the aging mouse brain. Nat Neurosci 22:1696-1708.

Xin M, Yue T, Ma Z, Wu FF, Gow A, Lu QR (2005) Myelinogenesis and axonal recognition by oligodendrocytes in brain are uncoupled in Olig1-null mice. J Neurosci 25:1354-1365.

Xu Q, Ji XF, Chi TY, Liu P, Jin G, Chen L, Zou LB (2017) Sigma-1 receptor in brain ischemia/reperfusion: Possible role in the NR2A-induced pathway to regulate brain-derived neurotrophic factor. J Neurol Sci 376:166-175.

Yang H, Shen H, Li J, Guo LW (2019) SIGMAR1/Sigma-1 receptor ablation impairs autophagosome clearance. Autophagy 15:1539-1557.

Ye P, Li L, Richards RG, DiAugustine RP, D'Ercole AJ (2002) Myelination is altered in insulin-like growth factor-I null mutant mice. J Neurosci 22:6041-6051.

Yona S, Kim KW, Wolf Y, Mildner A, Varol D, Breker M, Strauss-Ayali D, Viukov S, Guilliams M, Misharin A, Hume DA, Perlman H, Malissen B, Zelzer E, Jung S (2013) Fate mapping reveals origins and dynamics of monocytes and tissue macrophages under homeostasis. Immunity 38:79-91.

Yoo AS, Krieger C, Kim SU (1999) Process extension and intracellular Ca2+ in cultured murine oligodendrocytes. Brain Res 827:19-27.

Zhang G, Li Q, Tao W, Qin P, Chen J, Yang H, Liu H, Dai Q, Zhen X (2023) Sigma-1 receptor-regulated efferocytosis by infiltrating circulating macrophages/microglial cells protects against neuronal impairments and promotes functional recovery in cerebral ischemic stroke. Theranostics 13:543-559.

Zhang SZ, Wang QQ, Yang QQ, Gu HY, Yin YQ, Li YD, Hou JC, Chen R, Sun QQ, Sun YF, Hu G, Zhou JW (2019) NG2 glia regulate brain innate immunity via TGF-β2/TGFBR2 axis. BMC Med 17:204.

Zhang Y, Zhang X, Wei Q, Leng S, Li C, Han B, Bai Y, Zhang H, Yao H (2020) Activation of Sigma-1 Receptor Enhanced Pericyte Survival via the Interplay Between Apoptosis and Autophagy: Implications for Blood-Brain Barrier Integrity in Stroke. Transl Stroke Res 11:267-287.

Zhang Y, Argaw AT, Gurfein BT, Zameer A, Snyder BJ, Ge C, Lu QR, Rowitch DH, Raine CS, Brosnan CF, John GR (2009) Notch1 signaling plays a role in regulating precursor differentiation during CNS remyelination. Proc Natl Acad Sci U S A 106:19162-19167.

Zhang Y, Chen K, Sloan SA, Bennett ML, Scholze AR, O'Keeffe S, Phatnani HP, Guarnieri P, Caneda C, Ruderisch N, Deng S, Liddelow SA, Zhang C, Daneman R, Maniatis T, Barres BA, Wu JQ (2014a) An RNA-sequencing transcriptome and splicing database of glia, neurons, and vascular cells of the cerebral cortex. J Neurosci 34:11929-11947.

Zhang Y, Chen K, Sloan S, Bennett M, Scholze A, O'Keeffe S, Phatnani H, Guarnieri P, Caneda C, Ruderisch N, Deng S, Liddelow S, Zhang C, Daneman R, Maniatis T, Barres B, Wu J (2014b) An RNA-Sequencing Transcriptome and Splicing Database of Glia, Neurons, and Vascular Cells of the Cerebral Cortex. Journal of Neuroscience 34:11929-11947.

Zhao J, Ha Y, Liou GI, Gonsalvez GB, Smith SB, Bollinger KE (2014) Sigma receptor ligand, (+)-pentazocine, suppresses inflammatory responses of retinal microglia. Invest Ophthalmol Vis Sci 55:3375-3384.

Zhao N, Huang W, Cătălin B, Scheller A, Kirchhoff F (2021) L-Type Ca(2+) Channels of NG2 Glia Determine Proliferation and NMDA Receptor-Dependent Plasticity. Front Cell Dev Biol 9:759477.

Zhao X, Zhu L, Liu D, Chi T, Ji X, Liu P, Yang X, Tian X, Zou L (2019) Sigma-1 receptor protects against endoplasmic reticulum stress-mediated apoptosis in mice with cerebral ischemia/reperfusion injury. Apoptosis 24:157-167.

Zhemkov V, Geva M, Hayden MR, Bezprozvanny I (2021) Sigma-1 Receptor (S1R) Interaction with Cholesterol: Mechanisms of S1R Activation and Its Role in Neurodegenerative Diseases. Int J Mol Sci 22.

12 Acknowledgements

I would like to express my heartfelt gratitude to all those who have contributed to the successful progress of my project.

First and foremost, I extend my sincere appreciation to my mentor, Prof. Frank Kirchhoff, for his great support and encouragement throughout the entire research process. Thank you for accepting me into your group and for your profound influence on my academic experience in Germany.

I am deeply grateful to my supervisor, Dr. Wenhui Huang, for providing invaluable guidance and expertise in my academic work. Your insights were instrumental in shaping the direction of my PhD project, and your constant encouragement has strengthened my determination. I extend my warmest wishes for a happy new life for your family of three.

I would like to thank all the current and former members of the Kirchhoff team for their collaboration and dedication. Special thanks to Dr. Xianshu Bai, who has been both a teacher and a friend to me. Your patience in listening and inspiring me, as well as sharing both laughter and tears, have meant a great deal. My appreciation also goes to Dr. Anja Scheller, who helped to load thousands of slices from me. I am grateful to Qilin Guo and Lipao Fang for their assistance in my experiments and their support whenever I needed help. To my dear Davide Gobbo, thank you for your support in all aspects of my life in Germany. You, Phillip Rieder, and Emeline Buttigieg always made our lab life filled with laughter. I thank Rhea Seth for the company I needed at every moment. I would also like to express my gratitude to Ting Zhang and Paula Gelonch-Capell for their contributions to this project. Many thanks to lab technicians Daniel Schauenburg and Frank Rhode, as well as secretary Ute Legler, whose work was crucial in carrying out the experiments. I extend my gratitude to every member of the lab for the past five years, including Ahmad Lotfinia, Yasser Medlej, Na Zhao, Mariza Bortolanza, Erika Meyer, Naielly Rodrigues da Silva, Gebhard Stopper, Laura Caudal, and Laura Stopper. I cherish every moment I have spent with you all.

I would like to thank all my friends in Homburg. Thank you to Dr. Renping Zhao for always sharing with me his experiences in his studies and work, as well as his delicious food. Thank you to Dr. Zhao and Dr. Bai' s child, Caroline Zhao, who has brought me such pure joy and healing. Thank you to Yiwen Yao, Dr. Qinghua Luo, and Anqi Sheng for accompanying me to spent beautiful time in different cities in Europe. Thank you to Dr. Na Zhao and Dr. Qinghai Tian for driving me around the surrounding areas and enjoying the beautiful scenery.

A special thank you goes to the China Scholarship Council for the financial support of my PhD study abroad. I am also thankful to the funding agencies that financially supported my project.

Lastly, and most importantly, I want to thank my family for their unwavering understanding and encouragement to be my strongest support during my scientific journey.

To each one of you, I extend my heartfelt thanks for your valuable contributions and companionship. I wish you all the very best.

13 Curriculum Vitae and List of Publications

The curriculum vitae was removed from the electronic version of the doctoral thesis for reasons of data protection.